5-20-2011

Design and Development of Nanoconjugates for Nanotechnology

Ashley Dung Quach
University of New Orleans

Recommended Citation

Design and Development of Nanoconjugates for Nanotechnology

A Dissertation

Submitted to the Graduate Faculty of the
University of New Orleans
in partial fulfillment of the
requirements for the degree of

Doctor of Philosophy
in
Chemistry

By

Ashley Dung Quach

B.A., University of New Orleans, 2004

May 2011

Dedication

This dissertation is dedicated to my amazing and knowledgeable husband, Thang Ky Nguyen. Without his infinite love, support, encouragement, patience, care, and sacrifice, I would not be able to fulfill my current education.

Acknowledgements

I would like to express my great appreciation to my advisors, Professor Zeev Rosenzweig and Professor Matthew A. Tarr. Their tremendous and invaluable wisdom, guidance, support, and encouragement have always been a big part of my success.

I would also like to genuinely acknowledge Professor Seth Pincus and his staffs at Children's Hospital Research Institute for their knowledge, wisdom, counsel, encouragement, and generosity by discussing my projects, offering a working place, and allowing me to use their facilities in the aftermath of Hurricane Katrina.

I have benefited immeasurably from the association with my past and present group members at the University of Orleans, for whom I am always grateful. I wish to mention Liane Rossie, a former post-doc who taught me how to handle little things around the lab as an undergraduate student. I want to thank Lifang Shi, a former group member who introduced nanomaterial synthesis to me when I started my research as a graduate student. She was a great influence on how I conduct most of my experiments. Then there are Arriel Wicks and Venkata Kethineedi, the two lab members that I have spent most of my research time with. We have done research and been to many conferences together. Thank you both for listening to and discussing all my silly reasoning about life and work. I also wish to thank Gayatri Sahu, who has contributed a lot of effort to my third project. Thank you very much for not only helping me to get my work done, but also for being a good friend. My special thanks also go to other past and present group members, whom I have interacted with, worked together, and learned many unique things from.

I am especially grateful for the love and support from my parents and my sister throughout the course of my graduate school. Thank you all for just being there and offering

help when I need the most. And last but not least, I would also like to acknowledge the importance of my beautiful baby boy, Ryan Ky Nguyen. You are my new joy of life, my inspiration, and my biggest source of determination to finish this degree.

Table of Contents

List of Figures

List of Schemes and Table

Abstract

Nanotechnology builds devices from the bottom up with atomic accuracy. Among the basic nano-components to fabricate such devices, semiconductor nanoparticle quantum dots (QDs), metal nanocrystals, proteins, and nucleic acids have attracted most interests due to their potential in optical, biomedical, and electronic areas. The major objective of this research was to prepare nano-components in order to fabricate functional nano-scale devices.

This research consisted of three projects. In the first two projects, we incorporated two desirable characteristics of QDs, which are their abilities to serve as donors in fluorescence energy transfer (FRET) and surface energy transfer (SET) as well as to do multiplexing, to engineer QD-based nanoconjugates for optical and biomedical applications. Immobilizing luminescent semiconductor CdSe/ZnS QDs to a solid platform for QD-based biosensors offers advantages over traditional solution-based assays. In the first project, we designed highly sensitive CdSe/ZnS QD SET-based probes using gold nanoparticles (AuNPs) as FRET acceptors on polystyrene (PS) microsphere surfaces. The emission of PS-QD was significantly quenched and restored when the AuNPs were attached to and then removed from the surface. The probes were sensitive enough to analyze signals from a single bead and for use in optical applications. The new PS-QD-AuNP SET platform opens possibilities to carry out both SET and FRET assays in microparticle-based platforms and in microarrays. In the second project, we applied the QD-encoded microspheres in FRET-based analysis for bio-applications. QDs and Alexa Fluor 660 (A660) fluorophores are used as donors and acceptors respectively via a hairpin single stranded DNA. FRET between QD and A660 on the surface of polystyrene microspheres resulted in quenching of QD luminescence and increased A660 emission. QD emission on polystyrene

microspheres was restored when the targeted complementary DNA hybridized the hairpin strand and displaced A660 away from QDs.

The third project involved fabrication of different nanoconjugates via self-assembly of template-based metal nanowires and metal nanoparticles using oligonucleotides as linkers. These nanoconjugates can serve as building blocks in nano-electronic circuits. The template method restricted the oligonucleotides attachment to the tip of the nanowires. Nanowires tagged with hybridizable DNA could connect to complementary DNA-modified metal crystals in a position-specific manner.

Nanotechnology, Nanoconjugates, Quantum Dots, Metal Nanocrystals, Metal Nanowires, Peptides, Oligonucleotides, DNA, Surface Energy Transfer (SET), Fluorescence Resonance Energy Transfer (FRET), Multiplexing, Microspheres, Probes, Biosensors, Self-Assembly

Chapter 1

Introduction

1.1 Significance

Nanotechnology has been one of the fastest growing, most challenging, and most exciting fields nowadays. In his famous talk, "There's Plenty of Room at the Bottom", at Caltech in 1959 for the American Physical Society, Richard Feynman was the first to suggest the fabrication of nano-devices from nano part-assemblies[1]. Since then, nanotechnology has emerged from purely scientific to technical fields and public awareness[2,3] because of its tremendous potential in terms of manufacturing cost and conducting size. High-tech devices can be widely available and create much less environmental waste. In simple expressions, nanotechnology is understood as engineering tiny machines. In scientific terms, nanotechnology is defined as a study of matters at atomic or molecular levels involving processing, separation, consolidation, and deformation. It ranges from development of conventional equipment to engineering of new micron scale functional devices based upon self-assembled and controllable nanometer components. These components include nano-objects such as nanospheres, nanowires, nanotubes, and nanosheets and biomolecules such as protein and nucleic acids. The nano-objects can be made of organic, inorganic, organometallic, polymer or ceramic materials. The assembly of these nano-components into defined architectures can take place by variable attractions between them, or being driven by particular interactions with template-based chemistry. When the word "nano" is mentioned, it is acknowledged as physical entities that have structural sizes from 1 to 100 nm in at least one dimension. Below, scheme 1.1 is an illustration of relative size of a Qdot nanocrystal compared to other biomolecules.
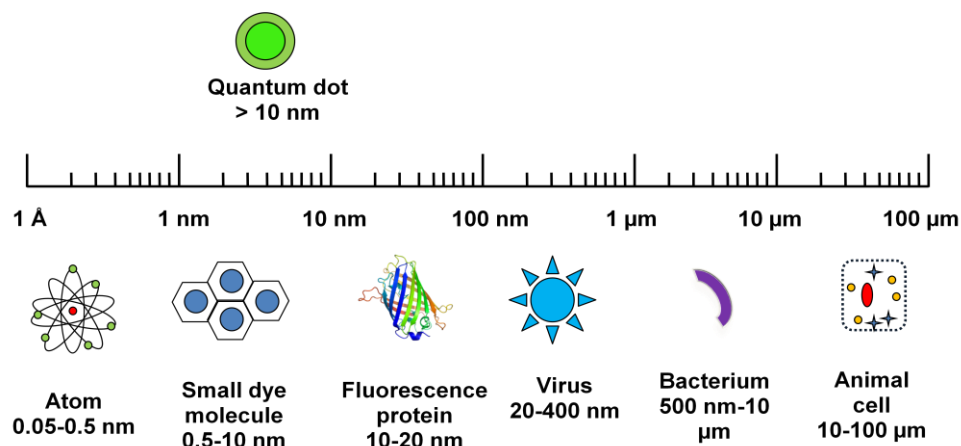
Scheme 1.1 *Relative size ranges of a quantum dot nanocrystal and other biomolecules*

Even though there have been increasing concerns about toxicity and long-term environmental impacts, nanotechnology with its amazing promise has created new materials and nano-devices with an enormous number of scientific and commercial applications including energy production, electronics, and medicine. Among basic nano-components to build such devices, synthetic materials like metal nanocrystals and semiconductor nanoparticle quantum dots (QDs) and biomolecules like proteins and nucleic acids have attracted most interests due to great individual and combined potential in exciting optical [4-9], biomedical[10-17], and electronic[18-23] fields. Scheme 1.2 illustrates the ideas of combining metal nanocrystals and/or semiconductor nanoparticles with proteins and/or nucleic acids to fabricate unique nanoconjugates that can be used to build nano-devices in such fields. The goal of many research projects that aim to develop such fields in nanotechnology therefore has been to design, synthesize such nano-component building blocks, and fabricate functional nano-scale devices from some or all of these basic nano-components. However, all the accomplishments so far in such fields are still far from what Feynman had envisioned. More studies of the nanoconjugates still need to be

2

explored and developed to contribute to the fabrication of such functional nano-devices. With

research experience in optical and magnetic nanomaterials for biomedical applications during the

last decade[12,24-27], our lab has also explored, designed, and developed such nano-devices .
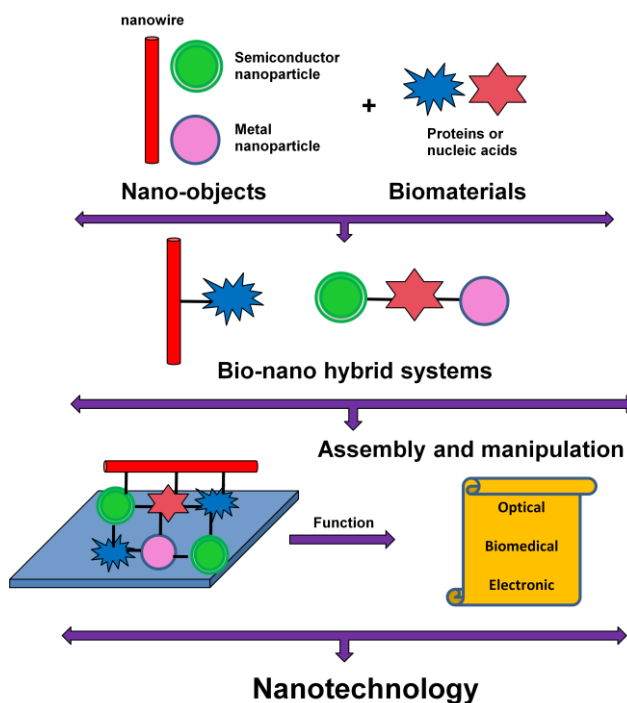
Scheme 1.2 *The conceptual generation of biomolecule–nanoparticle/nanorod conjugates to yield functional devices*

Luminescent semiconductor nanocrystal QDs, an exciting inventing class of fluorescent

probes, are considered a viable alternative to molecular fluorophores in luminescence bioassays.

Because of their distinctive electronic properties, QDs have many unique characteristics such as

broad absorption spectra, narrow and symmetrical emission peaks, good emission quantum

yields, large molar extinction coefficients, long fluorescence lifetimes, large Stokes shifts, low

photochemical degradation, and size-tunable wavelength dependence. Due to such benefits, QDs

are excellent donor fluorophores for fluorescence resonance energy transfer (FRET) and surface energy transfer (SET) studies, as well as ideal candidates for multiplexing applications.

FRET is a distance-dependent interaction between the electronic excited states of two fluorophores in which excitation is transferred from a donor to an acceptor without emission of a photon[77,122]. The efficiency of the energy transfer process is proportional to the inverse sixth power of the distance between donor and acceptor ($1/R^6$). In other words, FRET measurements can be used as an effective tool for measuring the distance between two chromophores. FRET-based sensing pairs have been used to analyze protein binding affinity and protein conformational alteration[28-31]. Because of their distinctive characteristics, QDs are often used as donors in the FRET process. Especially, the wide excitation spectra of quantum dots allow selection of an excitation wavelength that is out of the acceptors' range. This eliminates "bleeding" of excited energy into the acceptor channel, which increases fluorescence intensity of the acceptor, thus leading to over-estimation of the FRET efficiency between the donor and acceptor. Several research groups have developed luminescent QDs as donors in FRET studies. Zhang et al. described a novel approach to improve the detection sensitivity of QD FRET-based nanosensors using single-molecule detection in a capillary flow[32]. The authors obtained great FRET efficiency due to the deformation of DNA in the capillary stream. Mauro et al. has synthesized FRET-based maltose-binding assays by attaching CdSe/ZnS quantum dots capped dihydrolipoic acid with maltose binding protein (MBP) molecules. The FRET assay investigated the interactions between MBP and the acceptor Cy3[33,34]. Likewise, Goldman's group has developed a hybrid quantum dot-antibody fragment FRET based TNT sensor[35]. Similar to FRET, SET involves non-radiative energy transfer from donors to acceptors. However, SET is caused by metal induced quenching. The main variation between the two types of energy

4

transfer is that the acceptor for FRET has to be a fluorophore while for SET the acceptor is a metal surface. As a result, no acceptor emission occurs, but quenching of the donor fluorescence does take place. The efficiency of SET and FRET processes are also different. SET efficiency is proportional to the inverse fourth power of the distance between the donor and the acceptor $(1/R^4)$[15]. FRET is highly sensitive and only happens when the donor-acceptor distance is no more than 100 Å, while SET is not as sensitive and occurs at distances of up to 220 Å[36]. SET interactions between QDs and metal surfaces have been explored. In 2007, Pons et al. showed that non-radiative quenching of the QD emission by proximal Au-NPs is due to long-distance dipole-metal interactions that extend significantly beyond the classical FRET range[17]. In 2009, Li and the group presented DNA detection via dipole-surface energy transfer between QD and gold nanorod (GNR)[37]. DNA hybridization between complementary strands of DNA on QD and GNR enclosed the proximity between the two probes causing QD quenching by transferring emission energy to GNR.

QD multiplexing is realized as the ability to simultaneously excite multicolored QDs that have different emission wavelengths. Applying QD multiplexing in bioassays enables researchers to detect several targets in a single measurement. Several research groups have reported the use of quantum dots in multiplexed applications. In 2001, Han et al. fabricated multicolor optical coding for biological assays by embedding different-sized quantum dots into polymeric microbeads at precisely controlled ratios[38]. Their imaging and spectroscopic measurements indicated that the QD-tagged beads are highly uniform and reproducible, yielding bead identification accuracies as high as 99.99% under favorable conditions. Their DNA hybridization studies demonstrated that the coding and target signals can be simultaneously read at the single-bead level. Wilson et al. applied combination of layer-by-layer (LBL) self-

assembly and magnetic separation to encode magnetic microspheres with multiple colors of semiconductor QDs. Three sets of microspheres with different spectral codes were combined to form a suspension array that was used to screen three different types of explosive in the same sample[39]. Yezhelyev et al. used QDs emitting at 525 nm, 565 nm, 605 nm, 655 nm and 705 nm and directly conjugated them to primary antibodies against HER2, estrogen receptor, progesterone receptor, EGF receptor and mTOR, respectively[40]. The multicolor bioconjugates were used for simultaneous detection of five clinical significant tumor markers in breast cancer cells, MCF-7 and BT-474.

Regardless of the above achievements, most of the published QD-based energy transfer probes were based on nanometric solution assays. Due to their small size in solution, when attached to other biomolecules, QDs easily form aggregates, which can affect their true potential[41]. Additionally, multiplexing of QD FRET-based probes has only been mentioned but never explored[42]. As a result, the need to fabricate more stable and versatile QD-based probes for FRET studies in a broader range of biological assays is evident. Also, combining both FRET and multiplexing in the same study offers superior research capability. Moreover, new methodologies should be facile, allow easy purification, avoid aggregation, and provide enhanced signals. To accomplish these goals, QDs can be combined with microspheres by different approaches. Among these, coating of QDs on microspheres surface via layer-by-layer (LBL) method (Scheme 1.3) is preferred due to uniform distribution of QDs[41,43].
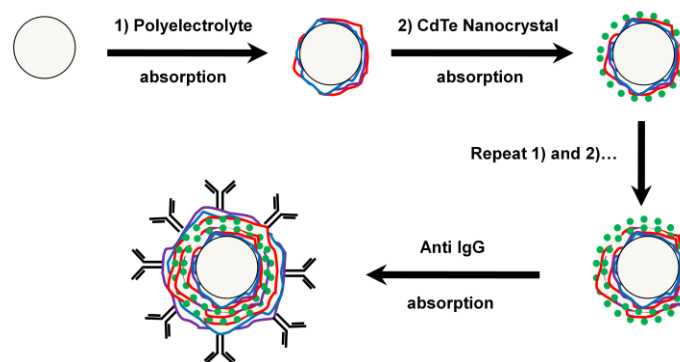
Scheme 1.3 *Illustration of the procedure used to prepare CdTe QD-microsphere bioconjugates via layer-by-layer assembly*

Indeed, this type of QD-encoded microsphere for biosensors has become an interesting approach in recent research due to the need for multiplexing and high-throughput detection. The microbead probes have been proven to be more flexible and reproducible compared to traditional solution-based microarrays[44]. Moreover, the bead can act as an amplifying platform that carries multiple QDs to substantially enhance signal-to-noise ratio. In 2008, Ma et al. investigated the adsorption of rabbit IgG onto CdTe QD/polystyrene microbeads[45]. The process, which was primarily dependent on pH conditions and ionic strength, performed best at the isoelectric point due to electrostatic interactions. The probes were later employed in the detection of goat anti-rabbit IgG antibody in fluoroimmunoassays with a limit of detection range of 1-100 ng/mL. In 2009, Li et al.[44] synthesized QD-coated encoded silica beads for multiplex coding. The silica beads were highly monodisperse and reproducible. By simply combining, mixing, and matching between different color QDs and different kinds of silica beads, many unique coding probes were developed to detect DNA utilizing DNA hybridization. In 2010, Dong et al.[46] incorporated CeTe QDs on poly(styrene-co-acrylic acid) microbead surface via layer-by-layer self-assembly. The probes provided great detection and labeling capabilities towards DNA and protein thanks to the large surface area of the polybeads and distinctive properties of QDs. When combined with

highly sensitive stripping voltammetry, the encoded beads delivered a detection limit of 0.52 fmol/L and a dynamic range spanning 5 orders of magnitude. However, incorporating energy transfer studies in QD-encoded microspheres can still be a challenge because the outer polymer layer to protect QDs prevents them from transferring energy to the outside environment. To solve this problem, we have developed a research approach in which we covalently attach QDs to biocompatible microsphere surface without coating the outer layer. As a result, QDs will be able to transfer energy to their surroundings to enable FRET studies. This in turn enables the development of a whole new generation of QD-based energy transfer probes.

In the past several decades, metal nanocrystals have revealed surprising benefits from conventional industry to clinical therapeutic. Noble metals such as gold, platinum, or silver attracted a lot more interest due to their non-toxic characteristics. One other direction that has also created attention is fabricating nano-electronic devices from nano-component building blocks. Since the first theoretical molecular rectifier was developed by Aviram and Ratner in 1974[47], the development of components to assemble nano-based-electronic devices has advanced significantly. As early as 1981, Murray and co-workers prepared a rectifier from a two-layer conducting polymer via electrochemistry[48,49]. Fifteen years or so later, single layers of conducting organic molecules, which were inserted in between micrometer-sized planar electrodes, have been developed by many research groups: unimolecular electrical rectification by Metzger et al. in 1997[50], electronically configuration molecular-based logic gates by Collier et al. in 1999[51] and negative differential resistance devices by Chen et al. in 1999[52]. However, preparing these structures remains challenging due to the need for connecting molecular switching elements to the molecular wires in complex nano-circuits. Additionally, in a nano-electronic device, the electronic and electromagnetic properties depend on elemental

construction, size, and shape of nano-components[53]. In 2002, Kovtyukhova and Mallouk presented a theory of site-specific assembly of electronic logic and memory circuits using metal nanowires as building blocks[54]. The authors proposed different ideas to connect molecular switching components to metal nanowires. The overall idea of self-assembling from small building blocks proposed parallel synthesis of large numbers of individual components. Consequently, such method reduces the basic physical limitations and processing costs compared to "top-down" approach[55]. The authors also pointed out that surface chemistry, length, diameter, and transport properties of metal nanowires can be precisely controlled by synthesis. Nanowires could form an array that contained memory or logic elements at the small cross points (Scheme 1.4). These small cross points would be less likely overlapped with a defect in self-assembled monolayer. This in turn would offer devices with extremely high density of memory or logic. Metal-based nanowires present many advantages over carbon nanotubes and semiconductor nanowires. First, the coupling chemistry for metal nanowire surface is established and straightforward. Second, they have low resistivity which is a big plus in electronic circuits.
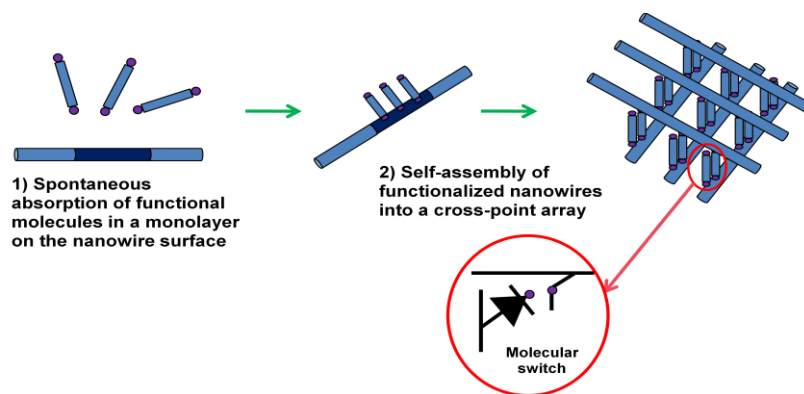
Scheme 1.4 *Schematic drawing of the assembly of a two-dimensional cross-point array from metal nanowires and functional molecules. In order for the cross-point array to act as a functional memory or logic device, a configurable switch is needed at each junction.*

Among many connecting chemistry approaches in this area, using short DNA or oligonucleotide as a tool to join template-based metal nanowires presents great potentials. Oligonucleotides are considered a "smart" tool since its hybridizing binding affinity can be not only specific, complementary, and reversible, but also synthetically mismatched-designed for binding kinetics. Nanoparticle positioning can be carefully controlled at the sub-nanometer scale using oligonucleotides as templates[56]. Consequently, DNA can contribute a major step toward creating nano-architectures with applications in nano-electronic and photonic device assembly. DNA hybridization has been successfully applied by different groups. Mirkin's group has presented a number of publications on colorimetric sensors via assembling of single-stranded DNA coated AuNPs and AgNPs[57-62]. Alivisatos and co-workers also published many studies of building nano-structures using discrete DNA-gold building blocks in which the number of DNA strands is controlled[63-67]. Recently, Wang and co-workers investigated photonic interaction between QDs and AuNPs connected by DNA self-assembled in discrete nanostructures[68]. Despite the potential advantages, little work has been done to explore much further in this research direction. However, the potential of using this approach to fabricate nano-scale electronic devices is too great to be abandoned. Indeed, understanding and fabricating simple site-specific nano self-assemblies will enable us to contribute small steps towards building such nano-scale electronic devices. As a result, we have designed functionalized single-stranded oligonucleotides and synthesize template-based metal nanowires to explore many different possible self-assemblies.

1.2 Objectives

The major objective of this PhD research is to design and develop nanoconjugates that combine synthetic nano components such as luminescent quantum dots (QDs) and metal nanocrystals with biomolecules such as proteins and nucleic acids to form a new generation of nanometric probes for optical, biomedical, and electronic applications. This major objective is divided into three individual projects for the above applications. The first two projects aim at developing QD-based nanoconjugates on microsphere platform while the third one focuses on self-assembling of template-based metal nanowires and metal nanoparticles using DNA hybridization as a tool.

In the first two projects, QD-encoded microspheres offer non-aggregated FRET-based probes that are stable and versatile with enhanced signal-to-noise ratios for optical and biomedical applications. The most exceptional properties of these bio-devices are that they can be used for the following things on a single bead: i) surface energy transfer (SET) between a QD and a gold nanoparticle, ii) FRET plus multiplexing simultaneously between a quantum dot and an organic dye, and iii) fluorescence imaging. These works for the first time ever, integrates SET and FRET on a microbead platform. In addition, incorporating simultaneously FRET, multiplexing, and fluorescence imaging on a non-aggregated microbead platform offers a new research direction for nano-based bio-devices. The microbead acts as an amplifier platform carrying multiple QDs to enhance signal to noise ratio significantly compared to traditional solution-based quantum dot probes. Quantitative analysis and imaging can simply be detected at a single bead level. The ability to enhance signal-to-noise ratio presents great potentials by improving the limit of detection. Furthermore, detection of DNA (either a single strand or several strands or simultaneously) can be performed by combining FRET and multiplexing.

11

The third project creates controllable and site-specific self-assemblies among nano-components such as metal nanoparticles/nanowires using oligonucleotides as linkers for nano-circuits. With oligonucleotides being attached to metal nanowires embedded in a template, oligonucleotides are restricted to locate just on the tips of the metal nanowires. Next, dissolving the template allows nanowires that are tagged with hybridizable DNA be in a position-specific manner. Complementary strands of the oligonucleotides can be attached to intended positions on other metal nanowires or nanoparticles. The final step is to mix the two oligonucleotide-modified nano-components to achieve site-specific self-assemblies.

1.3 Quantum dots

1.3.1 Fundamental

The desire to thoroughly investigate the cellular level of living organisms has driven tremendous research interests in the last two decades towards a new class of fluorescent nano-probes: semiconductor luminescent quantum dots (QDs). These materials are nanometer scale spheres with physical dimensions within the range of the exciton Bohr radius[69-71]. QDs have very broad absorption spectra, narrow and symmetrical emission spectra, tunable size-wavelength dependence, and low photochemical degradation. Hence, luminescent QDs have been considered to be better suited for biochemical labeling compared to conventional fluorophores. QDs have been integrated in many bio-applications such as cellular/cancer imaging[72-75], biosensor[76-78], and immunoassays[79-81] instead of organic fluorophores. QDs are neither atomic nor bulk semiconductors; rather, each dot contains thousands of combined atoms of elements from groups 12 -16 of the periodic table. That is why QD stands as a bridge gap

between semiconductor bulk solid state and single atom state just like any other nanoparticle. Hence, QDs show a mixture of physical and chemical properties of both semiconductor states[82].

We need to look at different energy states of semiconductor material to understand thoroughly why QDs have such a mixture properties. In semiconductors, there is an energy band gap between the valance band (ground state) and conduction band (excited state). As the temperature rises or light is introduced, an electron from the valance band can absorb (photon or themal) and jumps up to the conduction band. Once electrons reach the conduction band (10^{-15} to 10^{-14} s), they stay there briefly (10^{-8} to 10^{-5} s), and relax down to the lowest energy state of the conduction band (10^{-12} s or less) and then to the valance band (10^{-9} to 10^{-7} s). If this relaxation is by photon emission, the phenomenon is called fluorescence[83]. When introduced light is in near or visible range, the color of light emitted by the semiconductor material is determined by the width of the energy band gap. However, in QDs, the particle diameter corresponds to the system of quantum confinement, in which the spatial extent of the electronic wave function is related to the dot size. Quantum confinement of both the electrons and holes in all three dimensions leads to a fixed energy band gap and fixed color of light emitted. As a result, a decrease in dot size corresponds to an increase in the energy band gap of the semiconductor material. This is called quantum-size effect. As the quantum dot size increases, the gap decreases. Consequently, both the absorption and emission of QDs shift to lower wavelengths (higher energies) as the size of the dots gets smaller (scheme 1.5). In other words, the absorption and emission wavelengths are dot size dependent, which can be controlled precisely through synthetic conditions. All these unique characteristics are shown in figure 1.2.

$r_{CdSe\ core}$ (Å)	13.5	17.5	21.5	24.0
$\lambda_{Max\ em.}$ (nm)	510	555	590	610
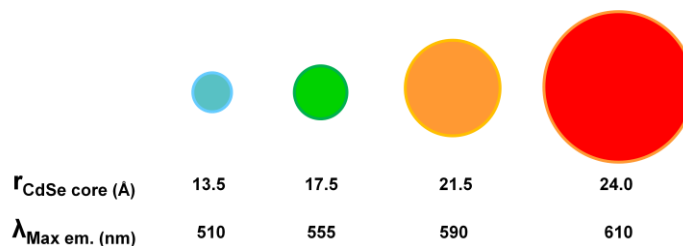
Scheme 1.5 *Schematic illustration of size-tunable emission of four different quantum dots*

1.3.2 Synthesis Conditions

Since the synthesis of high quality QD in trioctylphosphine oxide/ trioctylphosphine (TOP/TOPO) media was first developed by Murray in 1993[84], chemistry has been somewhat modified by other research groups for better synthesis conditions, shell coating thickness, and stability control. For more than a decade, QDs have been synthesized under various media including TOPO/TOP[85,86], reversed micelles[87,88], polymer films[89-91], sol-gel systems[92,93] and aqueous solution[94,95]. Among the elements which QDs are composed of, CdX (X= S, Se, Te) dots offer more utility due to distinctive physical properties of absorption/emission in the UV-VIS-NIR range. However, the molecular structures of CdX QDs are not ideal. Surface defects can cause electron leakage from individual nanocrystals, which lead to poor photoluminescence and widen the luminescence peaks of QDs[96]. To diminish the effect of surface defects and surface oxidation, a thin layer of a wider band gap semiconductor material, such as ZnS, is coated on the surface of the core CdX quantum dots[97-99] This coating process, which enhances the emission quantum yield, as well as chemical and photo stability of luminescent QDs, is called surface passivation. Furthermore, the ZnS shell also helps chemically manipulate surface of QDs with different solubility and chemical reactivity for particular applications.

14

1.3.3 Surface Modification

For biological compatibility, hydrophobic TOPO molecules, which are employed as capping ligands on the surface of luminescent QDs, must be replaced with hydrophilic ones containing polar terminated groups. These replaced hydrophilic ligands not only help QDs disperse in aqueous solution, but also preserve the large quantum yield original TOPO-capped QDs. These ligands usually are thiol functionalized compounds such as dihydrolipoic acid (DHLA), dithiothreitol (DTT), or mercaptoacetic acid (MAA). One of the earlier works that used DHLA to modify the QD surface was carried out in 2000 by Mattoussi et al[100]. In this work, the authors modified TOPO-capped CdSe/ZnS QDs with DHLA to make them water soluble before attaching them to an engineered recombinant protein. Many other groups have used the same kind of ligands to modify the TOPO-capped QD surface before using them in aqueous solution. In 2003, Jaiswal and coworkers used DHLA-capped QDs in live cell imaging[101] while Zimmer and coworkers used them for in vivo imaging[102] in 2006. Then in 2010, Vannoy et al. studied self-assembly of lysosome fibrils utilizing DHLA-modified CdSe/ZnS[103]. DTT, although not used as frequently as DHLA, has also been utilized to create hydroxyl groups on the QD surface. In 2001, Pathak and coworkers used DTT to replace TOPO[104] before applying them for in situ hybridization. In 2008, Banerjee and coworkers combined DTT and 1,10-diaza-18-crown-6 on CdS:Mn/ZnS QDs to detect cadminum ions[105]. In 2009, Duncan found that the combination of photoenhancement and DTT help improve the quantum yield of QDs without the appearance of spectral broadening and blue shift[106]. Mercaptoacetic acid (MAA) was also a popular choice to exchange with TOPO on the QD surface. In 2005, Derfus and coworkers capped QDs with MAA and studied its effect on the photooxidative process and cytotoxicity of CdSe/ZnS QDs[107]. In 2008, Jeong modified CdSe

QDs with MAA before attaching them on single-walled carbon nanotubes[108]. Then in 2010, Noh replace TOPO with MAA on CdSe QDs before adding electrolyte to cause fluorescence quenching due to QD aggregation[109].

QDs also can be made biocompatible via cross-linking with a thin shell of silanols, a thick shell of polymer, or organic dendrons. Coating with an outer layer of silica, polymer, or organic dendrons on TOPO-capped QDs have been a preferred choice for stabilizing QD surface and for in vitro and in vivo bioapplications. As early as 2000, Mulvaney and coworkers coated a thick layer of silica on metal clusters and CdS QDs to stabilize their surface in aqueous solution[110]. The silica shell, however, has gotten thinner and thinner to reduce the overall size for bioapplications. In 2005, Zhou achieved 28-nm SiO_2 encapsulated QDs via 3-mercaptopropyl trimethoxysilane (MPS) in a weak alkaline solution in ambient atmosphere at room temperature[111]. Then in 2010, Amato presented silica encapsulated QDs with high biocompatibility in the 50-200 nm range[112]. There are also many studies on polymer coating QDs, especially polyethylene glycol (PEG) with different molecular weights, before using in live cells[113]. In 2008, Warnement and coworkers tested QDs coated with custom PEG derivatives in bioassays[114]. These PEG derivatives were self-assembled on the QD surface and showed improved passivation in biological environments and were less vulnerable to unwanted protein adsorption to the QD surface. Organic dendrons are able to provide stable surface coating to QDs with just a thin layer (as thin as 1-2 nm) of closed packed and tangled ligand shell[115]. In this paper, Wang et al. also pointed out the photochemical stability of QDs after dendron coating. In another publication, Liu and coworkers used dendrons to encapsulate CdSe/ZnS QDs before detecting pathogens[116]. So far, hydrophilic QDs have been applied in immunoassays[117-120], in situ hybridization[104,121,122], cellular[107,123-125], and in vivo[126,127] multiplex labeling.

1.3.4 Fluorescence Resonance Energy Transfer (FRET)

Fluorescence resonance energy transfer (FRET) is defined as a non-radiative energy transfer process between two chromophores, one donor and one acceptor[83,128]. One very important parameter for FRET to occur is that the distance between the two chromophores has to be less than 10 nm. Others include the spectral overlap of the donor emission and acceptor absorption, as well as the relative orientation of the donor emission dipole moment and the acceptor absorption dipole moment. The process happens when the donor in its excited state transfers a non-radiative energy to the acceptor (Figure 1.2). As a result, the fluorescence intensity of donor is quenched, while the acceptor fluorescence is increased. The efficiency of the energy transfer process is proportional to the inverse sixth power of the distance between donor and acceptor ($1/R^6$).
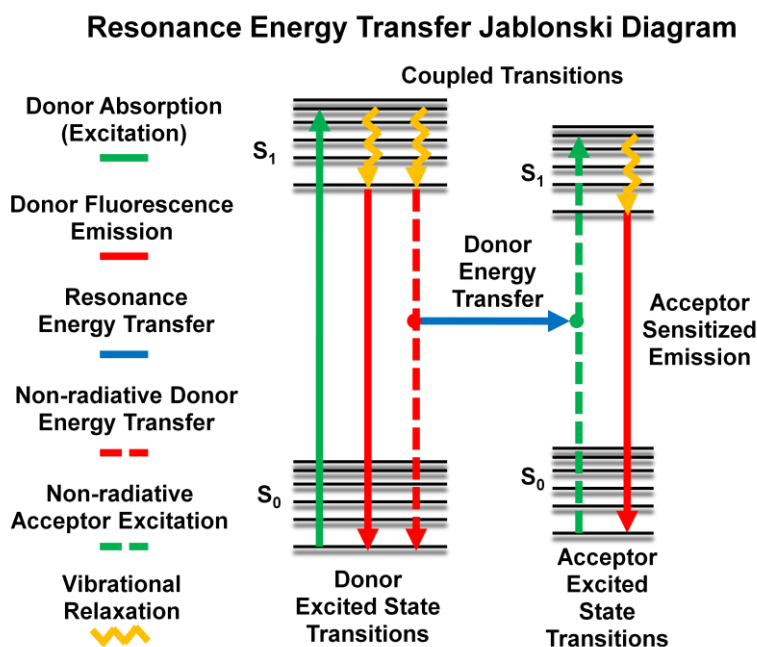
Scheme 1.6 *Jablonski Diagram of Fluorescence Resonance Energy Transfer*

17

1.3.5 Surface Energy Transfer (SET)

Similar to quenching in FRET caused by dipole-dipole exchanges, metal-induced quenching is related with dipole-surface energy transfer (SET)[15]. Even though both FRET and SET efficiency depend on the spectral overlap of the acceptor's absorption with the donor's emission, SET efficiency is proportional to inverse fourth power ($1/R^4$) of the distance between donor and acceptor. Yun[36] et al. investigated the strength and weakness of FRET and SET in 2005 to find out the overall length resolution of each method as a function of separation distance. Based on experimental analysis, he realized that FRET is highly sensitive and only detectable in 100 Å donor-acceptor distance while SET is not as sensitive but detectable up to 220 Å range. AuNPs are common acceptors in SET process.

1.3.6 Bioapplications

The most applications of QDs in biological research have been imaging, which plays an important role in exploring the complex spatial–temporal relationship between biomolecules from the cellular and the integrative level. QDs have been applied for both in vitro and in vivo imaging in many studies. Yet, there are other common applications that have successfully utilized QDs unique optical characteristics such as biosensors and immunoassays.

1.3.6.1 Cellular Imaging

Before the invention of QDs, in vitro and in vivo studies are accompanied by organic fluorophores, which usually have narrow absorption, broad emission, and low photobleaching threshold. These characteristics have restricted the efficiency of organic fluorophores in long-term imaging and 'multiplexing' (simultaneous detection of multiple signals). In 1998,

Brunchez[129] and Chan[130] solved the above problems by simply replacing those organic fluorophores with QDs via demonstrating water soluble QDs for bioapplications. Their work marked the beginning of an era of cellular imaging using QD bioconjugates. Among recent publications, in 2008, Wang et al.[131] revealed conjugation of QD to transferring (TRF), an iron transporting protein, and its application to label human HepG2 cells via the transferrin-receptor system. The probes were found accumulated around cytoplasm area after 12 hour-incubation but not the nucleus of the cells. In 2009, Yordanove and coworkers[132] demonstrated cellular imaging using poly(butylcyanoccrylate) coated CdSe/CdS QDs. Poly(alkylcyanoccrylate) polymer was believed very promising among many drug carriers due to their biocompatibility, biodegradability, low cytotoxicity, easy preparation and purification, ability to alter drug biodistribution and to overcome some biological barriers. Later, in 2010, Wu and Weil described multifunctional protein-hybrid that was applied to mammalian cell imaging[133]. By exploring hidden functional groups below protein surface, the authors realized that linear protein backbone with a defined numbers of amino acid, carboxylic acid, hydroxyl, as well as thiol groups would stabilize nanocrystals suited for bioapplications.

To better understand how QDs interact with biomolecules; researchers went one step further by imaging QD probes on live cells. In 2008, application of silicon carbide 3C-SiC QDs with no protective shell to live cells was revealed by Botsoa and coworkers[134]. SiC was believed chemically inert, stable, and biocompatible. The 3C-SiC QDs was formed by electrochemical anodization and etching. The authors found that he 3C-SiC QDs localized in the nucleus area after being incubated overnight (around 15 hours) to 3T3-L1 fibroblasts cell line. Even though the exact mechanisms of how 3C-SiC QDs travel and interact with biomolecules inside the cells were not understood, it was evident that the probe causes no toxicity to cells.

Payne's group, in 2009, described pyrenebutyrate-mediated delivery of QDs to the cytosol of living monkey kidney cells[135]. QDs were coated with a combination of cationic peptide-polyarginine and hydrobobic counterion-pyrenebutyrate. PA-QD probes traveled directly across the plasma membrane and bypassed the barrier of endocytic vesicles. In 2010, Lei et al. coated thiol-capped CdSe/ZnS QD with amino acid and then conjugated to Tat peptide for stem cell tracing in vivo[136]. The probes were injected into the tail veins of NOD/SCID beta2M null mice, whose tissue sections of major organs were analyzed later. The authors found that the internalized QDs become an in vivo tracer that provides useful information for stem cell transplantation.

1.3.6.2 Cancer Imaging

Statistically, cancer has become the leading cause of death for people younger than 85 year old in the United States since 1999[137]. There are close to 1.5 million new cancer cases and about 600,000 deaths from cancer predicted just in 2009 alone[138]. Obviously, the desire to better understand, detect, and diagnose cancer is being explored worldwide. Indeed, cancer targeting, detection and imaging using QDs have been one of the most interested research fields nowadays. Early in 2009, Zaman and his group conjugated single-domain antibody (sdAb) to PEGylated CdSe/ZnS QDs and applied it to imaging cancer cells[72]. The targeted sdAb EG2 in this study bound strongly to epidermal growth factor receptor (EGFR), a tumor marker for breast cancer. Imaging of SK-BR3 and MDA-MB468 breast cancer cells revealed that QD probes can also be used as a detecting purpose. In 2010, Li and the group synthesized aptamer-conjugated dendrimer-modified QDs and applied as tags for cancer cell targeting and imaging[73]. Aptamer is found to be an ultimate contender for molecular targets while dendrimer modifies hydrophobic

nanocrystals to make them better soluble in water. The target aptamer used in this work was

BDI-10, which can recognize the protein tenascin-C on the surface of human glioblastoma cell.

In vivo cancer imaging using QD probes has been doing very well in animal models; mice in particular.   There are multiple publications on imaging tumors in mice via QD bioconjugates.   In 2008, Chen et al.[139] reported the application of CdSe/ZnS core/shell QDs for imaging of human hepatocellular carcinoma metastasis (HCC) on HCCLM6 cells and grown tumor in mice from those cells.   The targeted biomolecules were alpha-fetoprotein (AFP) monoclonal antibody (Ab). The probe QD-AFP-Ab served both targeted imaging in vitro and in vivo with negligible acute toxicity to the models.   In 2009, Mulder et al.[74] investigated multimodality molecular imaging of tumor angiogenesis using αvβ3-integrin conjugated paramagnetic QDs. The analysis served to understand early detection and treatment of cancer. This publication was claimed to be the first that optimized the probes for both in vivo optical and magnetic resonance detection of tumor angiogenesis in mice.   And just recently, in 2010, Nurunnabi and coworkers injected near IR-QDs-cancer drug-loaded micelles into tumor bearing nude mice for simultaneously tumor therapy and imaging[75].   These micelles were dispersed quickly all over the entire animal body including the tumor. However, after 5 days, there was accumulation of fluorescent signals from the probes only at tumor site as well as shrinking of 79% of tumor size. This probe can be considered as both active and passive targeting, imaging and treatment of cancers in the early stages.

1.3.6.3 Biosensors

The second most popular usage of QDs in biological research is in sensor applications. Among recent applications, different surface coatings and templates of QDs have been

developed for better sensitivity. FRET-based biosensors are the most common means to detect specific protein, DNA, and metal ions. In 2008, Mattoussi's group illustrated the interaction between redox complexes and QDs using a peptide bridge to detect enzymatic activity[140]. QDs acted as FRET donor while metal complexes were FRET acceptor receiving charge transfer through a short peptide bridge. In 2009, Lee and Kang[141] studied the effects of dopamine concentration using FRET between dendrimer-QD and Alexa 488-antibody to better understand and determine Parkinson's disease. The degree of energy transfer was confirmed to be proportional to dopamine concentration. In 2010, Zhang and Hu[142] developed single QD-based nanosensor for multiplex DNA (HIV-1 and HIV-2) detection via coincidence and FRET approach. The QD probes also employed as a local nanconcentrator with notably enhanced coincidence-related fluorescent signals and FRET signals. Wang et al. used QDs to detect Cl^- ions in epithelial cells[76] in 2010. The targeted molecules on QD surface to capture Cl^- ions was an anion receptor, 1-(2-mercapto-ethyl)-3-phenyl-thiourea (MEPTU). QD fluorescence reduced proportionally to the concentration of Cl^- ions bound to the MEPTU as photo-induced electron transfer between QD and MEPTU occurred. Also in 2010, Banerjee and coworkers[77] doped manganese to traditional QD procedure to obtain CdS:Mn/ZnS QDs. The new probe was capable of selectively and sensitively detecting cadmium ions, alkali metal ions, and glutathione via electron transfer process to ion-captured organic ligands on QD surface. Upon the binding of various ions, initial fluorescence quenched as FRET occurred between manganese doped QDs and the ligands.

SET-based biosensors have also been studied more thoroughly even though they are not so common as compared to FRET-based biosensors. In 2009, Li and the group presented DNA detection via dipole-surface energy transfer (SET) between QDs and gold nanorods (GNRs)[15].

DNA hybridization between complementary strands of DNA on QDs and GNRs enclosed the proximity between the two probes causing QDs quenching by transferring emission energy to GNRs.

1.3.6.4 Immunoassays

Another big part of QDs in bioapplications explores immunoassays. Although similar to sensor, immunoassay is defined as a biochemical test that measures the concentration of a substance in solution. The star of immunoassays is antigen-antibody (Ag-Ab) binding specificity that produces a measurable signal accordingly. Because of their unique characteristics, QDs in this category are more advanced than organic fluorophores due to their fluorescence stability and multiplexing capability. Multiplexing has become a valuable tool in immunoassay utilizing QDs. In 2008, Zhang et al. synthesized high quality multicolor amphiphilic copolymer coated $CdSe/CdS/Cd_{0.5}Zn_{0.5}S/ZnS$ QDs for immunohistochemical analysis[79]. The copolymer coating not only made the core biocompatible, but also enlarged QD size enough to avoid FRET between two different color QDs. Polymer coated QDs were conjugated goat anti-human IgG and goat anti-rabbit IgG antibodies and mixed together before detecting human and rabbit antigens. Unlike conventional fluorophores, the two color QDs can be excited at the same wavelength which promoted multiplexing to identify single targets simultaneously. Recently, in 2010, Rauf et al. developed multiplexed immunoassays using QD barcoded magnetic microspheres[80]. Two different kinds of QDs attached on each bead surface (of total 4 kinds of optical encoding beads) via a layer-by-layer method utilizing unique streptavidin/biotin interaction , which also eliminated cleverly any potential non specific binding.

1.3.7 Cytotoxicity

Cytotoxicity has become a tremendous concern for in vivo QD applications. In the last two years, there have been a significant number of researches that carefully study QD cytotoxicity. When QDs were first invented, cadmium-based QDs were favorable and used in most applications due to their unique physical properties of absorption/emission in the UV-VIS-NIR range. However, long-term side effects from these cadmium-based QDs have concerned researchers if cadmium can be degraded into ion forms. That is why in vitro and in vivo studies of cadmium-based QDs with different surface coatings have been studied by many groups. In recent publications, in 2008, Zhang et al.[143] reported PEGylated CdSe/CdS QD toxicity in porcine skin and in human epidermal keratinocytes (HEK cells). The QDs were discovered just in the intercellular lipid bilayers of the stratum corneum (SC) in 24 hour-incubation. In HEK, cell viability reduction corresponded to 1.25 nM to 10 nM at 24 hours and 48 hours. Potential inflammation was found based on analysis of cytokines IL-6, IL-8, IL-10, TNF-α and IL-1β in HEK cells. The combined study of skin and cells concluded that any open wound, cut, or alteration to outer skin layer SC would expose QDs to viable skin cells and damage them at 1.25 nM concentration or higher. Later of 2008, Geys et al. examined the in vivo acute toxicity and prothrombotic effects of commercially available carboxyl- and amine-QDs[144]. After the injection, the authors saw an effect of surface charge for all the parameter tested. QDs accumulated mostly in lung, liver, and blood. At high injection dosage of 3,600 pmol/mouse, QDs caused pulmonary vascular thrombosis with carboxyl-QDs to be more potent than amine-QDs. In 2009, Jiang and the group[145] coated their CdTe/CdS QDs with reversible addition-fragmentation chain transfer glycopolymer of biotin, sugar, and amine groups for biocompatibility and colloid stability. Cell viability was then examined with the probe vs. non-

polymer QDs. The test showed cytotoxicity was insignificant to glycopolymer coated QDs at concentration up to 20 nM. Later in 2009, Lin and coworkers described a toxicity study in the kidneys of mice of Cd/Se/Te-based QD 705[146]. The authors tracked free Cd elevation in tissues by monitoring molar ratio of Cd/Te and induction of tissue in metallothionein as markers. The analysis showed that even though 100% of QD705 still remained in the body, free Cd was released after injection for 16 weeks. Since the free Cd ions associated with toxicity of QDs, this work showed that there is a considerable potential damage of QDs towards in vivo applications.

More and more QD toxicity studies were published in the beginning of 2010. Fu et al.[147] examined the toxicity of CdTe and CdTe/ZnSe core/shell QDs that were simply coated with mercaptosuccinic acid (MSA). The ZnSe shell was proven to increase the stability and biocompatibility of CdTe core. Cell viability was sustained over 80% at 100 μg/mL and 300 μg/mL concentration of MSA-CdTe/ZnSe QDs at 48 hour and 24 hour incubation, respectively. By the end of 2010, Wu et al. investigated several cellular aspects of cysteamine coated CdTe (Cys-CdTe) QDs when interacting with human hepatocellular carcinoma SMMC-7721 cells[148]. The QD probe was believed bound to cell membrane readily before internalizing thereafter. Fast endocytosis from early exposure of Cys-CdTe QDs only caused major damage on cell membrane and cell adherence ability, but high dosage and longer than 24 hour-incubation time would reduce cell metabolic activity significantly. Then, Hauck and coworkers demonstrated in vivo QD toxicity by coating CdSe/ZnS core/shell QDs with three different surface functional groups and injecting them in Sprague-Dawley rats[149]. The three surface coatings were polymer, PEG, and BSA. Bioditribution statistics indicated that QDs initially targeted the liver and spleen, but after several days to weeks, QDs showed up in the kidney. However, the authors found no significant toxicity observed in rats after the 15-nmol-injections of three QD probes over the

whole course of the long-term study. Also in 2010, Tan and coworkers[150] functionalized QD

with 6 different designs: anionic, hydrophobic anionic, cationic, hydrophobic cationic,

PEGylated cationic and hydrophobic PEGylated cationic to introduce carboxylate, amine, oleyl,

and PEG groups to QD surface before testing their intercellular interactions. Cell imaging and

viability revealed that these surface functional groups affect how QDs bind to surface, enter, and

localize in cells. The cationic and hydrophobic QDs had stronger interaction with cells

compared to anionic QDs; while PEG can help reduce the significant toxicity from cationic

groups. Moreover, hydrophobic QDs only labeled cell membrane and did not penetrate through

the cells; while PEGylated cationic QDs entered the cells easily.

Coating on QD surface is an important factor towards cytotoxicity. Polymer coating, so

far, has proven to reduce toxicity to cells and animals. However, understanding QD probes in

vivo degradation mechanisms will play a key role whether QD probes can be applied in human

clinical use at all.

1.4 Metal Nanoparticles and Nanowires

1.4.1 Fundamental

Nanoparticles are considered a connection gap between bulk materials and molecular

levels[2,3]. Compared to bulk materials at the same mass, nanoparticles exhibit enormous surface

area. That is why nanoparticles offer great potentials for future inventions. While a bulk

material has consistent physical and chemical characteristics regardless of its size, nanoparticle

presents size-dependent unexpected behaviors because each particle consists of hundreds to

thousands of atoms packed in a three dimensional captivity. Typically, nanoparticles or nano-

colloids are synthesized from wet chemical methods which are either water-based or organic

solvent-based[151]. Metal colloids are, however, commonly synthesized from the reduction of acid based solution containing position metal ions[152-154]. Throughout the reaction, positive metal ions will be reduced to neutral metal atoms. As more and more neutral atoms arise, the solution becomes supersaturated before those neutral atoms, with constant and vigorous stirring, precipitate and form into nano size particles. Metal nanoparticles express high electron density and strong optical absorption characteristics as opposed to quantum confinement effect of semiconductor nanocrystals (quantum dots) or to superparamagnetism in magnetic particles. Modern technology has driven the fabrication of metal nanoparticles into longer shape, metal nanowires, to link nano-components into nano-devices. Typical nanowires display very large aspect ratio (length-to-width ratio), from hundreds to thousands[155-158]. That is why they are known as one-dimensional (1-D) materials. Since metal nanowires are grown from metal nanoparticles, they also inherit the nanoparticle properties. However, high aspect ratio characteristic aims the nanowires into dielectrophoretic direction.

1.4.2 Synthesis Conditions of Metal Nanowires

The most common bottom-up approach to synthesize metal nanowires is in solution phase where the growth rate of different facets can be controlled by surfactant mixture[54,159-161]. One approach is to deposit chemical metal plating on the surface of high aspect ratio particles, such as DNA strands[162-164], carbon nanotubes[165-167], or to open and fill nanotubes[168-170]. The other approach is used for size-controlled metal nanowires by depositing precursor liquid solution into uniform and cylindrical porous template electrochemically (electro-deposition) or chemically (electroless-deposition) [171-173]. Once the pores are filled, metallic nanowires can be collected after removing the template. Synthesizing the nanowires by porous template-based approach is preferred over other methods due to simplicity, low cost, uniform sizes and shapes.

27

There are two popular choices of membrane being used including alumina and polycarbonate

membranes because of uniform pore sizes and ease of handling.

To enable electrochemical deposition, one side of the membrane is coated with a metal film

and using this metal film as a cathode for electroplating. On the other hand, before forming

electroless metal nanowires in the porous template, a catalyst must be applied to the pore walls

by a chemical reducing agent. This catalyst acts as a "molecular anchor" where the metal ions

are being reduced. As a result, solid metal tubes and wires begin to fill up the membrane pores.

The advantage of electroless vs. electro deposition is that it does not need a conducting layer as

cathode. Since Martin et al. first presented publically the electro-deposition in 1991[174] and

electroless-deposition in 1995[175], these template-based synthesis of metal and semiconductor

nanowires have been produced using similar principles before being utilized in applications.

Since then, Martin and co-workers have achieved more success in this area[171,176-181]. Many

successful studies by other research groups in this field include Kelley's [182-185], Mallouk's [186-188],

and Ugo's [189-191] . Furthermore, nanowires with multiple and different segments from several

materials can also be grown in the same template[187,192,193].

1.5 Peptides

Peptide, the short version of protein, is defined as polymers of multiple amino acids

connected by covalent amide bonds[194-196]. Because peptides are much shorter compared to

proteins, they can be made synthetically and applied to many biological studies. Peptides can be

created simply by water condensation, which eliminates a water molecule between the carboxyl

group of one amino acid and the amino group of the other. Technically, any amino acid can be

added to a peptide chain. When an amino acid is added, a water molecule must be removed.

Therefore, peptides can be designed accordingly to meet the research's purposes.

Most peptides would have an unreacted amino group at one end (called the amino terminus or N-terminus) and an unreacted carboxyl group at the other end (called the carboxyl terminus or C-terminus). The rule for writing peptide is to start from the left with N-terminus and to end from the right with C-terminus. Beside free amino group at the N-terminus and free carboxyl group at C-terminus, the middle amino acids will have their own side chain's ionizable groups, from weakly acidic to neutral to basic. Indeed, amino acids can be distinguished by their different side chains. There are only 20 main amino acids, but they are coded in all the genes of proteins found in all living organisms. The side chains in amino acids can be divided into several groups according to their main chemical features. Each group serves different purposes in biological system. For example, glycine and alanine carry aliphatic side chains for protein folding purpose; while cysteine and methionine carry sulfur side chains to form disulfide bond; and histidine and lysine provide positive charges under physiological conditions. Histidine amino acid has been known to bind strongly to metal ions via imidazole rings. Therefore, multiple consecutive (5 or more) histidine amino acids (polyhistidine) can certainly create a very stable and specific interaction with metal with high binding affinity. Polyhistidine has been applied from purifying proteins to removing heavy metals. Moreover, polyhistidine peptide has proven to play an important role in enhancing quantum yield for thiol ligand-coated QDs[33] by Medintz. Lately, polyhistidine has been proved to provide chemical functionality and stability[42,197-199] to QD bioconjugates before being utilized in bioapplications presented by Mattoussi and co-workers.

1.6 Nucleic Acids and Oligonucleotides

Nucleic acids are the most elemental components of all living cells[194-196]. They not only store, carry, and transmit but also duplicate genetic information for every cell, tissue, and organisms. There are two types of nucleic acids, ribonucleic acid (RNA) and deoxyribonucleic acid (DNA), which are polymeric chains (or polynucleotide strand) from multiple covalently attached monomers. And each polymeric chain has its own construction of monomers which are also called nucleotide sequence. Each monomer contains a five-carbon sugar (ribose in RNA and 2'-deoxyribose in DNA) and a heterocyclic base. DNA has two different types of heterocyclic bases: purines (include adenine (A) and guanine (G)) and pyrimidines (include cytosine (C) and thymine (T)) (Scheme 1.7). RNA has the same bases but uracil (U) is present instead of thymine. A is complementary to T (or U in case of RNA) while G is complementary to C and vice versa. Each base binds to its complement readily, specifically, and non-covalently under normal conditions.
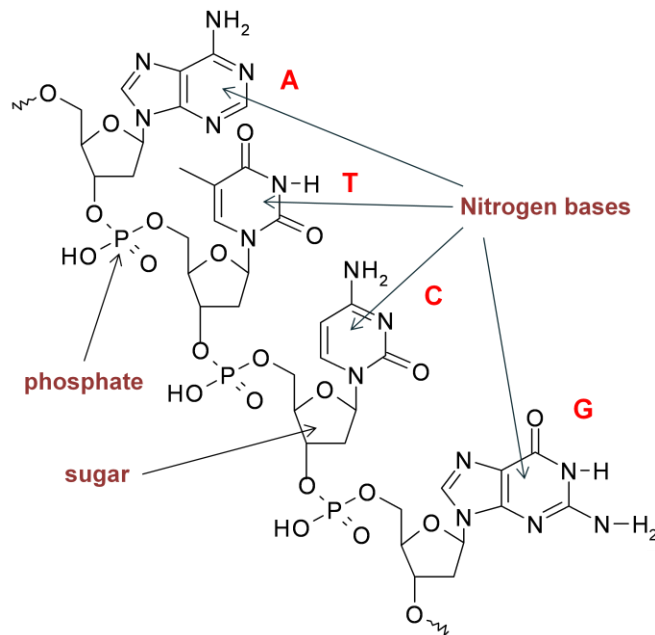
Scheme 1.7 *An oligonucleotide fragment containing the four nitrogen bases Adenine, Thymine, Guanine and Cytosine*

Whenever there is a sequence-specific binding between two or more complementary polynucleotide strands into a hybrid, it is called hybridization. The self binding of the double-stranded helical DNA has inspired self-assembled characteristics in many bioapplications. Colorimetric sensors via assembling of single-stranded DNA coated metal nanoparticles have been successfully developed by Mirkin's group[57-62]. Alivisatos and co-workers have built nano-structures using discrete DNA-gold building blocks in which the number of DNA strands is controlled[63-67]. Most recently, Wang and co-workers investigated photonic interaction between QDs and AuNPs connected by DNA self-assembly in discrete nanostructures[68].

Nucleic acid structure can be totally depended on temperature of the outside environment. Hybrids can be separated by thermal melting (denaturation). The so-called melting temperature (T_m) is the temperature at which half of the polynucleotide chain is in double helical state and the other half is in random coil state. T_m, in other words, depends greatly on the length and sequence of the polynucleotide strands. Since each monomer is attached to the next via phosphodiester linkage, every nucleic acid polymer strand has a *sense* or *directionality*[194-196]. The phosphodiester bond starts from 3' carbon of one monomer and connects to the 5' carbon of the next. So, the first monomer carries an unreacted 5' phosphate while the last monomer holds an unreacted 3' hydroxyl group. That is why the two terminals of the polymer chain are distinguishable by different unreacted groups. Technically, DNA is written from left to right as 5' to 3' with letters of bases in the middle.

There is a much shorter version of polynucleotide chain called oligonucleotide (around 100 bases or fewer). Even though oligonucleotides exist as bond cleavage of long DNA or RNA segments, they are frequently synthesized chemically by attaching individual monomers, and

their length is signified as "mer". For example, a 30-monomer nucleic acid polymer fragment can also be called a 30-mer. Just like DNA and RNA, oligonucleotide binds readily to their particular complementary oligonucleotide, which is also called antisense. Since oligonucleotide is short and can be synthetically made, it is often used as a probe to detect DNA or RNA. There are many publications of oligonucleotide used in DNA (RNA) microarrays[200-203], southern blots[204-206], fluorescent in situ hybridization (FISH)[207-209], and synthesis of artificial genes[210-212].

Chapter 2

Experimental

This chapter describes general information about chemicals, supplies, and instrumentation used in synthesis, conjugation, and characterization for all projects. More detailed experimental information will be mentioned later in each individual chapter.

2.1 Chemicals and Supplies

All chemicals were used as received without any further modification. Technical grade (90%) trioctylphosphine oxide (TOPO), technical grade (90%) trioctylphosphine (TOP), cadmium oxide (99.99+ %), selenium powder (-100 mesh, 99.5+ %), lauric acid (98+ %), technical grade (90%) hexadecylamine (HDA), cystamine $\geq$ 98% (RT), sodium borohydride powder $\geq$ 98%, nickel (II) nitrate hexahydrate 99.999% trace metal basis, diethyl zinc $(Zn(Et)_2)$ solution 1.0 M in heptane, hexamethyldisilathiane $((TMS)_2S)$, 16-mercaptohexadecanoic acid (MHDA, 90%), methanol anhydrous (99.8%), chloroform (99.5+ %), DL-Dithiothreitol (DTT), and Tris(2-carboxyethyl)phosphine hydrochloride solution 0.5 M pH 7.0 (TCEP) were purchased from Sigma-Aldrich. Polystyrene microspheres were purchased from Miscospheres-nanospheres and Polysciences, Inc. Citrate-stabilized gold nanoparticles were purchased from Ted Pella. Custom polyhistine peptides were purchased from CPC Scientific. Qdot® 525 ITK™ carboxyl quantum dot 8 µM solution, all molecular fluorophores, and all custom single-stranded oligonucleotides were purchased from Invitrogen. Orotemp 24 gold plating solution, silver 1025 RTU solution, and nickel sulfamate were purchased from Technic Inc. Alumina and polycarbonate membranes with different pore sizes were purchased from Whatman.

2.1.1 Custom polyhistidine peptides

Synthetic 10-amino acid-polyhistidine peptides were designed to attach to QD surface. The peptide consists of two lysine (K) amino acids next to N-terminus and two glutamic acid (E) amino acids next to C-terminus for better water solubility. The middle part of the custom peptide contained 6 histidine (H) amino acids for strong binding to the ZnS surface of the QDs. The overall structure of polyhistidine peptide is H_2N-K-K-H-H-H-H-H-H-E-E-COOH.

2.1.2 Custom single stranded oligonucleotides

The three main single strands of oligonucleotides (main ss-DNA1, DNA2, and DNA3) and their complements were custom-made following the pattern used by Medintz et al.[42] with a slight modification (Table 1). Other oligonucleotides were designed so that their 5' end was protected by a disulfide (S-S) bond and later thiolated to attach to a gold surface. Oligo1 was complement to oligo2; and oligo3 was complement to oligo4.

Oligonucleotides	Sequence	5' Mod	3' Mod	Length (bp)	MW
Main ss-DNA1	5'-CCGAGC*TGGATTAAGTATGCTGCATAC*GCTCGG-3'	Amine C6	C3 S-S	33	10,503.9
Complement1	3'-*ACCTAATTCATACGACGTATG*TACATT-5'	No	No	27	8,218.4
Non-complement1	3'-TTTGACATTAAGCGTCGCTAGTAGCGA-5'	No	No	27	8,315.4
Main ss-DNA2	5'-CCGAGC*AGCTAGGAGTTGTAAGATACT*GCTCGG-3'	Amine C6	C3 S-S	33	10,219.6
Complement2	3'-*TCGATCCTCAACATTCTATGA*TACATT-5'	No	No	27	8,169.4
Main ss-DNA3	5'-CCGAGC*GTTCCGATATGCGAATGCGCC*GCTCGG-3'	Amine C6	C3 S-S	33	10,132.6
Complement3	3'-*CAAGGCTATACGCTTACGCGG*TACATT-5'	No	No	27	8,260.4
Oligo1	5'-AAAGGCATTAGCG-3'	S-S C6	No	13	4,008.6
Oligo2	3'-CCGTAATCGCAAA-5'	S-S C6	No	13	3,928.6
Oligo3	5'-AAACTTATGGTAC-3'	S-S C6	No	13	3,958.6
Oligo4	3'-GAATACCATGGGG-5'	S-S C6	No	13	4,024.6

Table 1. *Custom single stranded oligonucleotides*

2.2 Instrumentation

2.2.1 Fluorescence Spectroscopy Measurements

2.2.1.1 Microplate Reader

Absorption and emission spectra of QDs in solution were measured using a SpectraMax M2 microplate reader (Molecular Devices, Inc.) equipped with a Xenon flash lamp source and a photomultiplier (R-3896) detector. The system is featured with a spectrophotometer for absorbance measurements and a spectrofluorometer for fluorescence measurements. Samples can be read in either a cuvette or a 96-well plate. SoftMax Pro software is used for data analysis. The microplate reader in our lab is also called multi-detection microplate reader because it can detect both absorbance and fluorescence signals at multiple wavelengths thanks to the built-in excitation monochromator and emission monochromator. First, the output of a xenon light source is irradiated directly to a concave holographic grating (excitation monochromator), which allows the selected range of wavelengths to pass through. Then, the excited light passes through 1-mm fiber optic bundles to a cuvette port or microplate port. Before reaching the cuvette, the incident light is reflected by an oval mirror and directed to the cuvette. The collected light then enters the emission monochromator before reaching the photomultiplier tube. In microplate mode, the light passes through another fiber optic to a different focusing oval mirror. The incident light enters the sample from the top of the microplate. The light given off from the sample travels to the emission monochromator and to the photomultiplier tube before being collected and processed.

2.2.1.2 Spectrofluorometer

Absorption spectra of fluorophore and quantum dot (QD) solutions were obtained by Varian UV-VIS-NIR spectrophotometer system (CARY 500 Scan). Emission spectra of fluorophore and QD solutions were measured using PerkinElmer LS 55 luminescence spectrometer equipped with a with a 75-W continuous Xe arc lamp as a light source. In general, to obtain emission spectra, light from Xe lamp first travels through an excitation monochromator, which tunes the different excitation wavelengths. Next, the selected wavelengths reach the sample. Emitted light from the sample then passes through an emission monochromator, where certain emission wavelengths can be filtered out before reaching photomultiplier tube.

2.2.1.3 Monochromator

Monochromator is defined as an optical wavelength selector which selectively narrows the range of incident light into a small band of light. The colors of light are separated based on the two common techniques called optical dispersion (prism) and diffraction grating (grating) which are illustrated in scheme 2.1[213]. There are four major components in a monochromator: an entrance slit, a collimating lens, a dispersing device (prism or grating), and an exit slit. As the incident light passes through the entrance slit, it is collimated before being dispersed by the prism or grating. Only certain wavelengths leave the monochromator by moving the dispersing element or the exit slit.
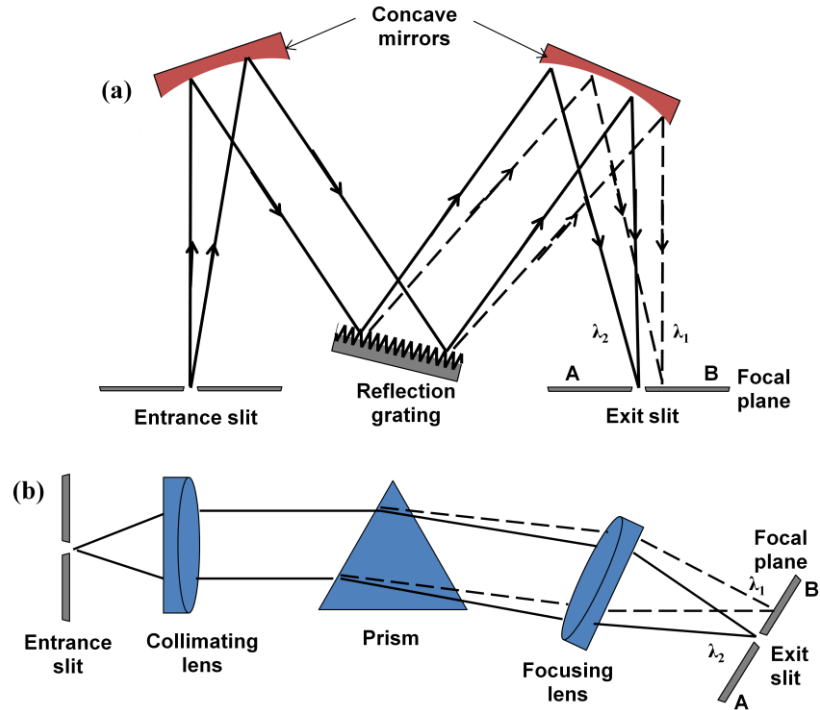
Scheme 2.1 *Two types of monochromator: (a) grating and (b) prism*

2.2.1.4 Photomultiplier tube (PMT)

Photomultiplier tube (PMT) in general is a type of photon transducer which is very sensitive to ultraviolet and visible radiation and exceptionally rapid in response time. It contains multiple photoemissive surfaces that emit a large amount of electrons when struck by electrons from the photosensitive area. Up to 10^6 to 10^7 electrons are created after one incident photon. However, because of amplifying characteristic, the PMT can be damaged when being exposed to elevated power of radiation. In details, a photo cathode surface releases electrons upon a photon strike. Then there are several electrodes (or dynodes) placed in a series so that the later is more positively potential than the former. The first dynode, which is higher positive potential than the photo cathode, will attract the first release of electrons, then multiplying before allowing them to go to the next dynode. Electrons naturally travel from one dynode to the next due to higher

positive attraction. The final batch of electrons, which is a cascade of electrons, is collected at an anode to be processed and read out. Scheme 2.2 illustrates the internal electrical circuit of a PMT.
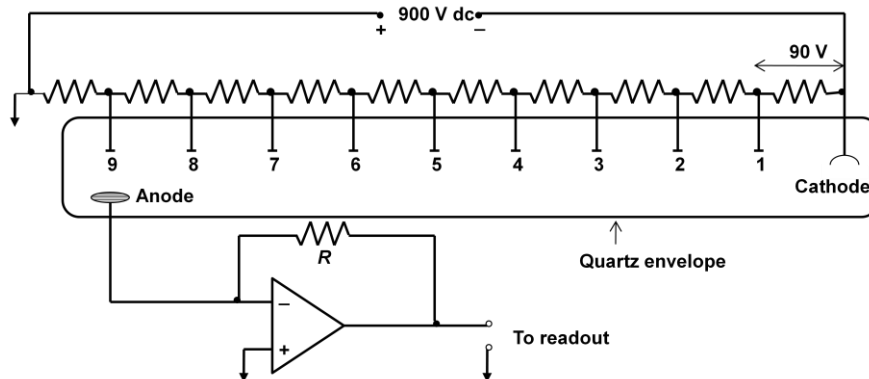
Scheme 2.2 *An internal electrical circuit of a photomultiplier tube*

2.2.2 Digital Fluorescence Microscopy

A fluorescence microscope typically detects fluorescence and phosphorescence properties of a sample as opposed to only collecting the reflection and absorption characteristics as in a regular optical microscope. In an inverted fluorescence microscope, the excited light passes through a series of filters before hitting the sample from below through an objective lens. A suitable combination of filters for excitation and emission wavelength plays an important role in getting proper fluorescence microscope images. Those filters, which are included in a filter cube, are the excitation filter, dichroic mirror, and emission filter. The emitted fluorescence is focused and collected by the same cube that is used for excitation. This phenomenon is also called epifluorescence. This method is believed to improve the signal-to-noise ratio because only reflected excitation light and emission light get to the objective simultaneously. A dichroic mirror in the series of filters then separates the excitation and emission photons. After the light

passes through the emission filter, different sizes of objective with certain numerical aperture are used to collect and magnify the fluorescence signals. The numerical aperture of a microscope objective is a measurement of its ability to gather light and resolve fine specimen detail at a fixed object's distance[214]. In all projects, luminescence images were obtained using a digital luminescence imaging microscopy systems. The systems consisted of inverted fluorescence microscopes Olympus IX51 and Olympus IX71 equipped with 100 W Hg lamps as a light source. Roper CCD 3392 camera and high performance color charge-coupled device camera (CCD, Olympus DP 70) were used to collect digital imaging in each microscope, respectively. A 0.300 m imaging triple grating monochromator/spectrograph Model SpectraPro 2300i coupled with an inverted fluorescence microscope Olympus IX70 was used to collect emission spectra and fluorescence images of QD-encoded polystyrene microspheres (Scheme 2.3). Roper Scientific software Win Spec/32 was used for spectral analysis of these emission spectra.
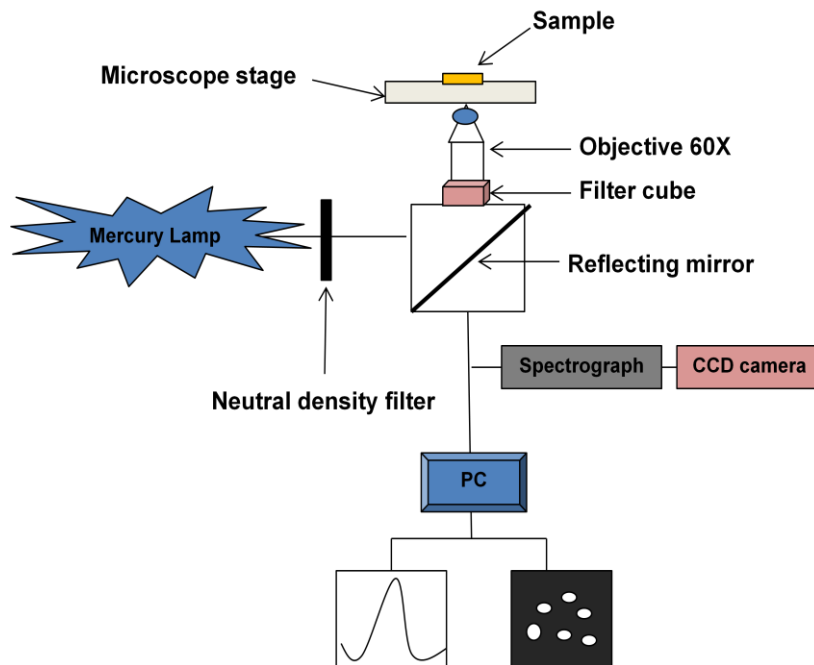
Scheme 2.3 *Digital fluorescence microscopy system*

Filter cubes containing a 385 nm, 420 nm or 480 nm band-pass excitation filters; 465 nm

and or 505 nm dichroic mirrors; and 475 nm or 515-nm long pass emission filters were used to

collect spectral imaging. The fluorescence images were collected via various objectives of 10X,

20X, 40X, and 60X with numerical apertures of 0.3, 0.5, 0.75, and 1.25, respectively. The

software Image-pro Plus and DP Controller were used for imaging analysis.

2.2.3 Charge-Coupled Device (CCD)

In spectroscopic imaging studies, a charge-coupled device (CCD) is usually incorporated

with an imaging sensor to convert incident radiation into an electrical signal. CCD is used more

often in professional, medical, and scientific fields due to required high-quality image data. A

CCD is basically a multichannel transducer consisting of an array of small photoelectric-

sensitive elements arranged in a two-dimensional pattern on a single semiconductor chip. The

most common material used to develop this semiconductor chip is silicon, often p-type silicon.

In the chip, there is a photoactive area (placed on an epitaxial layer of silicon) and transmission

area (the CCD) facilitating one another. The chip itself is only a few millimeters in size but

contains circuitry with dense matrix of photodiodes where photons can be converted to electrons.

When an image is captured, capacitor arrays in photoactive area accumulate electrical charges

proportional to the light intensity of the image in their potential wells. Then the control circuit

causes each capacitor in the array to relocate its contents to its neighbor in the transmission area.

Subsequently, all contents can be sent across the chip as shift register. Then the last capacitor in

the array transfers its charges into a charge amplifier, which converts all the charges into

voltages. These voltages will next be digitized and stored in memory. The total number of

electrons held in each capacitor will determine the upper limit of the dynamic range of the CCD.

There are three main structures of common CCD image sensors including full-frame, frame-transfer, and interline-transfer. In a full-frame CCD, after all photons are converted to electrons, parallel serials of image data are transferred one row at a time to an amplifier. All integrated charges must be clocked out of the serial register before the next parallel line of image data arrives. Even though full-frame features high density pixel array for high-resolution digital imaging and all image area is active, there is no electronic shutter. A mechanical shutter must be inserted to avoid smearing images as the device is clocked or read out.

With frame-transfer CCD, instead of 100 percent fill factor to detect all incoming photons, half the silicon area is covered by an opaque mask as storage arrays. The image data can be collected from the other half and transferred in parallel manner to opaque mask just like full-frame CCD in just a few percent of smearing. While the opaque mask is reading and storing that set of data, the first half array area is busy collecting the next image data set. A mechanical shutter is not required, but twice the silicon area is needed to be comparable of a full-frame CCD; hence, a bit higher in cost and much faster in speed. The Roper CCD 3392 camera and high performance CCD Olympus DP 70 in our lab belong to this type of design, frame-transfer.

The last design is interline CCD, which applies the frame transfer concept one step further. It masks every other column of the image sensor for storage. In other words, only one pixel shift has to take place to transmit from image row to storage row. Shutter times become much faster (a microsecond or less), smear is almost diminished, but cost is the highest among the three designs. So, each kind of CCD architecture is selected depending on each unique circumstance.

2.2.4 Potentialstat/Galvanostat

Metal nanowires were synthesized via electrodeposition using Potentialstat/Galvanostat model 263A from EG&G Instruments. In this model, a high-performance current-to-voltage (±200 mA and ±20 V) converter circuit was incorporated for precision, fast, and low-drift current measurements, free of degradation from cell-cable resistance, capacitance, and inductance. Low pass filters were used to eliminate noise arising in the electrochemical cell. The electrochemical cell consisted of 3 electrodes in which a platinum wire was used as counter electrode, Ag/AgCl was used as reference electrode, and a layer of metal coating in the back of the sample against copper tape was used as working electrode.

2.2.5 Scanning Electron Microscopy (SEM)

Scanning Electron Microscope (SEM) JEOL Model 5410 with energy dispersive X-ray spectrometer (EDS) was used to image metal nanowires and their assemblies. This model offers high-speed, non-damaging scan control, simple positioning, high resolution imaging, and stable observation of heated/cooled samples in high vacuum. SEM is considered a highly versatile instrument for measurement and analysis of microstructure morphology and chemical composition characterizations[215]. SEM, in general, uses a high-energy beam of electrons (electron gun) to bombard the sample surface and scan it in a raster pattern. The collected surface signals or so-called secondary electrons, which come from the interaction of electrons and atoms from the sample, provide surface topography, composition, and electrical conductivity, etc. This secondary electron signal is able to reach a limit of less than 10 nm resolving surface structures. Indeed, SEM's magnification can be as high as 250 times the

42

magnification limit of the best light microscopes producing high resolution images of samples of just nanometers in size.

2.2.6 Transmission Electron Microscopy (TEM)

For even better imaging resolution and characterization of smaller nanoparticles, transmission electron microscopy was performed on a JEOL Model 2010 LaB6 at 200 kVvoltage with an attached EDAX Genesis analyzer. In a typical TEM, a beam of electrons from electron source will be accelerated, filtered by electromagnetic lens system, transmitted through and interacted with a thin sample at sample holder before forming an image on a screen. Since the image is produced by the interaction of the electron beam transmitted through the thin sample, transmission of the electron beam greatly depends upon density and composition of the specimen being examined. TEM is capable of observing atomic scale resolution imaging. Material morphology, internal crystal and chemical structures can be identified easily by the combination of bright-field, dark-field, and electron diffraction[216,217]. Making very thin samples before TEM observation is always a must. That is why TEM analysis can be very costly and time-consuming due to sample preparation compared to other characterization techniques.

Chapter 3

Polystyrene-Quantum Dot-Gold Nanoparticle SET-based Probes for Bioassays

3.1 Introduction and objectives

QDs have been used as a popular probe to conjugate with different biomolecules in solution. Because the QD surface is so sensitive to the outside environment, coupling them to biomolecules and utilizing them in various buffer environments can result in aggregation and alteration of the unique photochemical properties of the QDs[41]. To eliminate this undesirable effect, QDs can be attached to the surface of a biocompatible microsphere or microbead surface. Furthermore, the huge surface area from the bead itself presents other advantages as well. First, a large number of QDs can be attached on one single bead so that the bead can act as an amplifier platform carrying multiple QDs to substantially enhance the signal-to-noise ratio. Second, purification steps are much easier because the heavier beads can be separated from unbound substances just by centrifugation. Among different kinds of QD-encoded beads, coating of QDs on microsphere surfaces via layer-by-layer (LbL) method (Scheme 1.1) is preferred due to the uniform distribution of QDs[41,43]. In this study, we applied and simplified this LbL method by employing covalent attachment of just one layer of QDs onto polystyrene microsphere surfaces without an outer polymer shell. The purpose was to enable analysis and develop QD-based energy transfer probes for biosensors on microsphere platforms. There are two basic energy transfer categories: fluorescence resonance energy transfer (FRET) between two fluorophores and surface energy transfer (SET) by metal induced quenching. The main difference between the two types of energy transfer is that the acceptor for FRET has to be a

fluorophore while for SET the acceptor is a metal surface. For FRET, the efficiency of the

energy transfer process is proportional to the inverse sixth power of the distance between donor

and acceptor ($1/R^6$) [83,128]. After the donor is excited, energy can be transferred to excite the

fluorophore acceptor so that the acceptor fluorescence increases and the donor fluorescence

quenches. For SET, the efficiency of the energy transfer process is proportional to the inverse

fourth power of the distance between the donor and acceptor ($1/R^4$)[15], and the acceptor is a metal

instead of a fluorophore. As a result, no fluorescence occurs, but quenching of the donor

fluorescence does occur. FRET is highly sensitive and only occurs when the donor-acceptor

distance is no more than 100 Å, while SET is not as sensitive and occurs at distances of up to

220 Å[36].

QD-based probes for SET studies were previously fabricated by different groups by

linking gold nanoparticles to the surface of luminescent QDs. In 2005, Chang and co-workers

previously developed solution assays for proteolytic activity with fairly long response time that

utilized QDs and gold nanoparticles (AuNPs) as donors and acceptors[218]. In 2007, Pons et al.

indicated that non-radiative quenching of the QD emission by proximal Au-NPs is due to long-

distance dipole-metal interactions that extend significantly beyond the classical FRET range[17].

In 2009, Li and the group presented DNA detection via dipole-surface energy transfer (SET)

between QD and gold nanorod (GNR)[37]. DNA hybridization between complementary strands of

DNA on QD and GNR enclosed the proximity between the two probes causing QD quenching by

transferring emission energy to GNR. Even though QD is a donor transferring energy to

acceptor GNR, this process is preferred as metal-induced quenching, because gold is not a

fluorophore but a metal.

All of these assays were used in homogeneous systems and were limited by the chemical and photostability of the linked organic molecules. However, this work for the first time incorporated a QD-AuNP SET pair on a polystyrene microsphere platform. QDs served as donors transferring non-radiative energy to acceptor AuNPs. Since gold is a metal, only quenching of QDs could be observed.

3.1.1 Water Soluble Quantum Dots

To achieve the above objective, QDs need to be water soluble and chemically accessible for later coupling chemistries before being attached on polystyrene surfaces. A variety of mercaptocarboxylic acids have been used to replace TOP/TOPO on QD surfaces (chapter 1) to make them water soluble and chemically accessible. While the thiol groups attach directly to QD surfaces, carboxylic acid groups on the other end of the molecule provide QDs with hydrophilicity[219]. Even though thiol-capped QDs are very common, the mercaptocarboxylic acid-modified water-soluble QDs are not very stable. Photodegradation studies reveal that the SH group coordinated to the QD surface inevitably undergoes photooxidation followed by the formation of disulfide bonds, which leads to the precipitation of the QDs[34]. This photochemical instability can be predicted by the relatively weak interaction (non-covalent bond) between the QD surface and the thiol ligand. Hence, these hydrophilic QDs have a very short shelf life. To avoid such problems, it is necessary to use another ligand with better binding affinity to modify the QD surface. Polyhistidine peptide emerges as an ideal candidate for this purpose. Binding affinity of multiple histidine amino acids is much stronger compared to just simple thiol attachment to Zn on the QD surface. This greater binding would provide better ligand coating for water soluble QDs to be involved in any chemical modification. Medintz et al. showed that

polyhistidine peptides play an important role in enhancing the quantum yield for thiol ligand-coated QDs[33]. Mattoussi and co-workers have successfully improved functionality and stability to QD bioconjugates with polyhistidine peptides before being utilized in bioapplications[42,197-199]. The thickness of the QD-His surface coating is small enough to allow energy transfer from QD to take place at the surface of the particles.

To start, we synthesized TOPO-capped or so-called organic CdSe/ZnS QDs. Next, we performed ligand exchange to make the QDs water soluble. After careful consideration, we decided that 16-mercaptohexadecanoic acid would first be exchanged with TOP/TOPO ligand on the ZnS surface to provide water-soluble QDs. This mercaptocarboxylic acid was chosen for the thiol exchange because it is one of the least photochemically active ligands[31], and it also provides an aqueous friendly environment for later binding of subsequent polyhistidine ligands to the QD surface. Then, synthetic polyhistidine peptides of 10 amino acids K-K-H-H-H-H-H-H-E-E were attached to the ZnS shell (Scheme 3.1).
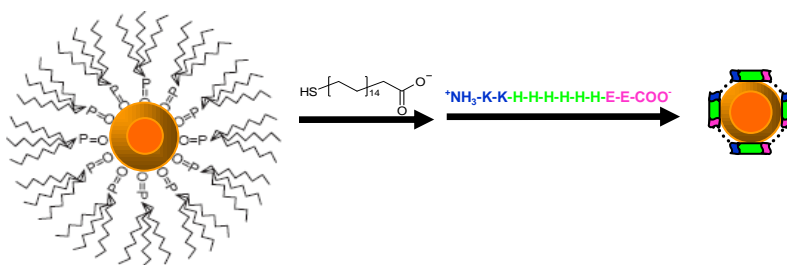
Scheme 3.1 *Chemical modification of QD-TOPO to QD-His*

The 6-histidine part of the peptide binds strongly to the ZnS surface while lysine (K) and glutamic acid (E) amino acids provide multiple carboxyl and amino groups for greater aqueous

compatibility and more than one coupling chemistry. Attaching QD-His to polystyrene-COOH

microspheres (6-8 µm) and aminated gold nanoparticle could be carried out easily with EDC

coupling which is explained in detail in scheme 3.2.
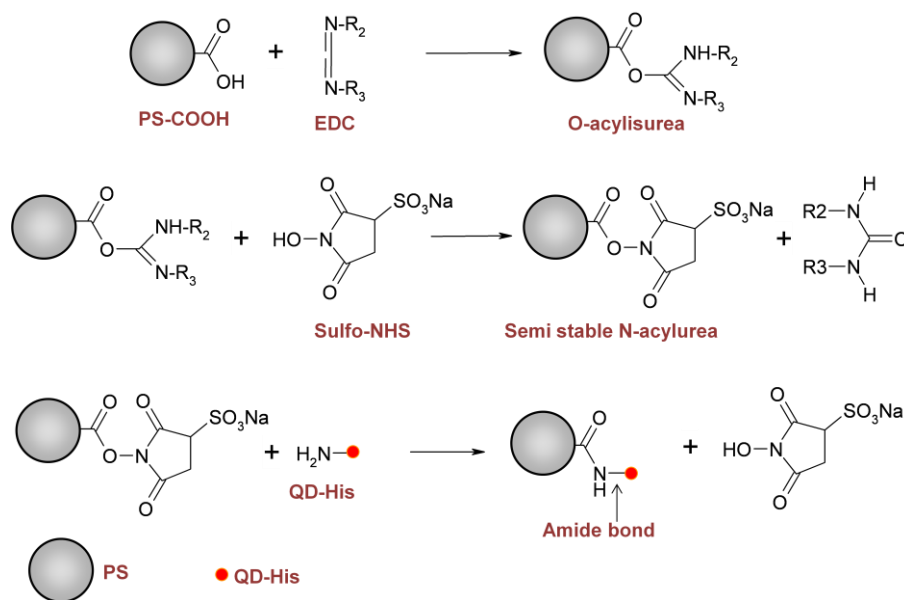
Scheme 3.2 *EDC coupling of carboxylated-polystyrene and QD-His*

3.1.2 Quantum Dots and Gold Nanoparticles as SET Donors and Acceptors

Since the QD-AuNP SET interaction is designed to occur on a microsphere platform, QDs

and AuNPs need to be covalently attached to the PS surface. The carboxylated polystyrene beads

were first activated with excess EDC/NHS before being attached to amino groups of QD-His in the

second step. The fluorescence of these PS-QDs shows very high quantum yield vs. non-fluorescence

carboxylated-PS. Next, excess di-amino disulfide linkers were attached to the AuNP surface.

Cystamine has been used as a bi-functional building block in which the thiol groups bind to the gold

surface leaving the free amino groups available for further modification chemistry[220,221]. The most

favorable attachment situation of cystamine di-thiol on the surface of gold involves a cleavage of the

48

disulfide bond[220]. Previous spectroscopic data suggest that di-thiol binds preferably through a single thiol end to gold surfaces[222].
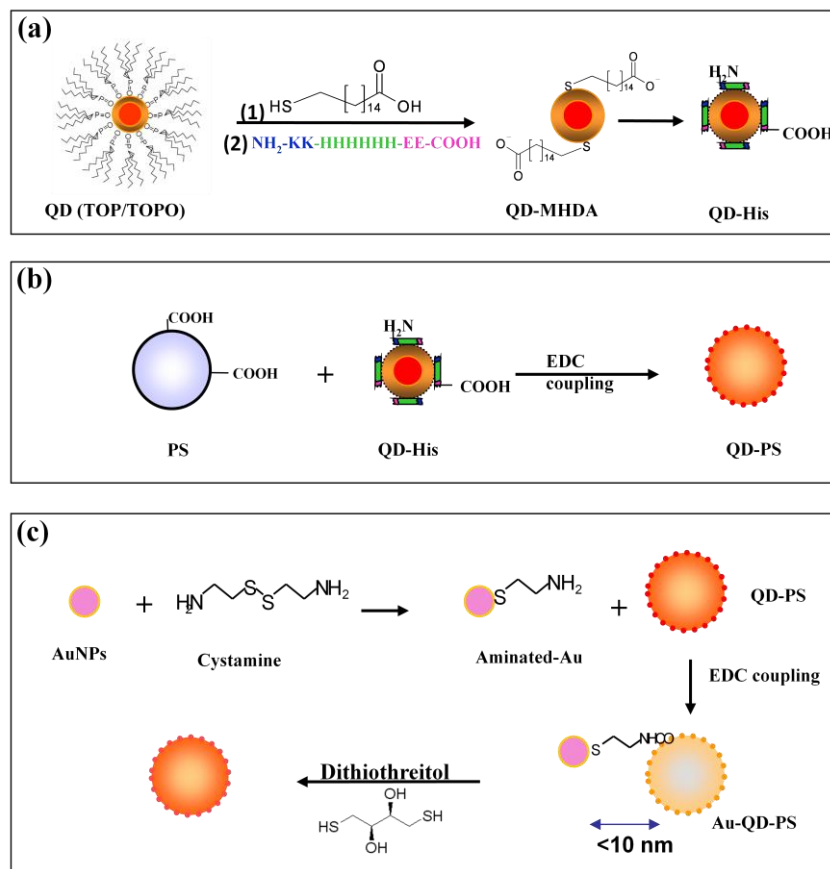
Scheme 3.3 *Schematic diagram of (a) water soluble QD-His from TOPO-capped QD via exchange ligands between TOPO and MHDA molecules plus attachment of synthetic His-tags, (b) QD-His covalently attaches to PS surface via EDC coupling, and (c) SET between Au and QD on polystyrene surface; and fluorescence restoration of PS-QD after the removal of AuNP from the microbead surface.*

EDC coupling is again applied among these aminated-gold nanoparticles and the PS-QD surface. Since QDs and AuNPs are covalently attached by a short linker, the distance between them is considerably less than 220 Å. This narrow distance between QD and gold nanoparticle is a crucial requirement for SET to take place. As QDs are being excited by UV light, fluorescence will be diminished because of their energy is transferred to gold nanoparticles in close proximity. However, the fluorescence of PS-QDs can be restored as gold nanoparticles are removed from

49

the system (Scheme 3.3). AuNPs are displaced from PS-QD surfaces when excess dithiothreitol (DTT) exchanges with cystamine linker between QDs and AuNPs.

3.2 Experimental

3.2.1 Synthesis of TOPO-Capped Luminescent Quantum Dots

Trioctylphosphine oxide (TOPO) capped CdSe/ZnS quantum dots were prepared following a method first proposed by Peng[223-225] with a slight modification. Briefly, 12.7 mg of cadmium oxide and 200-250 mg of lauric acid were mixed under a nitrogen atmosphere. The mixture was heated to ~200 °C to fully dissolve the cadmium oxide (clear color). Then, 2.0 g of TOPO and 2.0 g hexadecylamine were added to the solution under constant stirring. The temperature was raised to 250°C before being cooled down slowly to around 200°C. 80 mg selenium powder was then dissolved in 2.0 mL of trioctylphosphine before being rapidly injected into the solution under vigorous stirring. The temperature was increased to 280°C before being cooled down upon the desired color of quantum dots. For shell coating, a 2.0 mL TOP solution containing 250 µl $(TMS)_2S$ and 1 ml $Zn(Et)_2$ was drop-wise injected into the solution. The reaction mixture was kept at 200°C for one hour before being cooled to room temperature and washed three times with methanol, centrifuged at 5,000 rpm for 10 minutes each, and re-dissolved in chloroform. The resulting solution could be stored at room temperature in the dark for several years.

3.2.2 Water-Soluble Quantum Dots via polyhistidine-peptide (QD-His)

In our lab, water soluble QD-MHDA was prepared from QD-TOPO by ligand exchanging of TOPO molecules with 16-mercaptohexadecanoic acid molecules. The metal

binding affinity of polyhistidine to ZnS is much stronger than simple thiol binding. Hence, this strong binding affinity helped diminish photooxidation of thiols on the QD surface. Multiple carboxyl and amino groups from lysine (K) and glutamic acid (E) amino acids provided the QD surfaces with multiple carboxyl and amine groups for better aqueous compatibility and chemical accessibility. First, water soluble 16-mercaptohexadecanoic acid (MHDA)-capped QDs were prepared following a procedure published by Bawendi[50] with a slight alteration. About 25 mg MHDA was heated to 75-80°C until completely melted dissolved. Then 3 mL of chloroform + 3 mL of ~ 1.0 μM TOPO-QDs were added to the above solution and stirred overnight at 65-75°C. The solution was cooled down to room temperature before being mixed with 5-6 mL of aqueous tetramethylammonium hydroxide pentahydrate (pH ~10) and stirred constantly for 30-45 minutes. A two-phase solution resulted after a few hours. The top aqueous layer, containing the 16-MHDA coated QDs, was collected, centrifuged, and washed with DI H_2O to remove any by products. Spin dialysis was performed with 100,000 Da cut off molecular weight centrifuge tubes.

QD-MHDA was then incubated with 10-20 molar excess of histag peptide K-K-H-H-H-H-H-H-E-E at room temperature under constant stirring for 1-2 hours. The final product was washed by spin dialysis with DI water via 100,000 Da cut off molecular weight centrifuge tubes before being stored at 4°C in the dark.

3.2.3 Amino-Functional Gold Nanoparticles via Cystamine

To ensure that AuNPs were entirely coated with cystamine, excess cystamine was used for functionalizing. 2.0 mL of citrate-stabilized, 5.0 nm gold nanoparticles (AuNPs) at 5.0×10^{13} particles/mL were incubated with 50.0 mg cystamine in 1.0 mL water for 2-4 hours at room

temperature. The product was then washed by spin dialysis with DI water via 30,000 Da cut off molecular weight centrifuge tubes before being stored at 4°C.

3.2.4 Conjugation of QD-His to Carboxylated-Polystyrenes

1.0 mL of 6 µm polystyrene-COOH in water was activated with 0.1 M 4-Morpholineethanesulfonic acid (MES) buffer (pH 5.5) before being incubating with a mixture of 3 drops of *N*-(3-dimethylaminopropyl)-*N'*-ethylcarbodiimide (EDC) and 1.0 mg *N*-hydroxysulfosuccinimide sodium salt (Sulfo-NHS) for 15 minutes at room temperature. The mixture was centrifuged and washed with 10 mM borate buffer (pH 8.0) or 10 mM MES buffer (pH 8.0) 3 times before being incubated with 400 µL of 2.0 µM QD-His for at least 2 hours at room temperature with constant mixing. The product was then centrifuged and washed with DI water several times before being stored at 4°C.

3.2.5 Conjugation of Cystamine-Au to Polystyrenes-QD and DTT cleavage

PS-QD was activated with 0.1 M MES buffer (pH 5.5) before being incubated with EDC/NHS for 15 minutes at room temperature. The mixture was washed several times with DI water before being incubated with 50-100 fold excess of cystamine-Au for 2 hours at room temperature. Then 5 mg/mL of DTT were incubated with PS-QD-Au before fluorescence signals were measured at 0, 10, 30, and 60 minutes. EDC/NHS activated QD-PS was used as a positive control.

3.3 Results and Discussions

3.3.1 TOPO-capped CdSe/ZnS Quantum Dots

Characterization of TOPO-capped CdSe/ZnS QDs was done by various analyses. High resolution imaging and characterization of TOPO-capped CdSe/ZnS QDs emitted at around 600 nm were performed by transmission electron microscopy (JEOL Model 2010 LaB6 with EDAX Genesis analyzer) to obtain size distribution and elemental analysis.
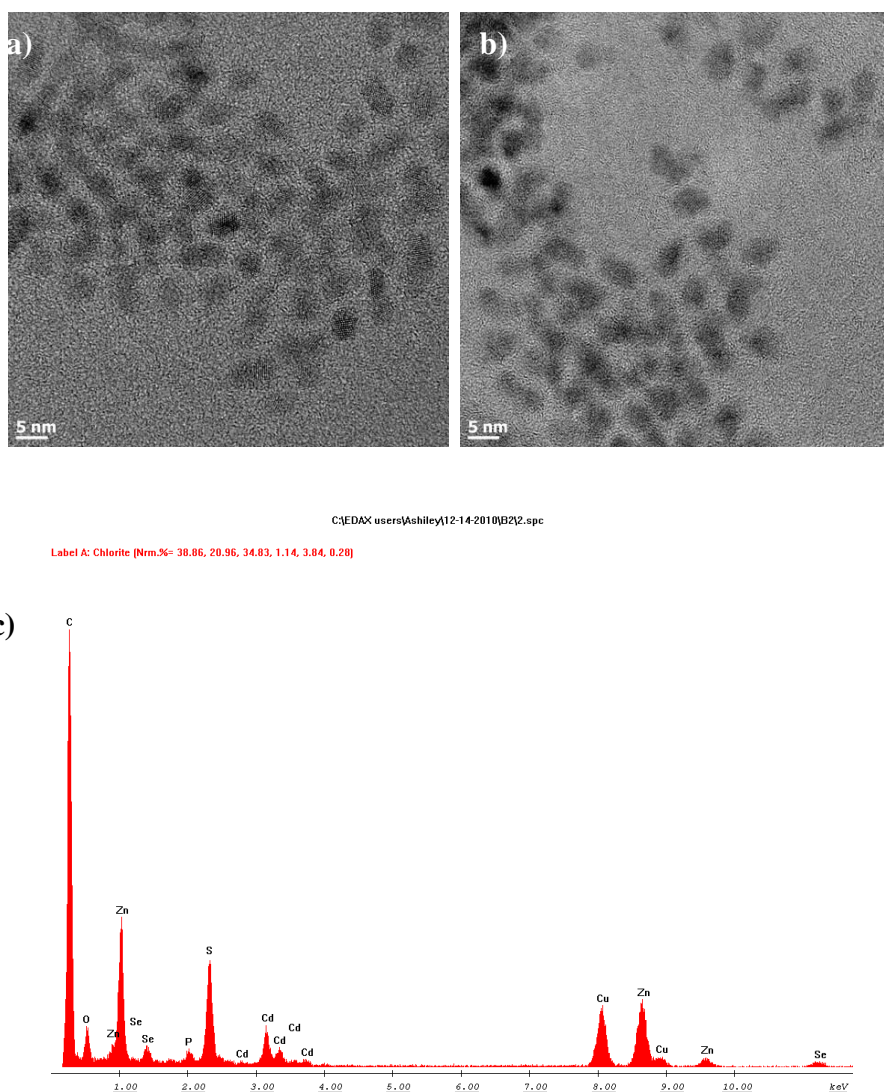
Figure 3.1 *(a), (b) TEM images, and (c) EDS of TOPO-capped CdSe/ZnS quantum dots.*

Sample preparation involved dropping QD-TOPO in chloroform on carbon-coated copper grids followed by air drying. Particle size measurements were carried out on raw TEM images. The average size of these QDs was about 5 nm corresponding to their emitted wavelength at 605 nm. EDS data show all elements (Cd, Se, Zn, S, O and P) which were intended to be included in the final semiconductor nanoparticle product.

Room light and fluorescence images of TOPO-capped QD solutions in chloroform were also taken along with fluorescence spectra to confirm that the emission wavelengths were coordinated with the colors viewed by UV lamp (Figure 3.2).
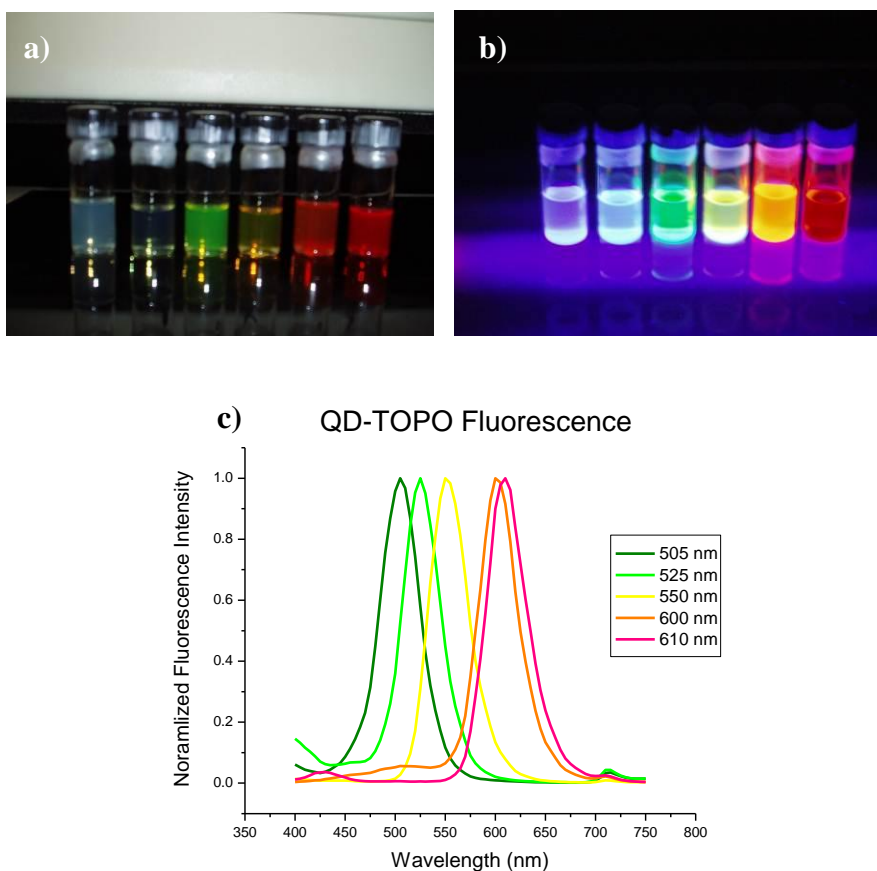
Figure 3.2 *(a) Room light image (b) fluorescence image and (c) fluorescence spectra of multiple-colored TOPO-capped CdSe/ZnS QDs.*

3.3.2 Photo-physical properties and fluorescence quantum yield of QD-TOPO, QD-MHDA, and QD-His

As mentioned earlier, we have carried out a ligand exchange reaction to replace hydrophobic TOPO ligands with MHDA ligands in order to provide the CdSe/ZnS QD with aqueous solubility. The MHDA ligands were then bound to peptide molecules that contained multiple histidine residues through Zn mediated chelation[8]. This increased the stability of the QDs in aqueous solution as well as their chemical accessibility.

Figure 3.3 illustrates the luminescence properties of 0.1 mM solutions of CdSe/ZnS QDs when coated with TOPO, MHDA and histidine peptides. Figure 3.3a shows that the luminescence intensity of the QDs slightly decreased when the TOPO ligands were exchanged with MHDA ligands. However, the luminescence intensity was partially recovered when the MHDA ligands were coated with the histidine peptide molecules. It was reported previously that His-tag binding to the thiol ligand-coated QDs increased their emission quantum yield [7]. More importantly, figure 3.3b showed that the normalized spectra of the QDs were almost identical. This indicated that the photophysical properties of the QDs were not significantly affected by these ligand exchange reactions.
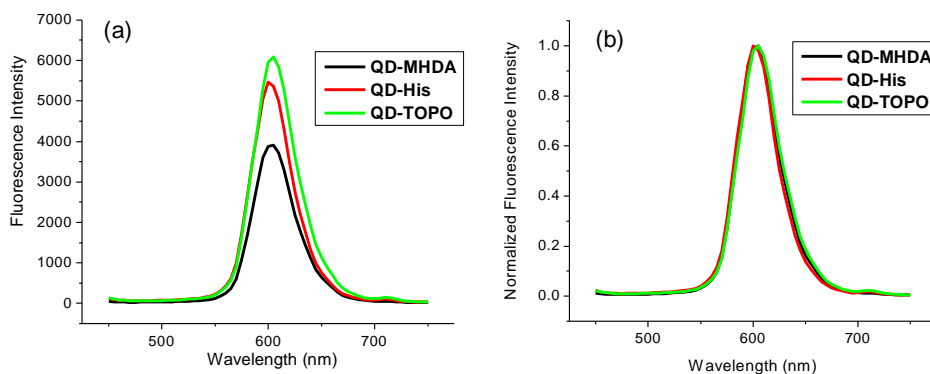
Figure 3.3 *(a) Emission spectra and (b) normalized emission spectra of QD-TOPO (green), QD-MHDA (red) and QD-His(black) (λ_{ex}=400 nm)*

Quantum yield (QY) values of QD-TOPO, QD-MHDA and QD-His were further determined using Rhodamine B with 590nm emission wavelength as a standard. All samples were excited at 550 nm and the emission intensity was measured at 590nm. The QY values for QD-TOPO, QD-MHDA and QD-His were recorded at 0.56, 0.37 and 0.46 respectively. These results were in agreement with previous studies in which the QY of peptide coated water soluble QD was found to be lower than the QY of TOPO-QD[8, 9].

To calculate the absolute quantum yield we used the following formula:

$$QY_{QD} = QY_{st} \ (G_{QD}/G_{st}) \ (\rho_{QD}^2/\rho_{st}^2) \qquad\qquad [1]$$
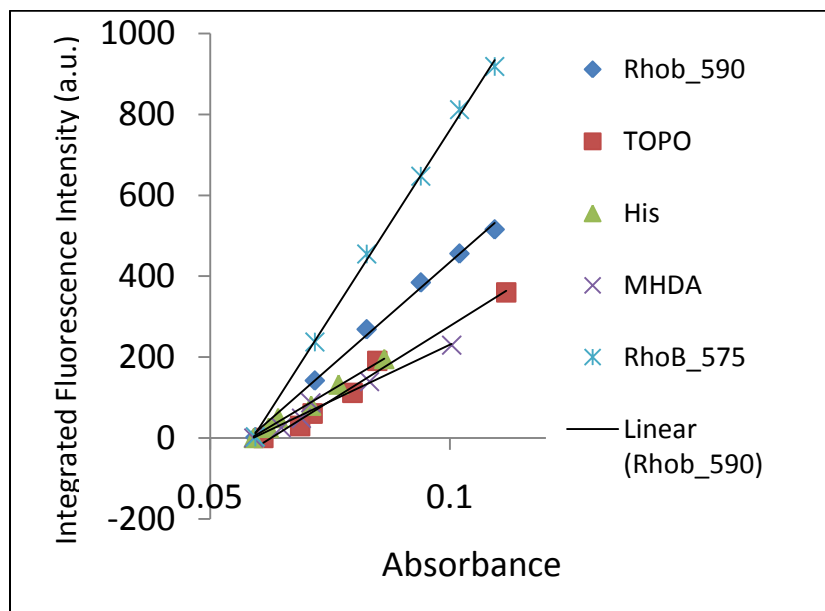
Figure 3.4 *Gradients of fluorescence vs. absorbance of Rhodamine B in ethanol, QD-TOPO in chloroform, and QD-MHDA and QD-His in DI water.*

QY_{QD} is the emission quantum yield of the QD sample. QY_{st} is the emission quantum yield of a standard sample. In our measurements Rhodamine B dissolved in ethanol was used as a standard with an emission quantum yield of 0.70. G_{QD} and G_{st} were the gradients of the QD and

Rhodamine B solutions. The gradients were the slopes of linear plots describing the fluorescence intensity versus absorbance at increased concentrations of QD and Rhodamine B (Figure 3.4). ρ_{QD} and ρ_{st} were the refractive indices of the solvents used to dissolve QD and Rhodamine B. The refractive indices were 1.4460 for TOPO-QD in chloroform, 1.333 for QD-His in water and 1.361 for Rhodamine B in ethanol.

3.3.3 Quantum Dot Coated Polystyrene (PS-QD)

Attachment of QD-His to polystyrene-COOH microspheres (6-10 µm) was carried out by carbodiimide or EDC coupling. EDC (1-ethyl-3-(3-dimethylaminopropyl) carbodiimide hydrochloride) coupling is common condensation chemistry between carboxyl groups and amino groups to produce a stable amide bond. EDC is often used in combination with N-hydroxysuccinimide (NHS) or sulfo-NHS to increase coupling efficiency. The carboxylated polystyrene beads were first activated with EDC/NHS before attaching to amino groups of QD-His. Figure 3.5 illustrates fluorescence and transmission images of PS-COOH and different color-emitting QD encoded on PS surface. No fluorescent signal was obtained from PS-COOH as expected, while PS-QD microbeads showed large fluorescent signals. Surprisingly, these QD-PS microspheres also showed much better fluorescent yield compared to microspheres encoded with conventional dye. The fluorescence intensity of dye coated PS microspheres was substantially reduced by self quenching of dye molecules in close proximity to one another on the surface. The greater fluorescence intensity represented a major advantage of QDs over conventional dyes in single microsphere-based sensors. Excess QD-His and conventional dye were provided to maximize occupancy of all available functional groups on polystyrene surface.
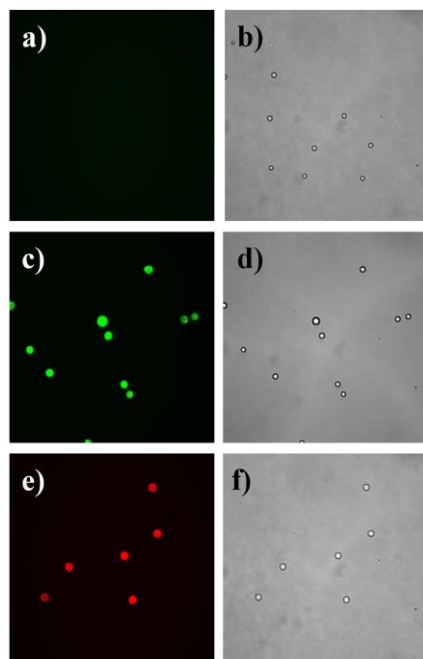
Figure 3.5 *First row: fluorescence images of a), PS-COOH c), PS-QD(535) and e) PS-QD(605); second row: transmission images of b) PS-COOH d), PS-QD(535) and f) PS-QD(605)*

Figure 3.6 shows PS microspheres coated with 535-nm and 605-nm emitting QDs. These PS-QD microspheres showed much stronger fluorescence intensity at the same laser exposure time (150 milliseconds) compared to PS-A488and PS-Rhodamine microspheres, respectively.
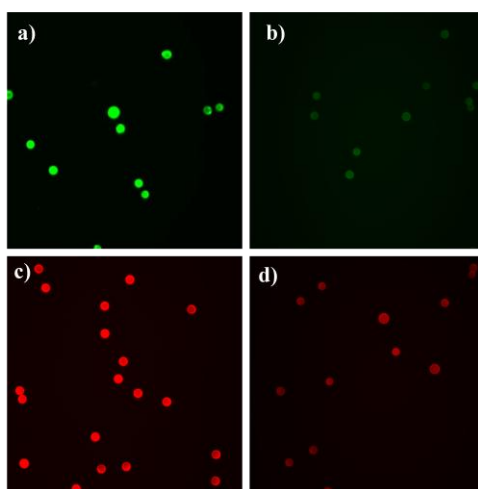
Figure 3.6 *Digital fluorescence images of green emitting (λex = 488 nm, λem = 535 nm) QD-PS (a) and PS-Alexa 488 (b); and red emitting (λex = 540 nm, λem = 605 nm) PS-QD (c) and PS-Rhodamine (d). Exposure times for all images were 150 msec.*

3.3.4 PS-QD-AuNP

After cystamine covered the AuNP surface (Scheme 3.4c), EDC coupling was again applied to link the PS-QD and amino-AuNP. Since QD and AuNP were covalently attached by a short linker, the distance between them was much less than 220 Å. This short distance between QD and AuNP was a crucial requirement for SET to take place. After being excited, non-radiative energy transfer occurred from donors (QDs) to acceptors (AuNPs). This SET transfer was confirmed by quenching of QDs as shown in figure 3.7a and 3.7b. TEM and EDS data also confirmed the presence of AuNP on the PS-QD surface (Figure 3.8).
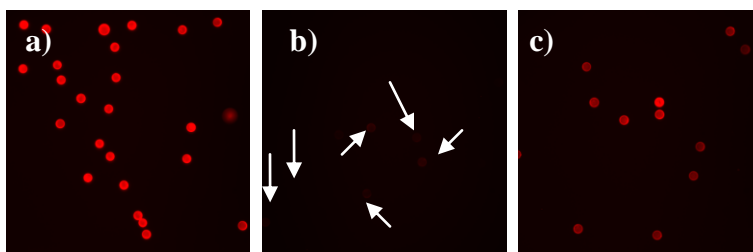
Figure 3.7 *Fluorescence images of (a) PS-QD605, (b) PS-QD605-Au and c) PS-QD605-Au incubated with 5 mg/mL DTT for 60 minutes.*
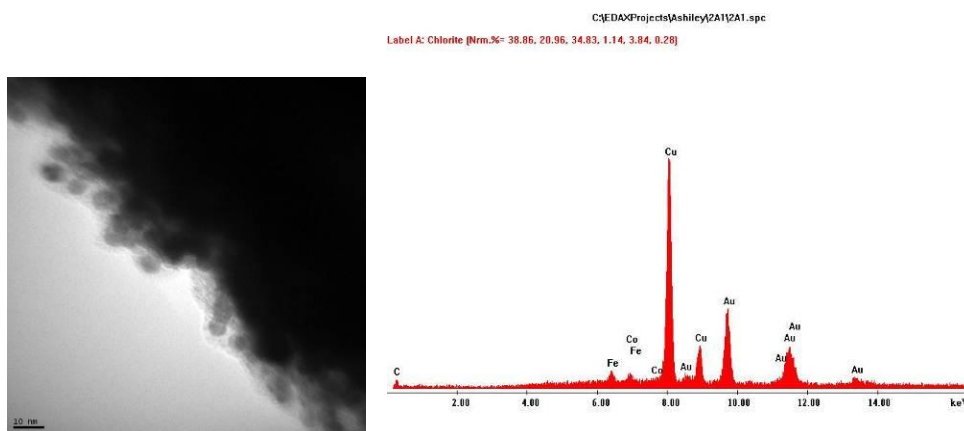
Figure 3.8 *TEM image (a) and (b) EDS of PS-QD-AuNP*

DTT was then used to displace the cystamine linker on the AuNP surface, removing AuNPs from the PS-QD surface. The use of 5 mg/mL of DTT resulted in suitable cleavage kinetics (0-120 minutes) for the analysis. Figure 3.9 confirmed fluorescence restoration of QDs after removal of AuNPs by treatment with 5 mg/mL DTT for 60 minutes. Figure 3.9a illustrates the average fluorescence spectra and figure 3.9b shows the peak fluorescence intensity of PS-QD605-Au incubated with 5 mg/mL DTT at different time points. EDC/NHS activated PS-QD was used as a positive control.
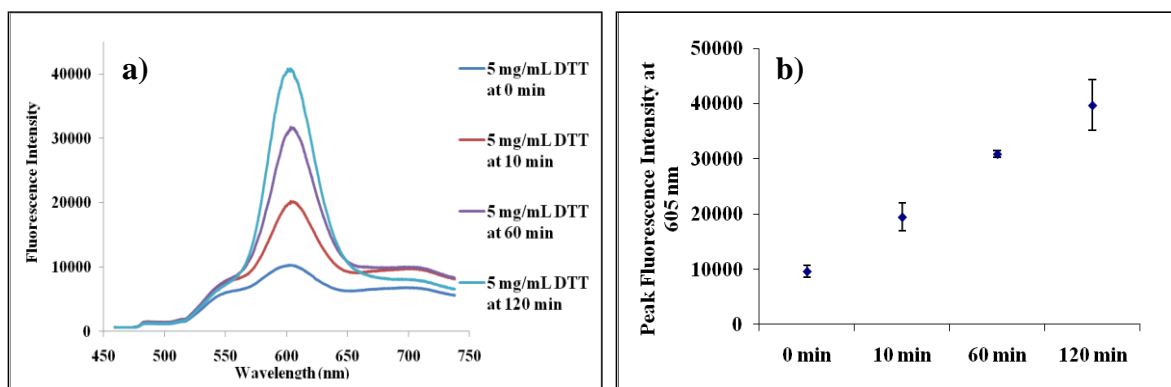
Figure 3.9 *Average fluorescence intensity of PS-QD-Au incubated with 5 mg/mL DTT at different time points. (a) Average fluorescence spectra and (b) peak fluorescence intensity @ 605 nm.*

3.3.5 DTT effect on Quantum Dot photoluminescence

As a control experiment, the effect of DTT the photoluminescence of QD-PS was investigated. The fluorescence signals of QD-PS when incubated with 5 mg/ml DTT for 1 hour and in the absence of DTT were analyzed (Figure 3.10). DTT quenching of QDs luminescence was found to be about 5% causing very small influence on fluorescence restoration of PS-QD.
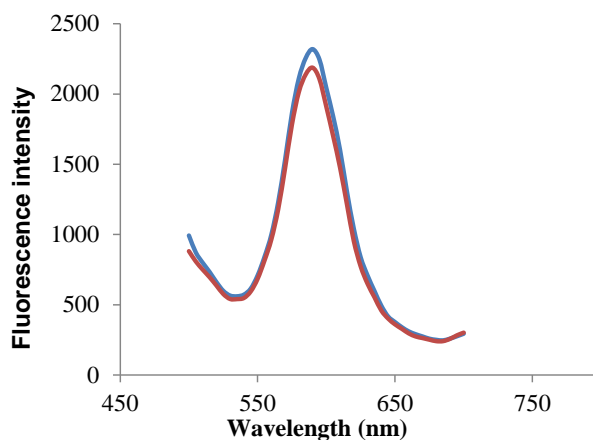
Figure 3.10 *Luminescence of QD-PS in the absence of DTT (blue line) and following incubation with 5 mg/ml DTT for 1 hour (red line).*

3.4 Summary

In summary, we demonstrated stepwise of preparation of small, stable, water soluble, and non-polymer coated QDs by ligand exchange of 16-mercaptohexadecanoic acids and attachment of synthetic his-tag peptides. Capping the QDs with histidine-containing peptides greatly increased their aqueous stability and photoluminescence properties. These QD-His particles were highly compatible with aqueous media and chemical accessibility for preparation of particle-based SET probes. QD-His were successfully attached to polystyrene microsphere surfaces providing QD-encoded beads that showed enhanced fluorescent signals compared to solution-based QDs. The fluorescence signal-to-noise ratios of polystyrene microbeads coated with QDs were significantly higher than the corresponding signal-to-noise ratios for polystyrene microbeads coated with conventional dyes because dye-coated PS suffered quenching due to close proximity of one dye molecule to another on the bead surface. The addition of AuNPs on PS-QD surfaces enabled the fabrication of particle-based SET biosensors. SET interactions between the QDs and AuNPs completely quenched the emission of the QD. The emission of the

QD was restored when the AuNPs were removed from the PS surface by DTT treatment. The new PS-QD-Au SET platform opens many new possibilities for carrying out SET and FRET assays in microparticle-based microarrays. For future development, the versatility of these assays could be greatly increased by replacing the linkers between the QDs and AuNPs to selectively respond to specific cleaving or displacement agents.

Chapter 4

Multiplexing of Polystyrene-Quantum Dot-Alexa A660 FRET-based Probes for DNA Detection

4.1 Introduction and objectives

Since the discovery of the human genome project, scientists have recognized the importance of DNA hybridization process. Thoroughly understanding this process will help develop postgenome technology with greater success[226]. Many research groups have attempted to fabricate different formats to detect DNA using DNA hybridization. Among the used formats, fluorescence resonance energy transfer (FRET) based-method has been utilized more often. In 2006, Zhang and co-workers studied quantum dot-based FRET nanosensors using single molecule detection in capillary flows[32]. The authors used DNA hybridization to connect Cy5 dye to 605-nm emitted QDs. In 2009, Jiang and co-workers fabricated cascaded FRET in conjugated polymer/quantum dot/dye-labeled DNA complexes for DNA hybridization detection[227]. Both their work and all other current-state of the art QD-based assays are in solution. However, the QD surface is so sensitive to the outside environment that coupling them to biomolecules and utilizing them in various buffer environments can result in aggregation and alteration of the unique photochemical properties of the QDs[41]. To reduce this unwanted effect, QDs can be attached to the surface of a biocompatible microsphere or microbead surface. Researchers favored this approach due to the following advantages. First, a large number of QDs can be attached on one single bead so that the bead can act as an amplifier platform carrying multiple QDs to substantially enhance the signal-to-noise ratio. Second, purification steps are much easier because the heavier beads can be separated from unbound substances just by

63

centrifugation. Among different kinds of QD-encoded beads, coating of QDs on microsphere surfaces via layer-by-layer (LbL) method (Scheme 1.1, Chapter 1) is preferred due to the uniform distribution of QDs[41,43]. However, incorporating FRET in QD-encoded microspheres using LbL method can still be a challenge because the outer polymer layer to protect QDs prevents them from transferring energy to the outside environment. To solve this problem, in our study, for the first time, we apply and simplify this LbL method by employing covalent attachment of just one layer of QDs onto polystyrene microsphere surfaces without an outer polymer shell. The purpose is to enable analysis and develop QD-based FRET probes for optical and biomedical detecting on microsphere platforms.

In details, we both developed FRET-based probes on a single microsphere surface to detect DNA and incorporated multiplexing characteristics from QDs into the application. As mentioned in chapter 3, with the use of QD-encoded microbeads for energy transfer assays, fluorescent signals from QDs were significantly enhanced and aggregation of QDs in solution was greatly eliminated. Since QDs are superior to conventional dyes due to their unique properties which create very broad absorption spectra, narrow and symmetrical emission spectra, tunable size-wavelength dependence, and low photochemical degradation, QDs are the best suited candidate for multiplexing where multiple emission signals can be simultaneously detected. In this work, two different color-emitting QDs were used for multiplexing and FRET with a fluorophore Alexa Fluor 660.

FRET was expected between donor QD and an acceptor thiol-reacted dye Alexa Fluor 660 (A660) attached to the QD via a hairpin single-stranded DNA (ss-DNA). This resulted in quenching of QD fluorescence and enhancing A660 emission without direct excitation of A660. The main-ss-DNA was designed such that it contained a sequence in which some complementary

monomers were located at both ends. This enabled the DNA to loop to itself and bring both ends

in close proximity (less than 10 nm) for FRET to occur[42]. A660 was chosen because it has very

broad absorption from below 300 to 750 nm, allowing multiplexing between different color

emitting QDs and the dye. QDs that emitted at 540 nm and 615 nm were used as multiplexing

FRET donors since their emission spectra are well-separated. Upon addition of a complementary

DNA that hybridizing to the hairpin ss-DNA, it was expected that the double-stranded DNA

would open up and relocate A660 further away from QD surface. Hence, the distance between

QD and the dye would larger than before, allowing for restoration of QD fluorescence. Scheme

4.1 illustrates step-by-step fabrication of the PS-QD-DNA-A660 probe before and after DNA

hybridization. Table 1 (chapter 2) includes the three modified main single-stranded

oligonucleotides (main-ssDNA1and main-ss-DNA3) and their complementary strands

(complement1 and complement3) that were used in this project.
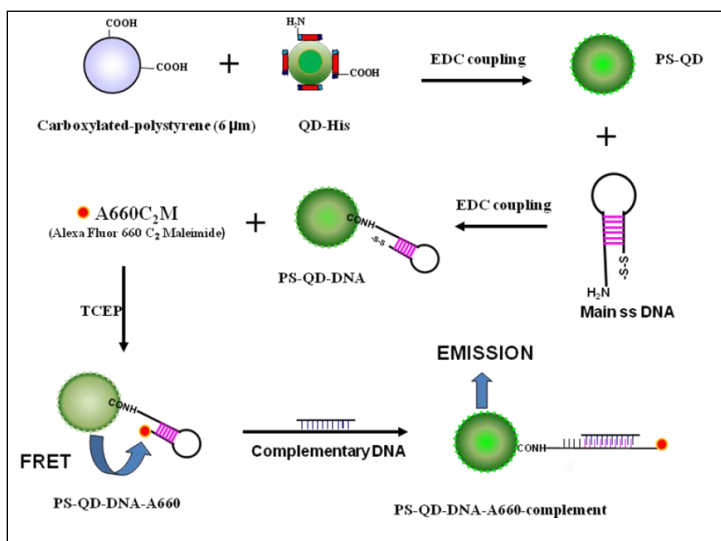
Scheme 4.1   *Schematic diagram of stepwise fabrication of PS-QD-DNA-A660 probe
before and after DNA hybridization*

For successful conjugation of all necessary steps for FRET to occur, the main-ss-DNA had to be carefully functionalized to provide available amino and thiol groups at either end for QD and fluorophore attachment. After attaching QD-His to PS surface, the available amine groups from the hairpin ss-DNA and the available carboxyl groups on PS-QD probes were conjugated to one another via EDC coupling. This coupling left a free end of the main-ss-DNA with an available thiol group for covalent attachment of the thiol-reactive A660 fluorophore. All conjugating steps and subsequent purification steps were done by centrifugation to eliminate the use of complex gel filtration columns.

4.2 Experimental

4.2.1 Synthesis of TOPO-Capped Luminescent Quantum Dots

Trioctylphosphine oxide (TOPO) capped CdSe/ZnS quantum dots were prepared following a method first proposed by Peng[7-9] with a slight modification. Briefly, 12.7 mg of cadmium oxide and 200-250 mg of lauric acid were mixed under a nitrogen atmosphere. The mixture was heated to ~200 °C to fully dissolve the cadmium oxide (clear color). Then, 2.0 g of TOPO and 2.0 g hexadecylamine were added to the solution under constant stirring. The temperature was raised to 250°C before being cooled down slowly to around 200°C. 80 mg selenium powder was then dissolved in 2.0 mL of trioctylphosphine before being rapidly injected into the solution under vigorous stirring. The temperature was increased to 280°C before being cooled down upon observation of the desired color of quantum dots. For shell coating, a 2.0 mL TOP solution containing 250 µl $(TMS)_2S$ and 1 ml $Zn(Et)_2$ was injected dropwise into the solution. The reaction mixture was kept at 200°C for one hour before being cooled to room temperature and washed three times with methanol, centrifuged at 5,000 rpm for 10 minutes

each, and re-dissolved in chloroform. The solution could be stored at room temperature in the dark for up to several years.

4.2.2 Water-Soluble Quantum Dots via polyhistidine-peptide (QD-His)

Water soluble 16-mercaptohexadecanoic acid (MHDA)-capped QDs were prepared following a procedure published by Bawendi[50] with a slight alteration. About 25 mg MHDA was heated to 75-80°C until completely melted. Then 3 mL of chloroform + 3 mL of ~ 1.0 μM TOPO-QDs was added to the above solution and stirred overnight at 65-75°C. The solution was cooled down to room temperature before being mixed with 5-6 mL of aqueous tetramethylammonium hydroxide pentahydrate (pH ~10) and stirred constantly for 30-45 minutes. A two-phase solution resulted after a few hours. The top aqueous layer, 16-MHDA coated QDs, was collected, centrifuged, and washed with DI H$_2$O to remove any by products. Spin dialysis was performed with 100,000 Da cut off molecular weight centrifuge tubes. QD-MHDA was then incubated with 10-20 molar excess of histag peptide K-K-H-H-H-H-H-H-E-E at room temperature under constant stirring for 1-2 hours. The final product was washed by spin dialysis with DI water via 100,000 Da cut off molecular weight centrifuge tubes before being stored at 4°C in the dark.

4.2.3 Conjugation of QD-His to Carboxylated-Polystyrenes

1.0 mL of 6 μm polystyrene-COOH in water was activated with 0.1 M 4-Morpholineethanesulfonic acid (MES) buffer (pH 5.5) before being incubated with a mixture of 3 drops of *N*-(3-dimethylaminopropyl)-*N'*-ethylcarbodiimide (EDC) and 1.0 mg *N*-hydroxysulfosuccinimide sodium salt (Sulfo-NHS) for 15 minutes at room temperature. The

mixture was centrifuged and washed with 10 mM borate buffer (pH 8.0) or 10 mM MES buffer (pH 8.0) three times before being incubated with 400 µL 2.0 µM QD-His for at least 2 hours at room temperature with constant mixing. The product was then centrifuged and washed with DI water several times before being stored at 4°C.

4.2.4 Conjugation of Rhodamine Red to main-ss-DNA

The hairpin main-ss-DNAs and their complements were designed following Medintz el al.[42] with a slight modification. Main-ss-DNA in 10 mM MES buffer (pH 7.5) was incubated with at least 100X Tris(2-carboxyethyl)phosphine hydrochloride (TCEP) at room temperature for up to 30 minutes. Then, a 2:1 ratio of Rhodamine Red C_2 maleimide in DMSO was added to the above main-ss-DNA solution. The reaction was incubated for about 2 hours at room temperature with constant mixing. No further purification was necessary.

4.2.5 Conjugation of main-ss-DNA-Rhodamine Red to PS-QD

PS-QD was activated with EDC/NHS in 0.1 M MES buffer (pH 5.5) and resuspended in 10 mM MES (pH 7.5). Various ratios of main-ss-DNA-Rhodamine Red from 0.2 to 4.0 nmol were added to every 200 µL of EDC-activated PS-QD. All samples reacted at room temperature with constant mixing for 2-4 hours. The product was washed and centrifuged with 10 mM Tris-HCl + 1 mM EDTA (pH 8.0) several times before being stored at 4°C.

4.2.6 Conjugation of main-ss-DNA to PS-QD

Main-ss-DNA was conjugated to PS-QD surface via EDC coupling at a ratio of 2.5 nmol main-ss-DNA for every 1.0 mL PS-QD. Similar steps were done as previously described to

activate PS-QD surface before main-ss-DNA in 10 mM borate buffer (pH 8.0) or 10 mM MES

buffer (pH 8.0) was added to the mixture. The mixture was then incubated with constant mixing

at room temperature for 2-4 hours. The product was washed and centrifuged with 10 mM Tris-

HCl + 1 mM EDTA (pH 7.5) several times before being stored at 4°C.

4.2.7 Attachment of Alexa Fluor 660 C$_2$ maleimide to PS-QD-main-ss-DNA

1.0 mL of PS-QD-DNA in Tris-HCl EDTA (pH 7.0, above solution) was incubated with

5 µL of 0.5 M TCEP for 30 minutes with constant mixing at room temperature. The solution

was then centrifuged and washed a couple of times with Tris-HCl EDTA (pH 7.5). Various

ratios from 1 to 10 nmol of Alexa Fluor 660 C$_2$ maleimide in DMSO were added to every 200

µL of PS-QD-DNA mixed constantly at room temperature for 1-2 hours. The solution was

centrifuged and washed several times with 10 mM Tris-HCl + 1 mM EDTA (pH 8.0) before

being stored at 4°C.

4.2.8 PS-QD-Rhodamine Red or PS-QD-A660 and complement DNA via DNA hybridization

PS-QD-DNA-A660 product from previous step was incubated with 10x molar excess of

complement DNA in the same buffer (10 mM Tris-HCl + 1 mM EDTA pH 8.0) for at least 2

hours at room temperature. No further purification step was necessary before analysis. All

samples were placed in a 96-well plate and measured using microplate reader.

4.3 Results and Discussions

As presented in Chapter 3, TOPO-coated QDs, QD-MHDA, and QD-His retained the same photophysical properties. After ligand exchanging, their quantum yields were not significantly affected. QD size measurements were carried out by analysis of raw TEM images. The average size of these QDs was about 5 nm corresponding to their emitted wavelength. EDS data showed all elements Cd, Se, Zn, S, O and P which were intended to be included the final semiconductor nanoparticle product. PS-COOH microspheres were evenly coated with QD-His by EDC coupling. PS-QD particles were monodisperse and not aggregated.

4.3.1 Absorbance and Emission Spectra

As stated in Chapter 1, FRET is defined as a non-radiative energy transfer process between two chromophores, one donor and one acceptor[83,128]. The process occurs when the donor in its excited state transfers energy non-radiatively to the acceptor. As a result, the donor's fluorescence intensity is quenched, while the acceptor's fluorescence is increased. There are three important requirements for FRET to occur: i) spectral overlap of the donor emission and acceptor absorption spectra, ii) the distance between the two chromophores must be less than 10 nm, and iii) donor and acceptor transition dipole orientation must be approximately parallel. Therefore, the dye absorbance/emissions and QD emission spectra were analyzed to observe the FRET effect.
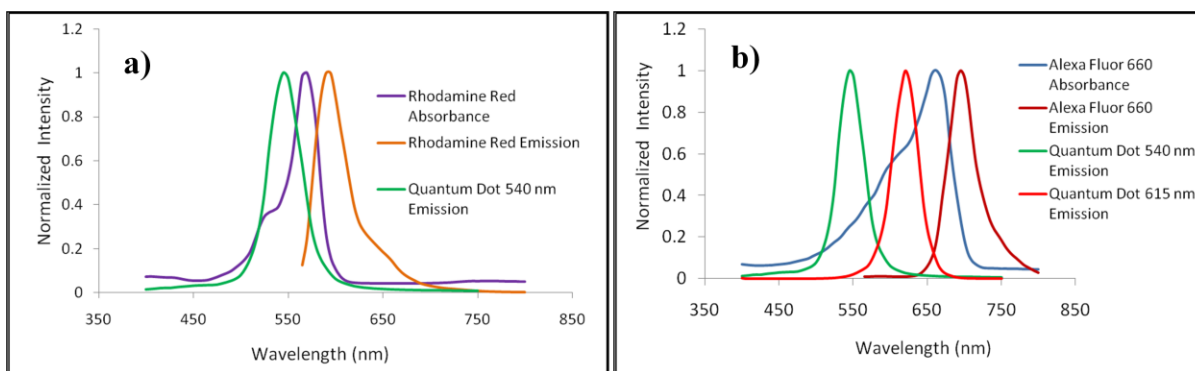
Figure 4.1 *Absorbance and emission spectra of a) QD(540) and Rhodamine Red dye and b) QD(540), QD(615), and A660 dye*

Figure 4.1 illustrates absorbance and emission spectra of Rhodamine Red, A660, and QDs. The spectra confirmed that the QD emission and the absorbance of the dyes overlapped. Moreover, the emissions of the dyes were also well-separated from QD emission. All samples were placed in 96-well plates and read by a microplate reader.

Figure 4.2 shows the FRET phenomenon between PS-QD(540) before and after conjugating to main-ss-DNA1-Rhodamine Red. The emission spectra were collected from samples placed in a 96-well plate and read by a microplate reader. The excitation wavelength was selected at 400 nm to avoid directly exciting the Rhodamine Red dye. Figure 4.2a demonstrates that Rhodamine Red emission increased as higher concentrations of main-ss-DNA1-Rhodamine Red were attached to the PS-QD(540) surface. Figure 4.2b illustrates the fluorescence restoration of PS-QD(540) after being hybridized with the complementary strands of main-ss-DNA1 (complement1 or comp1). Emission of Rhodamine Red at 595 nm decreased as emission of QDs at 540 increased. Therefore, FRET transfer was evident and significant enough for detection in the PS-QD(540)-DNA1-Rhodmaine probes. Despites preliminary success of PS-QD(540)-DNA1-Rhodmaine probes, we think these probes could be further improved. First, the sensitivity of this probe could be enhanced if signals of every single particle

71

platform were detected and averaged using more advanced analytical instruments. Second, fluorescence restoration could be higher by exploring better compatible buffer environments as well as DNA hybridization conditions.
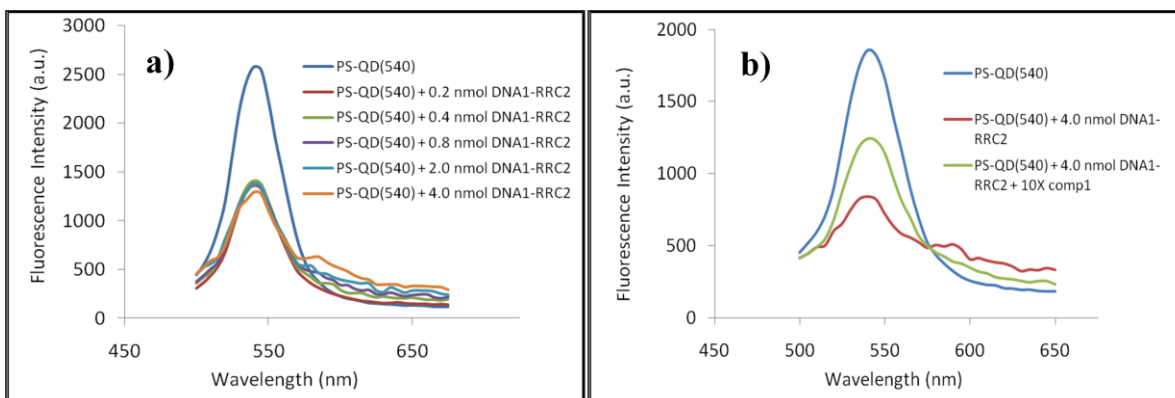
Figure 4.2 *Emision spectra of a) PS-QD(540) before and after conjugation with increased concentrations of main-ss-DNA1-Rhodamine Red (RRC2) and b) hybridization with 10X molar ratio of complementary strands (comp1).*

After analyzing FRET effect between PS-QD(540) and Rhodamine Red dye using main-ss-DNA1 as a linker, FRET effect beween PS-QD(540), PS-QD(615) and A660 dye were also examined using main-ss-DNA3 as a linker. Since A660 dye contained free amino groups in its molecular structure, main-ss-DNA3 had to be EDC-coupled to the PS-QD(615) surface first. Then, main-ss-DNA3 with available thiolated end was attached to A660 maleimide. This step was necessary to avoid any direct cross-linking of A660 to the PS-QD(615) surface. Figure 4.3 demonstrates that after the attachment of main-ss-DNA1 and main-ss-DNA3 to their surfaces, the photophysical and photochemical properties of PS-QD(540) and PS-QD(615) remained the same. After the attachment of A660, clear FRET signals occurred between PS-QD(540) to A660 as well as between PS-QD(615) to A660.
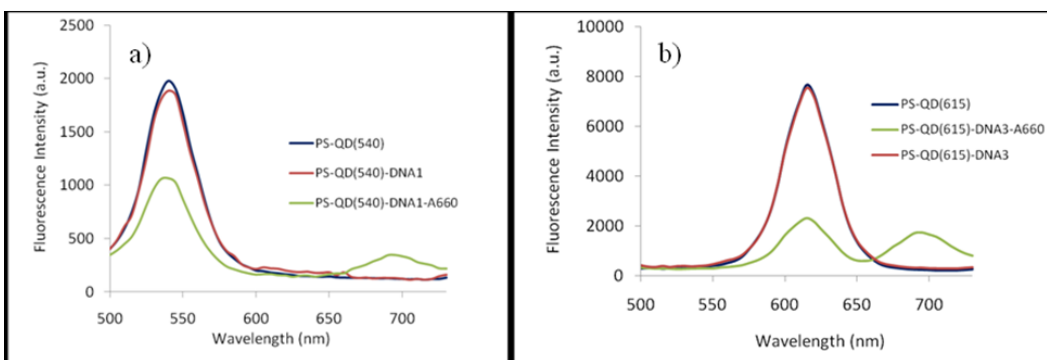
Figure 4.3 *Emission spectra of a)PS-QD(540) before and after attaching of DNA1 and A660; and b)PS-QD(615) before and after attaching of DNA3 and A660*

Figure 4.4a specifies that A660 had minimal non-specific binding to the PS-QD(615) surface under the experimental conditions. The excitation wavelength was selected at 400 nm to avoid direct exciting of A660 fluorophore. Figure 4.4b shows quantitative analysis of FRET as different concentrations of A660 fluorophore were attached to PS-QD(615)-DNA3. The emission of PS-QD(615) decreased as the concentration of A660 fluorophore increased accordingly. As 2.5 μM total concentration of A660 was incubated with PS-QD(615)-DNA3, A660 emission did not increase further. This indicates that all of the main-ss-DNA3 attached on PS-QD(615) surface bonded with A660. Figure 4.4c shows the quantitative fluorescence restoration of QDs at 615 nm after being incubated with different concentrations of complementary strands of main-ss-DNA3 (complement3 or comp3). When we used ten times (10X) the amount of complement3 (compared to main-ss-DNA3) to hybridize the main-ss-DNA3 on the PS-QD(615) surface, fluorescence restoration of PS-QD(615) became highest after 2 hours of hybridization. However, emission of A660 did not diminish accordingly. We believe that this happened because when all of the hairpin main-ss-DNA3 attached on PS-QD(615) surface bonded with A660, all of the attached A660 dye molecules could be in close proximity. As the complement3 hybridized with main-ss-DNA3, A660 was displaced away from the PS-

73

QD(615) surface and far away from each other, which reduced self-quenching effect of A660 dye.
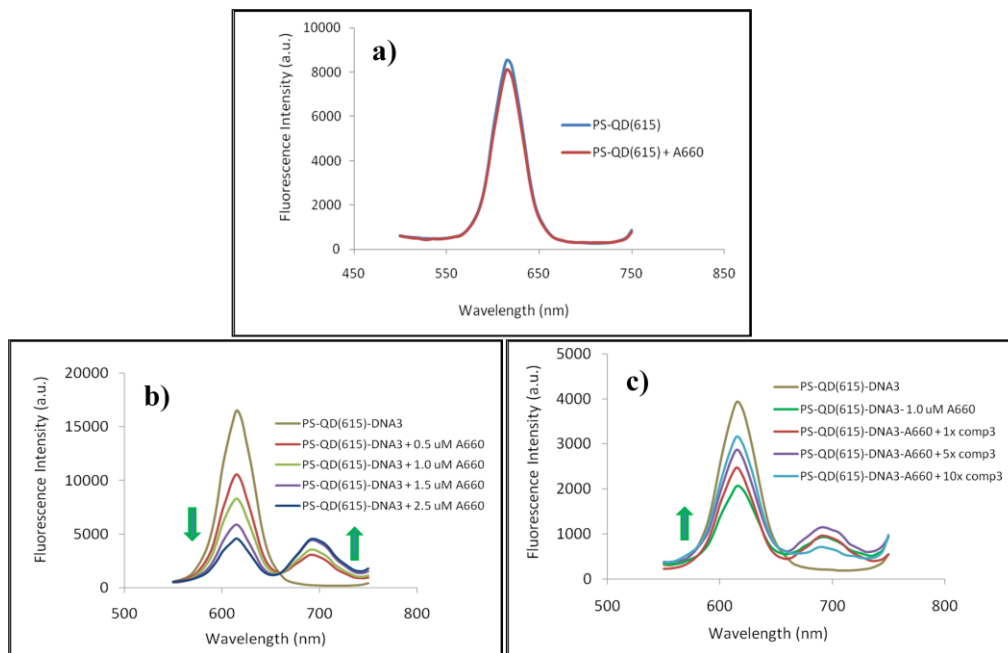
Figure 4.4 *Emision spectra of a)PS-QD(615) vs. PS-QD(615) incubated with A660, b)PS-QD(615)-DNA3 before and after attachment of increased concentrations of A660 dye and d)hybridization with increased concentrations of complementary strands (comp3).*

The last step in this project was to fabricate FRET and multiplexing between PS-QD(540), PS-QD(615) and A660. First, the PS-QD(540)-DNA1 and PS-QD(615)-DNA3 were mixed together before being attached with A660. Then, 10X complement1 and 10X complement3 were added to the PS-QD(540+615)-DNA-A660 for hybridization. Since complement1 is the exact complementary strand of main-ss-DNA1, it becomes non-complementary strand of main-ss-DNA3, and vice-versa. Figure 4.5 demonstrates that FRET occurred between PS-QD(540+615)-DNA and A660 because emission of A660 was present even without being directly excited at 400 nm. Moreover, after being incubated with 10X complement1 and complement3, hybridization of each complement took place and caused

74

specific fluorescence restoration of PS-QD(540) and PS-QD(615). As indicated in figure 4.5, there was some unexpected fluorescence restoration of PS-QD during the incubating process with non-complementary strands of DNA. However, the unexpected fluorescence restoration was lower than the expected signals. Overall, figure 4.5 shows that there was FRET and multiplexing between PS-QD(540), PS-QD(615) and A660. We believed that the unexpected fluorescence restoration could be minimized or eliminated through careful experimental conditions and careful designs of DNA sequences.
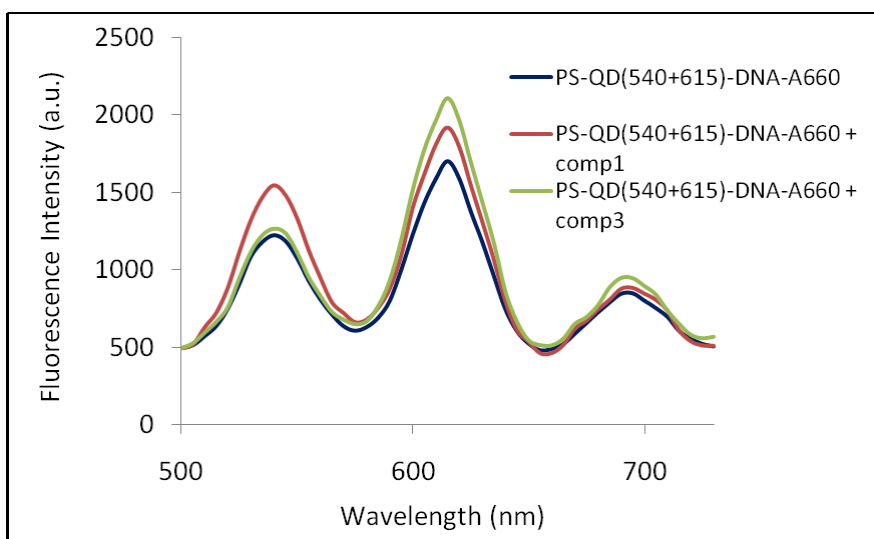
Figure 4.5 *Emission spectra of PS-QD(540)-DNA1-A660 and PS-QD(615)-DNA3-A660 before and after hybridization of 10X of complement1 and 10X of complement3.*

4.3.2 Fluorescence imaging

It was evident in Figure 4.6a that PS-QD(540) were monodisperse, non-aggregated, and emitted green fluorescence. After attachment of main-ss-DNA1-Rhodamine Red to the PS-QD(540) surface, the PS-QD(540) emission appeared light yellow (figure 4.6b). This was a result of a decrease of PS-QD(540) emission and an increase of Rhodamine Red emission at 590 nm. Overlapping of green (540 nm emission) and orange (590 nm emission) results in the

perception of yellow emission. After the incubation with complement1, which was

complementary strand of main-ss-DNA1, hybridization of DNA strands displaced Rhodamine

Red fluorophore further away from the PS-QD(540) surface. This in turn resulted in restoration

of 540-nm emission. Figure 4.6c confirms that the emission changed back to light green as some

of 540-nm emission returned.
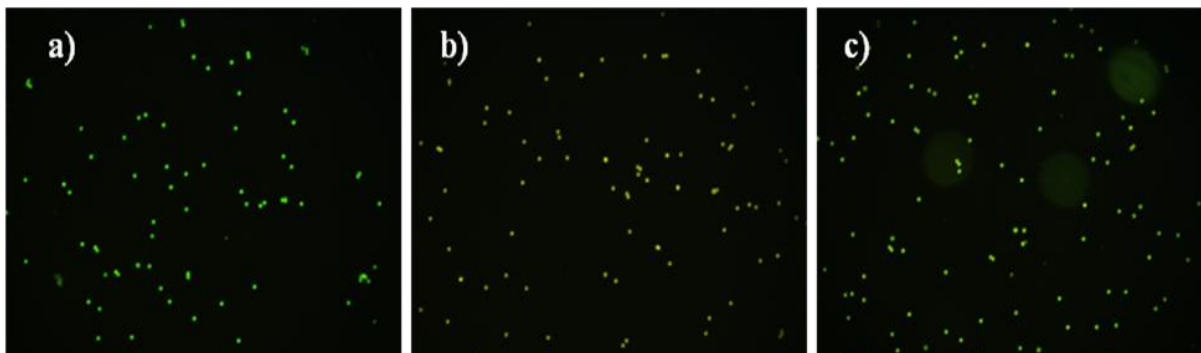
Figure 4.6 *Fluorescence images of a)PS-QD(540), b)PS-QD(540)-DNA1-RRC2, and c)PS-QD(540)-DNA1-RRC2+10X complement1*

Figure 4.7 demonstrates the monodisperse PS-QD(540) and PS-QD(615) microspheres

emitted green and red colors respectively. The brighter red particles compared to green particles

confirmed higher emission intensity of PS-QD(615) compared to PS-QD(540).
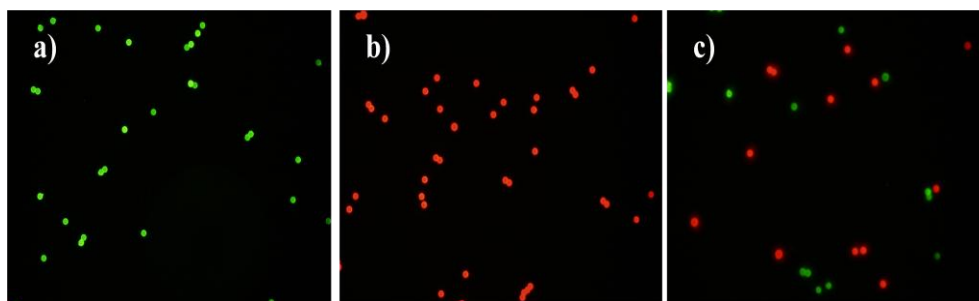
Figure 4.7 *Fluorescence images of a) PS-QD(540), b) PS-QD(615), and c) PS-QD(540) and PS-QD(615)*

Since A660 emitted at 695 nm, its deep red color could only be slightly detected by human eyes. Furthermore, our CCD camera detection decreased significantly as it approached 650 nm and longer emission wavelengths. Consequently, small changes in A660 signals could only be detected by microplate reader but not by the fluorescence microscope CCD camera. Figure 4.8 confirms that FRET signals between PS-QD(540), PS-QD(615) and A660 were hardly detected by fluorescence imaging (Figure 4.8). However, imaging of FRET and multiplexing using PS-QD platforms could be possible if we selected the right QD emission wavelengths vs. corresponding fluorophores and/or analyzed samples by instrumentation with better detection range.
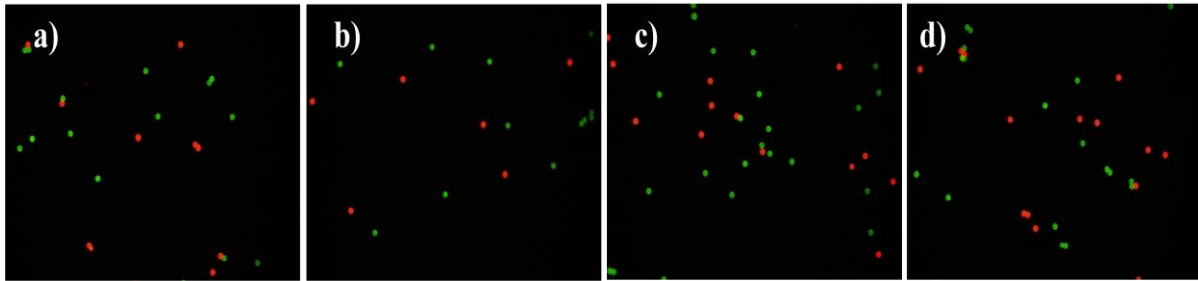
Figure 4.8 *Fluorescence images of a) PS-QD(540)-DNA1+ PS-QD(615)-DNA3, b)PS-QD(540)-DNA1-A660+PS-QD(615)-DNA3-A660, c) PS-QD(540)-DNA1-A660+PS-QD(615)-DNA3-A660 + complement1, and d) PS-QD(540)-DNA1-A660+PS-QD(615)-DNA3-A660 + complement3*

4.4 Summary

In summary, we presented for the first time the fabrication of multiplexing of QD-fluorophore FRET-based probes on microsphere surface to detect DNA. Similar to the method used in Chapter 3, we demonstrated stepwise preparation of small, stable, water soluble, and non-polymer coated QDs by ligand exchange of 16-mercaptohexadecanoic acids and attachment of synthetic his-tag peptides. Capping the QDs with histidine-containing peptides greatly increased their aqueous stability and photoluminescence properties. These QD-His particles were highly compatible with aqueous media and chemical accessibility for preparation of particle-based FRET probes. QD-His were successfully attached to polystyrene microsphere surfaces providing QD-encoded beads that showed much enhanced fluorescent signals compared to solution-based QDs. Emission spectra of QDs plus emission and absorbance spectra of Rhodamine Red and A660 fluorophores confirmed possible FRET and multiplexing interactions between QDs and the dyes. FRET from PS-QD(540) to Rhodamine Red while held together by main-ss-DNA1 was confirmed by quantitative data, fluorescence restoration of PS-QD(540), and color-changed fluorescence images before and after DNA hybridization.

To further explore multiplexing properties of the particle-based FRET probes, data of FRET signals between PS-QD(540) and PS-QD(615) to A660 were also quantified, analyzed, and confirmed. Both FRET and multiplexing occurred simultaneously in the same probe. After being hybridized with complementary DNA strands, specific fluorescence restoration of PS-QD(540) and PS-QD(615) were significant enough to be distinguished. Even though there was some unexpected fluorescence restoration of PS-QD when being incubated with non-complementary strands of DNA, signals from specific fluorescence restoration of PS-QD were still dominant. This unexpected limitation could be minimized or eliminated through careful

experimental conditions and careful designs of DNA sequences. In addition, imaging of FRET and multiplexing using PS-QD platforms could be possible if we select the right QD emission wavelengths vs. corresponding fluorophores and/or analyzed samples by instrumentation with better detection range. It is also feasible to multiplex more than two colors of QDs by carefully analyzing the overlapping of donor emission and acceptor absorbance. Moreover, we have identified other shortcomings which could be improved to raise the probes' sensitivity. One solution would be the utilization of more advanced equipments for individual microbead detections. We could also enhance fluorescence restoration by exploring better compatible buffer environments as well as DNA hybridization conditions.

Chapter 5

Nano-Structures from Metal Nanoparticles and Template-based Metal Nanowires Assemblies via DNA Hybridization

5.1 Introduction and objective

Atomic-sized devices present huge potential and interest for scientific technical, medical, and industrial fields. The electronic industry over the last few decades has grown tremendously since the start of smaller lithographically fabricated apparatus in silicon integrated circuits[54]. However, as we begin to build much smaller and faster electronic devices such as nano-circuits, miniaturization by lithography or so-called "top-down" approach has its own limitations compared to "bottom-up" molecular electronics. The first obvious disadvantage is that lithography itself does not work well below 50-nm patterning, which can be a problem for small detailed work of nano-circuits. Secondly, the self-assembly of individual elements as building blocks into mass production of complex nano-electronic circuits is preferred in terms of handling and production cost. This self-assembled method, indeed, remains one of the most promising methods for predicting, controlling, synthesizing, and organizing structures that are larger than molecules[228,229].

DNA has drawn significant attention for this self-assembled approach due to its extraordinary molecular recognition properties and structural features. By combining DNA's specific hybridization characteristics with individual synthetic nanometer components, we can design and develop any imaginable nano-structures. Short DNA or oligonucleotides are considered a "smart" tool to assemble components since their binding affinity can be not only be specific, complementary, and reversible, but also synthetically mismatched-designed for binding kinetics. By exploring DNA's structural properties and the unique base-complement rules,

nanoparticle positioning can be carefully controlled at the sub-nanometer scale using oligonucleotides as templates[56]. Consequently, DNA can play a major role in creating nano-architectures with applications in nano-electronic and photonic device assembly. DNA hybridization for self-assembly has been used successfully by many research groups[57-68]. Mirkin's group has presented a number of publications on colorimetric sensors via assembling of single-stranded DNA coated gold nanoparticles (AuNPs) and silver nanoparticles (AgNPs)[57-62]. Alivisatos and co-workers also published many studies of building nano-structures using discrete DNA-gold building blocks in which the number of DNA strands is controlled[63-67]. Recently, Wang and co-workers investigated photonic interaction between QDs and AuNPs connected by self-assembled DNA in discrete nanostructures[68]. However, all of these studies self-assembled only the same shape of nanomaterials, nanoparticles. As mentioned in details from Chapter 1, Mallouk and Kovtyukhova[54] explained why using metal nanowires as building blocks is a better choice compared to other nanomaterials. First, surface chemistry, length, diameter, and transport properties of metal nanowires can be precisely controlled by synthesis. Secondly, their low resistivity and established coupling chemistry are more advanced than carbon nanotubes and semiconductor nanowires. Furthermore, synthesizing the metal nanowires by porous template-based approach is preferred over other methods due to simplicity, low cost, uniform sizes and shapes. In 1999, Martin and co-works first developed template-synthesized micro- and nanowires for self-assembly of supermolecular architectures[230]. In this study, the authors used micro and nanowires along with nanoparticles as building blocks for their nano-structures, biotin/streptavidin chemistry and conducting polymer materials were used for component self-assembly. In addition, Mallouk and coworkers showed that thiolated single-stranded DNA could be attached precisely at the tips of template-based metal nanowires or along the nanowire at any

distance from the tips[231,232]. Because of this site-specific characterization, metal nanowires, in theory, can be assembled into any shape controllably. Despite the potential advantages, for almost a decade, little work has been done to explore much further in this specific research direction. Instead, many research groups have used DNA as templates to grow metal into nano building blocks[23,233-236]. This method, however, only provides the same kind of metal for the same building block and do not have good control over overall desired structures compared to the self-assemblies of template-based metal nanowires using DNA hybridization as a tool. Therefore, the objective of this project was, for the first time, to build simple nano-structures as electronic building blocks by using metal nanoparticles and nanowires that have selective-binding sites via DNA hybridization.

Common commercially available porous membranes including polycarbonate (PC) and anodic aluminum oxide (AAO) membranes were used as templates to produce uniform sizes and shapes of metal nanowires. Metal nanowires could be easily grown electrochemically using a metal cathode and a metal anode inside a metal plating solution. The metal anode in this case was the porous membrane that was metal-coated on its back side. To obtain gold or nickel nanowires, either gold or silver would be coated on the back side of the membranes. To obtain silver nanowires, on the other hand, only gold should be coated on the back side of the membranes. During the process of electrodeposition, metal ions suspended in the plating solution migrated under the influence of the electric field and were deposited onto the metal anode, or the metal-coated porous membrane. As metal ions were deposited into the pores, metal nanoparticles were formed on top of one another. Eventually, the aggregated metal nanoparticles grew vertically into metal nanowires with diameters corresponding to the pore sizes. The length

of these nanowires could be controlled by manipulating deposition time. Metal nanoparticles were obtained from commercial sources.

To achieve the project's objective, first, we fabricated metal nanowires electrochemically before attaching thiolated oligonucleotides onto the nanowire tips. Thiol interaction with metal surface is by far the most well-established method. It has attracted great interest due to the formation of well-organized self-assembled monolayers[237-244]. Our custom oligonucleotides were thiolated at 5' end for this purpose. Each strand was only 13-base-pairs long, including 3 base pairs as spacer that could be attached to a metal surface through a thiol linker. Table 1 (Chapter 2) includes the four thiolated single-stranded oligonucleotides that were used in this project: oligo1, oligo2, oligo3, and oligo4. Oligo1and oligo2 are complementary to each other and similarly for oligo3 and oligo4. As two different metal surfaces were coated with complementary strands of the above oligonucleotides, hybridization between the strands took place to assemble the metal surfaces together. To ensure that either metal nanoparticle or nanowire would be assembled at the tip of another nanowire, thiolated oligonucleotides were attached while the metal nanowires were still intact inside the membrane used for templated synthesis of the wire. Then the membrane was dissolved away leaving the metal nanowires with attached oligonucleotides at their tips for later DNA hybridization. As a result, the products of this design were metal nanoparticles or metal nanowires attached to one of the tips of the template-based metal nanowires.

To achieve other nano-structures for electronic building blocks, we intended to leave the other tip of the nanowires available for other nanocrystal attachments. Before attaching oligonucleotides to this tip of the nanowires, we had to remove the metal coating layer of the membranes. Since we encountered various metals that were coated in the back of the porous

membranes, removing the metal coating layers could significantly interfere with or completely dissolve the nanowire structures. Therefore, we explored another route of fabricating metal nanowires without involving the back coatings. Indeed, metal nanowires can also be grown chemically. One of the most popular wet chemical approaches involved the reduction of seeding metal nanoparticles to grow metal nanowires under ambient conditions[245,246]. Particularly, gold nanorods can be grown by wet chemical reduction of gold salts involving cetyltrimethylammonium bromide (CTAB), a surfactant-based solution[247]. Most recently, Zhou and co-workers presented a protocol to fabricate metal nanowires via an ambient and surfactantless synthesis[248]. Since the authors did not employ surfactant or catalyst seed particles, extensive washing steps of using strong acid/base solvents or organic solvents to remove surfactant or catalytic metal could be avoided. In this study, we incorporate their protocol to fabricate our own metal nanowires. This is very important because our oligonucleotide-modified metal nanowires will not contact non-compatible solvents that would alter the oligonucleotides' abilities to hybridize later.

5.2 Experimental

5.2.1 Synthesis of template-based metal nanowires via electrodeposition

Both anodic aluminum oxide (or alumina) membranes and polycarbonate membranes were metal coated on one side accordingly before being electrodeposited. Copper tape was used as a stable anchor for the membranes before the membranes were placed in electrochemical cells. Polycarbonate membranes were used more often than alumina membranes in this project due to their unique characteristics when working with oligonucleotides. Alumina membranes were dissolved using 0.5 M NaOH while absolute dichloromethane (CH_2Cl_2) were used for

84

polycarbonate membranes.

Orotemp 24 gold, silver 1025 RTU, and nickel sulfamate plating solutions were used for deposition of gold, silver, and nickel nanowires, respectively. Either gold or silver could be coated on one side of the membrane for conducting purpose. Negative 0.3 mA-negative 0.9 mA current and 5-30 minutes were applied to produce desired nanowire lengths.

5.2.2 Synthesis of template-based metal nanowires via electroless deposition

Experimental procedures for synthesizing Au, Ag, and Ni nanowires were conducted following a study by Zhou et al. in 2009 with a slight modification[248]. Either an alumina or a polycarbonate membrane was mounted between a custom 2 half-cell-U-tube. Typically, one half-cell was filled with 0.1 M of corresponding metal salts ($HAuCl_4$ for Au, $AgNO_3$ for Ag, and Ni(II)nitrate hexahydrate for Ni), while the other half-cell was filled with 0.5 M of solution of $NaBH_4$ in ethanol. The two solutions were reacted at room temperature from 30-60 minutes to obtain the desired length of the metal nanowires. Then the reagents were removed and the membrane was washed off of any residue with DI water.

5.2.3 DNA attachment to nanowires

Oligo1 and/or Oligo3 (table 1) in 10 mM Tris-HCl 1 mM EDTA pH 8.0 were incubated with 50 µL TCEP solution for 30 minutes at room temperature to cleave disulfide bond (S-S) at 5' end. Meanwhile, alumina anodic oxide membrane or polycarbonate membrane containing metal nanowires were wetted with 10 mM Tris-HCl 1 mM EDTA pH 8.0 for at least 30 minutes. Then thiolated oligos were incubated at 100:1 to number of metal nanowires for 2 hours at room temperature. DNA was conjugated to metal nanowires while they were still intact inside the

membrane to ensure that DNA only located on the tips of the wires. After DNA attachment, the sample was washed with DI water thoroughly and let air dry before being dissolved extensively in 50 mM NaOH for alumina anodic oxide membrane and CH_2Cl_2 for polycarbonate membrane to completely remove the membrane. After the membrane was dissolved away, nanowires containing DNA were resuspended in 10 mM Tris HCl 1 mM EDTA pH 8.0.

5.2.4 DNA attachment to nanoparticles

Oligo2 and/or oligo4 (table 1) in 10 mM Tris-HCl 1 mM EDTA pH 8.0 were incubated with 50 µL TCEP solution for 30 minutes at room temperature to cleave disulfide bond (S-S) at 5' end. 1,500:1 ratio[249] of thiolated DNA were mixed with nanoparticles (gold or silver). Sodium dodecyl sulfate (SDS) was added to bring the mixture to 0.01% of SDS and phosphate buffer was added to bring the mixture to 10 mM of phosphate buffer. The mixture was vortexed before being incubated at room temperature for 2 hours.

5.2.5 DNA hybridization

2:1 or more ratio of DNA conjugated nanoparticles were incubated to metal nanowires for at least 2 hours at room temperature. Up to 100 mM of NaCl was added to increase ionic strength. Sample was washed with DI water before being prepared for SEM imaging.

5.3 Results and Discussions

5.3.1 SEM imaging

Figure 5.1 and Figure 5.2 show the presence of electrochemical prepared standing Au nanowires after PC and AAO membranes were dissolved away. The nanowires were uniform in

diameter due to uniform pore sizes of the membranes. Their lengths were manipulated to desired

scale by simply controlling deposition time. Figure 5.1 indicates that even though intensive

washing of PC membrane was done with dichloromethane (CH_2Cl_2), there was still some

polycarbonate material left around the bottom of the nanowires. On the other hand, sodium

hydroxide (NaOH) at concentration of 3M removed AAO membrane completely (Figure 5.2),

the whole structure of the metal nanowires from top to bottom was clearly shown. EDS data

show the presence of Au element, which indicates the nanowires are Au nanowires.
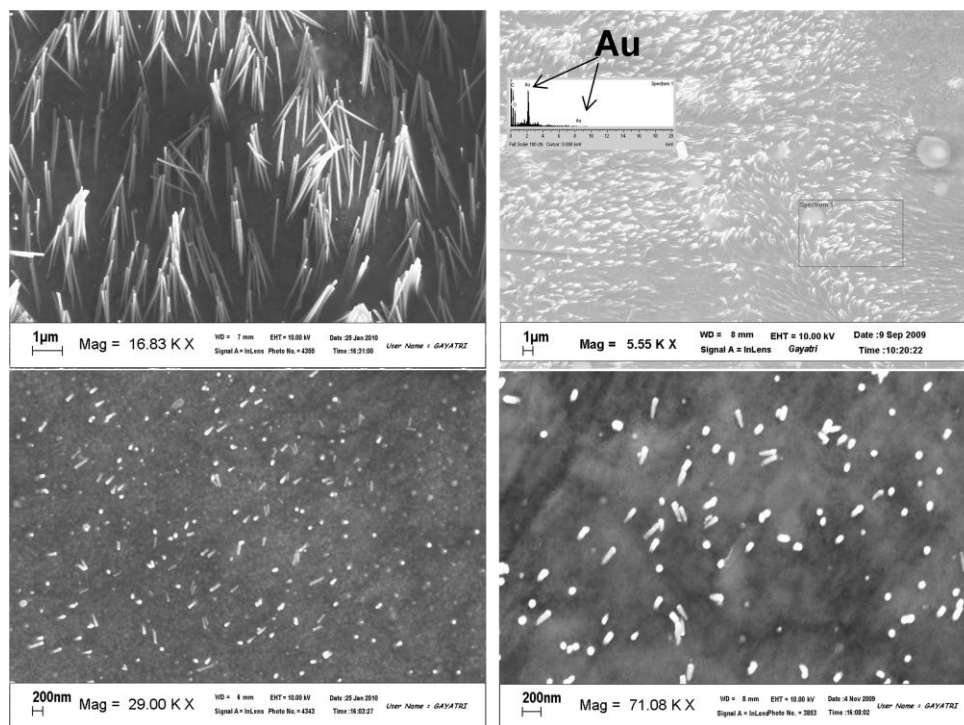
Figure 5.1 *SEM images of different lengths of standing Au nanowires grown from porous polycarbonate membranes. The membrane was dissolved away by dichloromethane. The pore size of the membrane is 30 nm. EDS data indicate the presence of Au element.*
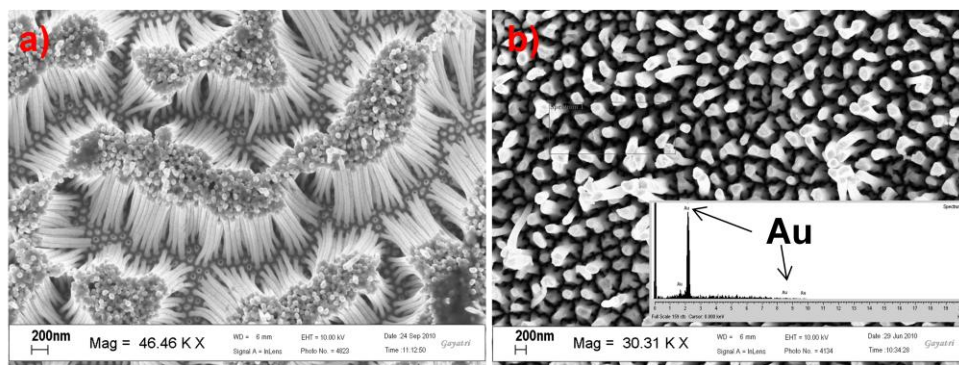
Figure 5.2 *SEM images of different lengths and diameters of standing Au nanowires grown from alumina membranes. The pore sizes of the membranes are a) 40 nm and b) 200 nm. EDS data indicate the presence of Au element.*

Figure 5.3 demonstrates that Au nanoparticles were attached on the tips of standing electrochemical and PC-templated Au nanowires. The image clearly shows the barrier between a gold nanowire and a monodisperse gold nanoparticle. This indicates that oligonucleotides were selectively attached to the tips of the Au nanowires. It also confirms the hybridization of complementary oligonucleotides that were used to modify the Au nanoparticles and the Au nanowires. EDS data confirm the presence of just Au element, which is an indication of both Au nanowires and Au nanoparticles.
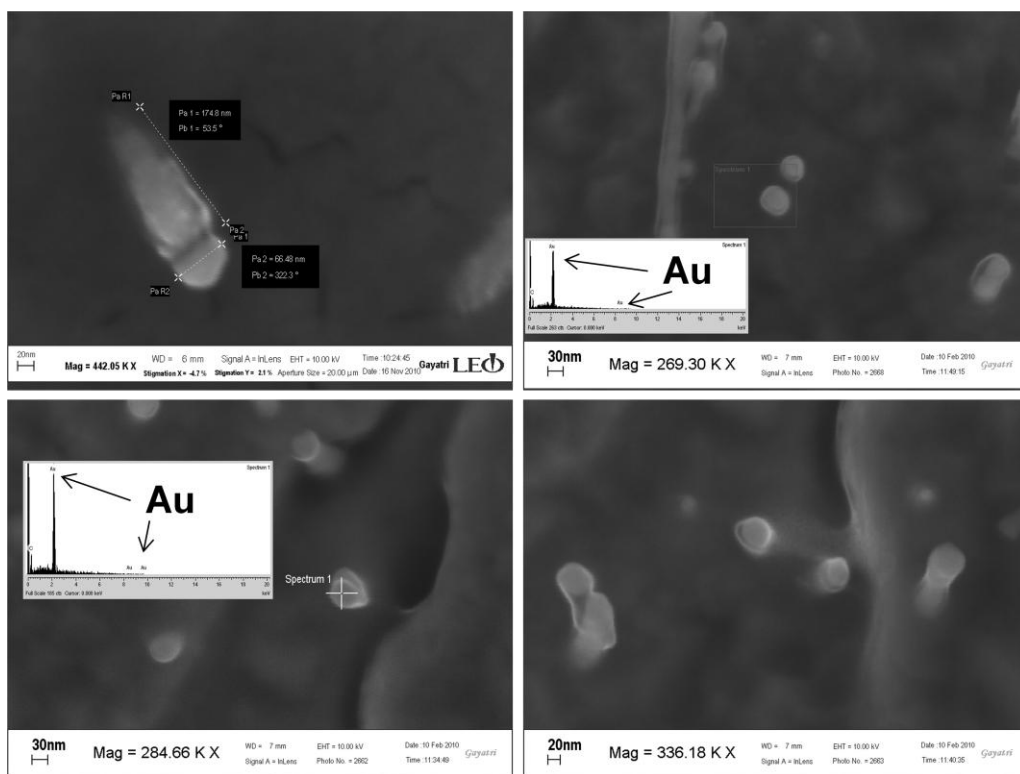
Figure 5.3 *SEM images of Au nanoparticles attached to the tips of standing electrochemical PC-templated Au nanowires. EDS data indicate the presence of Au element.*

Figure 5.4 illustrates that some individual Ag nanoparticles were connected to the tips of electrochemical and PS-templated Ni nanowires. However, it also shows that most of oligonucleotide-modified Ag nanoparticles were aggregated to form large Ag nano-clusters instead of monodisperse individual particles like oligonucleotide-modified Au nanoparticles in Figure 5.3.   We found that Ag nanoparticles tend to be easily aggregated when being surface-modified compared to Au nanoparticles. Indeed, it was reported by Cao and coworkers that Ag nanoparticles cannot be effectively passivated by alkylthiol-modified-oligonucleotides using the established protocols for modifying Au nanoparticles[250].   The authors figured the difference in mono-dispersion between oligonucleotide-modified Au nanoparticles Ag nanoparticles experimentally. From their conclusion, we believe that Ag nanoparticle surface could only be partially coated with thiolated oligonucleotides. Consequently, after the original citrate ligands

89

were exchanged with some oligonucleotides, the Ag nanoparticle surfaces lost their balance between negative-charge repulsion and attractive forces (which had made Ag nanoparticles monodisperse) and became aggregated. However, those nano-clusters clearly located at the tips of nanowires as intended. This indicates the DNA hybridization between oligonucleotides on the Ni nanowires and the Ag nano-clusters. In addition, EDS data show the presence of silver and nickel elements as in Ag nanoparticles and Ni nanowires respectively. Figure 5.4 also illustrates that not all the Ni nanowires were attached with an Ag nano-cluster even though excess molar ratio of oligonucleotide-modified Ag nanoparticles were incubated with Ni nanowires. This is simply because most of Ag nanoparticles were aggregated together which reduced the total number of individual Ag nanoparticles compared to that of Ni nanowires.
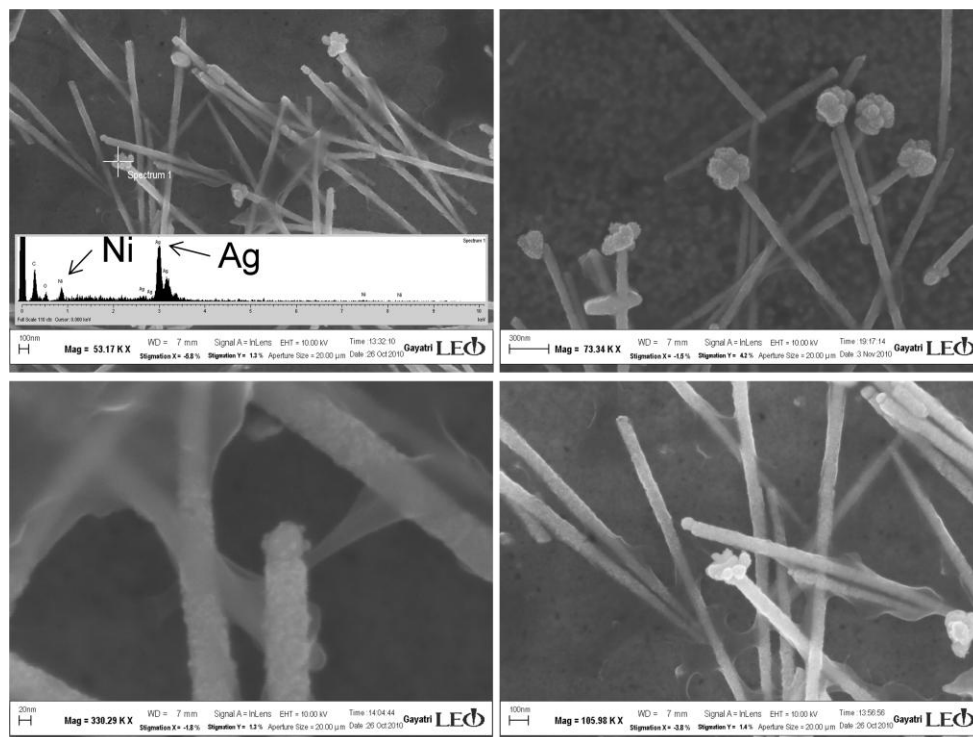
Figure 5.4 *SEM images of monodisperse Ag nanoparticles and Ag nano-clusters attached to the tips of electrochemical PC-templated Ni nanowires. EDS data indicate the presence of Ag and Ni elements.*
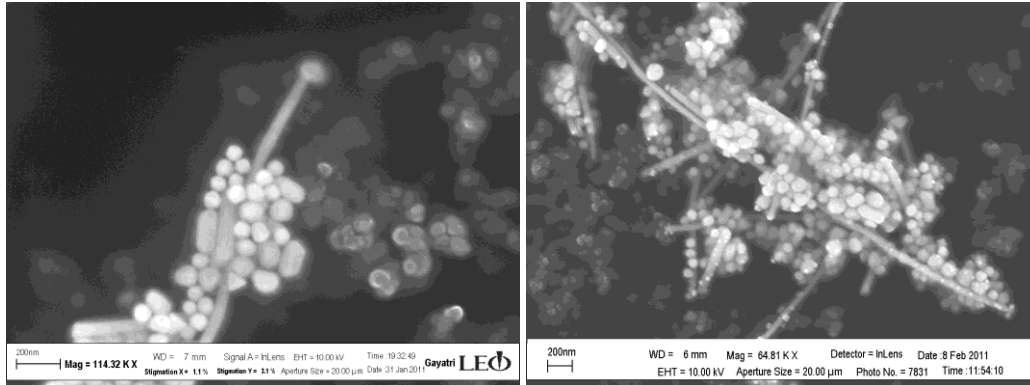
Figure 5.5 *SEM images of Au nanoparticles attached to the tips of chemical-Ni nanowires*

In Figure 5.5, Ni nanowires were fabricated chemically using PC membrane via homemade U-tube. Besides locating at the tips of the Ni nanowires, Au nanoparticles were clearly attached along the side of the nanowires as well. This indicated that thiolated oligonucleotides were bound along the side of the Ni nanowires. That happened because the nanowires were not fully deposited to fill up membrane pores, leaving void space around the side of the nanowires for thiolated oligonucleotides to attach. This limitation could be reduced by exploring solvents or a combination of solvents to constrict the pores of PC membranes which containing metal nanowires before the PC membrane is incubated with thiolated oligonucleotides.

5.4 Summary

We demonstrated stepwise fabrication of self-assembled template-based metal nanowires and/or metal nanoparticles using DNA hybridization as linkers. SEM images revealed that different metal nanowires were successfully synthesized electrochemically and chemically using

polycarbonate membranes and alumina membranes as templates. EDS data confirmed the presence of the proposed metal nanocrytals. So far, only polycarbonate (PC) membranes provided intended structures of metal nanoparticles on the tips of metal nanowires. Therefore, synthesis conditions needed to be carefully explored to fabricate other possible nano-structures. The success from PC membrane-based structures indicates that oligonucleotides which were attached to metal nanowires grown from PC membranes retained their necessary characteristics for self-assembled hybridization after the PC membranes were dissolved away. On the other hand, the lack of metal nanoparticles on the tips of metal nanowires grown from anodic aluminum oxide (AAO) membranes specifies that the structures of the attached DNA were altered somehow after the AAO membranes were etched away. Solvents that were used to dissolve PC and AAO membranes were believed to play an important role in altering the structures of attached DNA. Since chloroform and dichloromethane, which were used to dissolve PC membrane, were compatible with DNA, their presence did not affect the necessary characteristics for DNA hybridization. In contrast, sodium hydroxide, which was used to dissolve AAO membrane, could hydrolyze oligonucleotides and alter their structures. As a result, there was no DNA hybridization to self-assemble metal nanoparticles on the tips of metal nanowires grown from AAO membranes. By exploring compatible solvents or a combination of solvents that interact with PC and AAO membranes, we think that oligonucleotides can show their full potential as a smart tool to provide possible nano-structures for nano-electronic circuits through hybridization as envisioned. The possible complex nano-structures are dumbbell structures from one metal nanowire and two metal nanoparticles, T-junction structures from a triangle metal nanocrystal and three different metal nanowires, and even molecular switches from different type of metal nanocrystals and semiconductor nanocrystals.

Since self-assembling metal crystals using DNA hybridization as building blocks for nano-electronic circuits has only been done in our lab, our preliminary results are important for the following reasons. First, it provided straight forward stepwise methods for preparing specific and controllable self-assemblies of building blocks for nano-electronic circuits using DNA hybridization. Second, it showed that synthetic oligonucleotides as short as 13-base pairs can be used to modify the surface of various metal nanocrystals through thiol interaction. Third, the synthetic oligonucleotides can hybridize to their synthetic complementary so that counter oligonucleotide-modified metal nanocrystals can self-assemble to one another. Finally, by exploring DNA's structural properties and the unique base-complement rules this method opens up opportunities to specific, controllable, and simultaneous self-assemblies of extreme complex nano-structures of hundreds or even thousands of various material nano-components using DNA hybridization for nano-electronic circuits.

Chapter 6
Summary and Conclusions

A countless number of scientific studies in the field of nanosciences and nanotechnology have been carried out successfully in the last few decades pointing to a bright future for the field. As commercial applications of nanoscience and nanotechnology emerge through technology and transfer from academia to industry, the field has been gaining public recognition[2,3]. Since Feynman's first suggestion of fabricating nano-devices from nano building blocks back in 1959[1], the field has advanced dramatically. Combining synthetic nano building blocks like metal nanoparticles and semiconductor nanocrystals with biomolecules like proteins and nucleic acids led to unique nanoconjugates that could be used in a wide range of exciting optical [4-9,18,251], biomedical[10-17], and electronic[18-23,251,252] fields. The goal of many research projects that aim to develop such fields in nanotechnology therefore has been to design, synthesize such nano-component building blocks, and fabricate functional nano-scale devices from some or all of these basic components. However, the accomplishments so far in this research direction still need to be explored and studied extensively to meet Feynman's first envision of functional nano-devices. With research experience in optical and magnetic nanomaterials for biomedical applications during the last decade[12,24-27], our lab has also explored, designed, and develop nano-devices to apply in such fields. The major objective of this PhD research was to design and develop nanoconjugates that combine luminescent quantum dots (QDs) and metal nanowires with biomolecules to form a new generation of nanometric probes for optical, biomedical, and electronic applications. Our accomplishments and challenges we encountered were described in this dissertation.

One of the most desirable characteristics of luminescent semiconductor CdSe/ZnS QDs are their ability to serve as donor fluorophores in fluorescence resonance energy transfer (FRET) Direct excitation of acceptor molecules has been a problem in conventional FRET studies that involve molecular donor and acceptors. The use of QD donors alleviate this problem since luminescent QDs are characterized with broad excitation and narrow and symmetrical emission peaks. When used in FRET studies it is possible to excite the luminescent QDs with an excitation wavelength that is sufficiently removed from the excitation peaks of the acceptor molecules, thus preventing bleeding between the QD donors and molecular acceptors. Recently, there have been studies that go beyond traditional FRET publications and explore into the interactions between QDs and metal surfaces called surface energy transfer (SET). The SET process describes as non-radiative quenching of the QD emission by proximal metal surface. These studies allow better understanding of energy transfer of QDs to outside environment. There have been many successful research applications using luminescent QDs as donors in FRET and SET assays, including in our laboratory[15,17,32,253-255]. In these applications, nanoconjugates of QDs and molecular acceptors were used in homogeneous assays and were limited by the chemical and photostability of the linked organic molecules. This limitation was overcome in this PhD research through the attachment of QD-acceptor conjugates to the surface of biocompatible microspheres. Molecular acceptors were replaced with gold nanocrystals as acceptors to improve the photochemical stability of the nanoconjugates. The covalent attachment of hundreds of luminescent CdSe/ZnS QDs to a single microsphere resulted in very high brightness and considerably enhanced signal-to-noise ratio in FRET assays than the signal to noise level obtained in homogeneous FRET assays involving QD donors and molecular acceptors. Chapter 3 of this dissertation discusses the fabrication of luminescent polystyrene particles (PS) through

95

the covalent attachment of CdSe/ZnS luminescent QDs and gold nanocrystals (AuNP) to the

surface of the particles to form PS-QD-AuNP composite particles suitable for SET assays.

CdSe/ZnS luminescent QDs were synthesized and capped with trioctyl phosphine oxide (TOPO)

ligands following standard protocols[223-225]. To facilitate their covalent attachment to the

polystyrene microsphere surface the hydrophobic TOPO ligands were replaced with mercapto-

carboxylic acid (16-MHDA) molecules through a ligand exchange process to enable QDs

aqueous solubility. This particular ligand was chosen because it is least susceptible to oxidation

among thiol-based ligands. To further increase the aqueous solubility of the QDs we covalently

attached to the MHDA-modified QDs surface a synthetic polyhistidine peptide to form QD-His

conjugate. This his-tag layer had been shown to increase functionality and stability of thiol

ligand-coated QDs[42,197-199]. Furthermore, spectroscopic measurements indicated that QD-His has

higher emission quantum yield compared to QD-MHDA, probably due to more complete ligand

coverage on the QDs surface. Our histag peptide ligand was designed to contain two lysine

amino acids at the N-terminal and two glutamate amino acids at the C-terminal of the peptide.

This increased the density of amine and carboxylic groups on the QD surface, which increases

their aqueous stability and provides opportunities for subsequent coupling chemistry. QD-His

were covalently attached to the polystyrene particles and the resulting PS-QD microparticles

were intensely luminescent. The luminescence signal-to-noise ratios of the PS-QD particles were

significantly higher than the fluorescence signal-to-noise ratio of polystyrene particles that were

modified with organic fluorophores (PS-FL). Unlike in PS-QD, the fluorescence of PS-FL

particles is limited by the maximum density of organic fluorophores on the surface of the

microparticles. Excess density of fluorophores on the microparticles' surface results in

fluorescence quenching of the PS-PL particles. QD-PS particles were mono-dispersed in aqueous

solutions with minimal or no noticeable aggregation. The strong emission of the PS-QD particles was completely quenched when gold nanoparticles were attached to the PS-QD surface due to SET between the QD (donor) and the gold nanoparticles (AuNP) (quencher, acceptor). The emission of the PS-QD-AuNP conjugates was restored when the PS-QD-AuNP conjugates were incubated with DTT which displaced the AuNP from the surface of the microparticles. Continuing studies in our laboratory aim to apply this unique SET sensing platform to detect specific targets of biomedical interest.

The luminescence wavelength of semiconductor QDs depends largely on their diameter with smaller particles emitting blue light (short wavelength) while larger particles emitting red light (long wavelength). The narrow luminescent peaks are easily resolved spectrally and it is possible to excite QDs of multiple diameters and emission wavelengths with a single excitation source. These unique characteristics make luminescent QDs amenable to multiplexed assays. Chapter 4 discusses the development of above composite polystyrene particles that contain QDs and molecular acceptors on their surface and their application in multiplexed assays on DNA oligonucleotides. To identify oligonucleotides, self-assembly of DNA hybridization was chosen for its specificity in bioapplications. Compared to the last chapter, acceptors in this study were still intact connecting to donors via DNA linkers after recognizing targeted oligonucleotides. Since FRET was more sensitive than SET and detection range was within 10 nm, FRET pair on microsphere platform was a clear choice for this targeted-oligonucleotide study. In other words, the acceptors were organic fluorophores instead of AuNPs. The excitation wavelength was selected at 400 nm to avoid direct exciting of the fluorophores. As FRET occurred between PS-QD(540) and Rhodamine Red fluorophore, fluorescence images confirmed the color overlapping of QDs and Rhodamine emission. To further improve the assay by incorporating multiplexing to

unique characteristics of FRET QD donors and fluorophore acceptors, we chose A660 fluorophore so that its absorbance was wide enough to accommodate at least two well-separated QD emission wavelengths, 540-nm and 615-nm. As a result, both FRET and multiplexing could occur simultaneously. The emission spectra analysis indicated that both FRET and multiplexing took place between PS-(540) and PS-QD(615) and A660. After being hybridized with complementary DNA strands, specific fluorescence restoration of PS-QD(540) and PS-QD(615) was significant enough to be distinguished. Even though there was some unexpected fluorescence restoration of PS-QD when the probes were incubated with non-complementary DNA strands, signals from specific fluorescence restoration of PS-QD were still dominant. Unfortunately, captured images of FRET and multiplexing between A660 and PS-QD platforms did not distinguish color changes of QDs emission.

The ability to self-assemble individual elements as building blocks into mass production of complex nano-electronic circuits is preferred over miniaturization by lithography or so-called "top-down" approach in terms of handling and producing cost. Among different potential individual elements, metal nanowires are favored because their surface chemistry, length, diameter, and transport properties can be precisely controlled by synthesis. Furthermore, metal nanowires have low resistivity and established coupling chemistry, which is desired in nano-circuit self-assembly compared to other materials such as carbon nanotubes or semiconductor nanowires. Short DNA or oligonucleotides are ideal to be used as linkers to connect individual nano-components because they are specific, complementary, and reversible. Chapter 5 discussed the fabrication of nano-structures using metal nanowires and nanoparticles as building blocks. All components were self-assembled specifically using DNA hybridization as a tool. SEM images revealed metal nanowires were synthesized by template-based approach

electrochemically and chemically. By attaching oligonucleotides to metal nanowires incorporated in a template, oligonucleotides were restricted to be on the tips of the metal nanowires. Next, dissolving the template allowed nanowires that were tagged with hybridizable DNA to be in a position-specific manner. SEM images confirmed that various metal nanoparticles were attached only on the tips of various metal nanowires. EDS showed the presence of proposed nanocrystals. So far, only one nano-structure, in which metal nanoparticles were specifically self-assembled to the tips of PC template-based metal nanowires, was successfully fabricated. Other structures, including self-assembled dumb-bell structures of one metal nanowire with two metal nanoparticles or two metal nanowires and T-junctions or molecular switches of different metal nanowires, are still being explored and developed.

In conclusion, this dissertation has discussed the design, synthesis of synthetic nano building blocks like metal nanoparticles and semiconductor nanocrystals with biomolecules like proteins and nucleic acids, and fabrication of functional nano-scale devices in nanotechnology, to be applied in the optical, biomedical, and electronic fields. Chapter 3 discussed the success of the first project by demonstrating the development of a new generation of QD-based energy transfer probes. The fabrication of QD-AuNP nanoconjugates on biocompatible polystyrene microspheres permits quantitative SET studies and optical imaging. This approach enables new possibilities to carry out SET and FRET assays in microparticle-based microarrays. Data analysis and fluorescence images clearly showed emission of PS-QD was quenched and restored when the AuNPs were attached to and then removed from the surface as intended. The nano-components in this project were QD, AuNP, and histag peptide. Chapter 4 discussed the accomplished goals of the second project by designing and developing multiplexing of PS-QD-DNA-A660 FRET-based probes for DNA detection. The probe incorporated both FRET and

multiplexing between QDs and A660 fluorophores via hairpin oligonucleotides. Data analysis evidently indicated multiplexing and FRET transferred from PS-QD(540) and PS-QD(615) to A660. After being hybridized with complementary DNA strands, specific fluorescence restoration of PS-QD(540) and PS-QD(615) was significant enough to be distinguished. Even though there was some unexpected fluorescence restoration of PS-QD when being incubated with non-complementary strands of DNA, signals from specific fluorescence restoration of PS-QD were still dominant. Fluorescence images illustrated color change and fluorescence restoration of PS-QD(540) when Rhodamine Red fluorophores came close to and moved away from the surface. The nano-components in this project were QD, histag peptide, and DNA. Consequently, the QD-based nanoconjugates from both chapters 3 and 4 permitted the probes to be utilized as optical sensors when the distance between donors and acceptors were in close proximity or far away. The differences in the distance correlated quantitatively to QD fluorescence intensity. Additionally, DNA-detecting probes in chapter 4 demonstrated that they function as biomedical detectors. As the targeted complementary strands of DNA were hybridized with the probes, specific fluorescence restorations took place. Finally, to explore nanoconjugates for electronic nano-circuits, simple nano-structures were designed and self-assembled in chapter 5. This chapter discussed stepwise specific self-assemblies of metal nanoparticles and metal nanowires via DNA hybridization. SEM images and EDS analysis indicated the presence of the intended nanoconjugate structures. These structures illustrated the successful metal based-nanoconjugates for nano-circuits. Metal nanocrystals and DNA were the nano-components in this project. As all three chapters pointed out, the major objective of this PhD research, which was to design and develop nanoconjugates utilized in nanotechnology, specifically in optical, biomedical, and electronic fields, was successfully achieved.

Even though the goals were successfully accomplished in Chapters 3, 4 and 5, the probes can still be further improved. Both FRET and multiplexing signals from the DNA-biomedical detector nanoconjugates of chapter 4 could be enhanced and more specific for each color of QDs by creating compatible experimental conditions and careful designs of DNA sequences. In addition, fluorescence images of the FRET and multiplexing nanoconjugates could be distinguishable if we select the right QD emission wavelengths vs. corresponding fluorophores and/or analyze the probes using instruments with better detection range. Although the obtained nano-structures for electronic nano-circuits were fabricated by self-assembling among different metals via DNA hybridization, only one desired structure was achieved. However, with careful DNA sequence designs and proper experimental conditions, we would be able to build other complex nano-structures.

References

(1)   Stoddart, J. F. *Accounts of Chemical Research* **2001**, *34*, 410.

(2)   Schmid, G. *Nanotechnology: Volume 1: Principles and Fundamentals*; Wiley-VCH, 2008.

(3)   Ozin, G. A.; Arsenault, A. C. *Nanochemistry: A Chemical Approach to Nanomaterials*; 1st ed.; Royal Society of Chemistry, 2005.

(4)   Sugawara, M.; Mukai, K.; Nakata, Y.; Ishikawa, H.; Sakamoto, A. *Phys. Rev. B: Condens. Matter Mater. Phys.* **2000**, *61*, 7595.

(5)   Su, H.; Li, H.; Zhang, L.; Zou, Z.; Gray, A. L.; Wang, R.; Varangis, P. M.; Lester, L. F. *IEEE Photonics Technol. Lett.* **2005**, *17*, 1686.

(6)   Sadeghi, S. M. *Nanotechnology* **2009**, *20*, 225401/1.

(7)   Zhang, X.; Liu, H.; Tian, J.; Song, Y.; Wang, L.; Song, J.; Zhang, G. *Nanotechnology* **2008**, *19*, 285202/1.

(8)   Xu, X.; Georganopoulou, D. G.; Hill, H. D.; Mirkin, C. A. *Anal. Chem. (Washington, DC, U. S.)* **2007**, *79*, 6650.

(9)   Chen, C.-W.; Wang, C.-H.; Cheng, C.-C.; Wei, C.-M.; Chen, Y.-F. *J. Phys. Chem. C* **2011**, *115*, 1520.

(10)   Rosi, N. L.; Giljohann, D. A.; Thaxton, C. S.; Lytton-Jean, A. K. R.; Han, M. S.; Mirkin, C. A. *Science (Washington, DC, U. S.)* **2006**, *312*, 1027.

(11)   Smith, R. A.; Sewell, S. L.; Giorgio, T. D. *Int. J. Nanomed.* **2008**, *3*, 95.

(12)   Shi, L.; Rosenzweig, N.; Rosenzweig, Z. *Anal. Chem.* **2007**, *79*, 208.

(13)   Kyrsting, A.; Bendix, P. M.; Stamou, D. G.; Oddershede, L. B. *Nano Lett.* **2011**, *11*, 888.

(14)   Pissuwan, D.; Niidome, T.; Cortie, M. B. *J. Controlled Release* **2011**, *149*, 65.

(15)   Li, X.; Qian, J.; Jiang, L.; He, S. *Appl. Phys. Lett.* **2009**, *94*, 063111/1.

(16)   Liang, G.-X.; Pan, H.-C.; Li, Y.; Jiang, L.-P.; Zhang, J.-R.; Zhu, J.-J. *Biosens. Bioelectron.* **2009**, *24*, 3693.

(17)   Pons, T.; Medintz, I. L.; Sapsford, K. E.; Higashiya, S.; Grimes, A. F.; English, D. S.; Mattoussi, H. *Nano Lett.* **2007**, *7*, 3157.

(18)   Cui, Y.; Bjoerk, M. T.; Liddle, J. A.; Soennichsen, C.; Boussert, B.; Alivisatos, A. P. *Nano Lett.* **2004**, *4*, 1093.

(19)   Leschkies, K. S.; Divakar, R.; Basu, J.; Enache-Pommer, E.; Boercker, J. E.; Carter, C. B.; Kortshagen, U. R.; Norris, D. J.; Aydil, E. S. *Nano Lett.* **2007**, *7*, 1793.

(20)   Lee, W.; Min, S. K.; Dhas, V.; Ogale, S. B.; Han, S.-H. *Electrochem. Commun.* **2009**, *11*, 103.

(21)   Gorelik, L. Y.; Voinova, M. V. *Biosens. Bioelectron.* **2006**, *22*, 405.

(22)   Deng, J.; Song, Y.; Wang, Y.; Di, J. *Biosens. Bioelectron.* **2010**, *26*, 615.

(23)   Liu, J.; Geng, Y.; Pound, E.; Gyawali, S.; Ashton, J. R.; Hickey, J.; Woolley, A. T.; Harb, J. N. *ACS Nano* **2011**, *5*, 2240.

(24)   Ji, J.; Rosenzweig, N.; Griffin, C.; Rosenzweig, Z. *Analytical Chemistry* **2000**, *72*, 3497.

(25)   De Paoli, V. M.; De Paoli Lacerda, S. H.; Spinu, L.; Ingber, B.; Rosenzweig, Z.; Rosenzweig, N. *Langmuir* **2006**, *22*, 5894.

(26)   McNamara, K. P.; Nguyen, T.; Dumitrascu, G.; Ji, J.; Rosenzweig, N.; Rosenzweig, Z. *Analytical Chemistry* **2001**, *73*, 3240.

(27)   Crivat, G.; Da, S. S. M.; Reyes, D. R.; Locascio, L. E.; Gaitan, M.; Rosenzweig, N.; Rosenzweig, Z. *J. Am. Chem. Soc.* **2010**, *132*, 1460.

(28)   O'Connell, P. J.; Guilbault, G. G. *Anal. Lett.* **2001**, *34*, 1063.

(29)   Benson, D. E.; Conrad, D. W.; de, L. R. M.; Trammell, S. A.; Hellinga, H. W. *Science (Washington, DC, U. S.)* **2001**, *293*, 1641.

(30)   Looger, L. L.; Dwyer, M. A.; Smith, J. J.; Hellinga, H. W. *Nature (London, U. K.)* **2003**, *423*, 185.

(31)   Jares-Erijman, E. A.; Jovin, T. M. *Nat. Biotechnol.* **2003**, *21*, 1387.

(32)   Zhang, C.-y.; Johnson, L. W. *Analytical Chemistry* **2006**, *78*, 5532.

(33)   Medintz, I. L.; Clapp, A. R.; Mattoussi, H.; Goldman, E. R.; Fisher, B.; Mauro, J. M. *Nat. Mater.* **2003**, *2*, 630.

(34)   Clapp, A. R.; Medintz, I. L.; Mauro, J. M.; Fisher, B. R.; Bawendi, M. G.; Mattoussi, H. *J. Am. Chem. Soc.* **2004**, *126*, 301.

(35)   Goldman, E. R.; Medintz, I. L.; Whitley, J. L.; Hayhurst, A.; Clapp, A. R.; Uyeda, H. T.; Deschamps, J. R.; Lassman, M. E.; Mattoussi, H. *J. Am. Chem. Soc.* **2005**, *127*, 6744.

(36)   Yun, C. S.; Javier, A.; Jennings, T.; Fisher, M.; Hira, S.; Peterson, S.; Hopkins, B.; Reich, N. O.; Strouse, G. F. *J. Am. Chem. Soc.* **2005**, *127*, 3115.

(37)   Li, X.; Qian, J.; Jiang, L.; He, S. L. *Applied Physics Letters* **2009**, *94*.

(38)   Han, M.; Gao, X.; Su, J. Z.; Nie, S. *Nat. Biotechnol.* **2001**, *19*, 631.

(39)   Wilson, R.; Spiller, D. G.; Prior, I. A.; Bhatt, R.; Hutchinson, A. *J. Mater. Chem.* **2007**, *17*, 4400.

(40)   Yezhelyev, M. V.; Al-Hajj, A.; Morris, C.; Marcus, A. I.; Liu, T.; Lewis, M.; Cohen, C.; Zrazhevskiy, P.; Simons, J. W.; Rogatko, A.; Nie, S.; Gao, X.; O'Regan, R. M. *Adv. Mater. (Weinheim, Ger.)* **2007**, *19*, 3146.

(41)   Wang, D.; Rogach, A. L.; Caruso, F. *Nano Lett.* **2002**, *2*, 857.

(42)   Medintz, I. L.; Berti, L.; Pons, T.; Grimes, A. F.; English, D. S.; Alessandrini, A.; Facci, P.; Mattoussi, H. *Nano Lett.* **2007**, *7*, 1741.

(43)   Cai, W.-Y.; Feng, L.-D.; Liu, S.-H.; Zhu, J.-J. *Adv. Funct. Mater.* **2008**, *18*, 3127.

(44)   Li, J.; Zhao, X.-W.; Zhao, Y.-J.; Gu, Z.-Z. *Chem. Commun. (Cambridge, U. K.)* **2009**, 2329.

(45)   Ma, Q.; Song, T. Y.; Yuan, P.; Wang, C.; Su, X. G. *Colloids and Surfaces B-Biointerfaces* **2008**, *64*, 248.

(46)   Dong, H. F.; Yan, F.; Ji, H. X.; Wong, D. K. Y.; Ju, H. X. *Advanced Functional Materials* **2010**, *20*, 1173.

(47)   Aviram, A.; Ratner, M. A. *Chem. Phys. Lett.* **1974**, *29*, 277.

(48)   Abruna, H. D.; Denisevich, P.; Umana, M.; Meyer, T. J.; Murray, R. W. *J. Am. Chem. Soc.* **1981**, *103*, 1.

(49)   Denisevich, P.; Willman, K. W.; Murray, R. W. *J. Am. Chem. Soc.* **1981**, *103*, 4727.

(50)   Metzger, R. M.; Chen, B.; Hoepfner, U.; Lakshmikantham, M. V.; Vuillaume, D.; Kawai, T.; Wu, X.; Tachibana, H.; Hughes, T. V.; Sakurai, H.; Baldwin, J. W.; Hosch, C.; Cava, M. P.; Brehmer, L.; Ashwell, G. J. *J. Am. Chem. Soc.* **1997**, *119*, 10455.

(51)   Collier, C. P.; Wong, E. W.; Belohradsky, M.; Raymo, F. M.; Stoddart, J. F.; Kuekes, P. J.; Williams, R. S.; Heath, J. R. *Science (Washington, D. C.)* **1999**, *285*, 391.

(52)   Chen, J.; Reed, M. A.; Rawlett, A. M.; Tour, J. M. *Science (Washington, D. C.)* **1999**, *286*, 1550.

(53)   Ohtsu, M. *Optical and Electronic Process of Nano-matters*; 1st ed.; Springer, 2001.

(54)   Kovtyukhova, N. I.; Mallouk, T. E. *Chem.--Eur. J.* **2002**, *8*, 4354.

(55)   Huang, Y.; Duan, X.; Cui, Y.; Lauhon, L. J.; Kim, K.-H.; Lieber, C. M. *Science (Washington, DC, U. S.)* **2001**, *294*, 1313.

(56)   Le, J. D.; Pinto, Y.; Seeman, N. C.; Musier-Forsyth, K.; Taton, T. A.; Kiehl, R. A. *Nano Lett.* **2004**, *4*, 2343.

(57)   Storhoff, J. J.; Elghanian, R.; Mucic, R. C.; Mirkin, C. A.; Letsinger, R. L. *J. Am. Chem. Soc.* **1998**, *120*, 1959.

(58)   Cao, Y.; Jin, R.; Mirkin, C. A. *J. Am. Chem. Soc.* **2001**, *123*, 7961.

(59)   Storhoff, J. J.; Elghanian, R.; Mirkin, C. A.; Letsinger, R. L. *Langmuir* **2002**, *18*, 6666.

(60)   Cao, Y. C.; Jin, R.; Thaxton, C. S.; Mirkin, C. A. *Talanta* **2005**, *67*, 449.

(61)   Lee, J.-S.; Lytton-Jean, A. K. R.; Hurst, S. J.; Mirkin, C. A. *Nano Lett.* **2007**, *7*, 2112.

(62)   Lee, J.-S.; Ulmann, P. A.; Han, M. S.; Mirkin, C. A. *Nano Lett.* **2008**, *8*, 529.

(63)   Zanchet, D.; Micheel, C. M.; Parak, W. J.; Gerion, D.; Alivisatos, A. P. *Nano Lett.* **2001**, *1*, 32.

(64)   Zanchet, D.; Micheel, C. M.; Parak, W. J.; Gerion, D.; Williams, S. C.; Alivisatos, A. P. *J. Phys. Chem. B* **2002**, *106*, 11758.

(65)   Claridge, S. A.; Liang, H. W.; Basu, S. R.; Frechet, J. M. J.; Alivisatos, A. P. *Nano Lett.* **2008**, *8*, 1202.

(66)   Claridge, S. A.; Mastroianni, A. J.; Au, Y. B.; Liang, H. W.; Micheel, C. M.; Frechet, J. M. J.; Alivisatos, A. P. *J. Am. Chem. Soc.* **2008**, *130*, 9598.

(67)   Mastroianni, A. J.; Claridge, S. A.; Alivisatos, A. P. *J. Am. Chem. Soc.* **2009**, *131*, 8455.

(68)   Wang, Q.; Wang, H.; Lin, C.; Sharma, J.; Zou, S.; Liu, Y. *Chem. Commun. (Cambridge, U. K.)* **2010**, *46*, 240.

(69)   Alivisatos, A. P. *Science (Washington, D. C.)* **1996**, *271*, 933.

(70)   Yoffe, A. D. *Adv. Phys.* **2001**, *50*, 1.

(71)   Chan, W. C. W.; Maxwell, D. J.; Gao, X.; Bailey, R. E.; Han, M.; Nie, S. *Curr. Opin. Biotechnol.* **2002**, *13*, 40.

(72)   Zaman, M. B.; Baral, T. N.; Zhang, J.; Whitfield, D.; Yu, K. *J. Phys. Chem. C* **2009**, *113*, 496.

(73)   Li, Z. M.; Huang, P.; He, R.; Lin, J.; Yang, S.; Zhang, X. J.; Ren, Q. S.; Cui, D. X. *Materials Letters* **2010**, *64*, 375.

(74)   Mulder, W. J. M.; Castermans, K.; van, B. J. R.; oude, E. M. G. A.; Chin, P. T. K.; Fayad, Z. A.; Loewik, C. W. G. M.; Kaijzel, E. L.; Que, I.; Storm, G.; Strijkers, G. J.; Griffioen, A. W.; Nicolay, K. *Angiogenesis* **2009**, *12*, 17.

(75)   Nurunnabi, M.; Cho, K.-J.; Choi, J.-S.; Huh, K.-M.; Lee, Y.-K. *Biomaterials* **2010**, *31*, 5436.

(76)   Wang, Y. C.; Mao, H.; Wong, L. B. *Nanotechnology* **2010**, *21*.

(77)   Banerjee, S.; Santra, S.; Cullum, B. M.; Porterfield, D. M.; Booksh, K. S. *Proc. SPIE* **2010**, *7674*, 767403/1.

(78)   Medintz, I. L.; Pons, T.; Trammell, S. A.; Grimes, A. F.; English, D. S.; Blanco-Canosa, J. B.; Dawson, P. E.; Mattoussi, H. *J. Am. Chem. Soc.* **2008**, *130*, 16745.

(79)   Zhang, B. B.; Liu, X. H.; Li, D. N.; Tian, H.; Ma, G. P.; Chang, J. *Chinese Science Bulletin* **2008**, *53*, 2077.

(80)   Rauf, S.; Glidle, A.; Cooper, J. M. *Chem. Commun. (Cambridge, U. K.)* **2010**, *46*, 2814.

(81)   Zhang, L. W.; Yu, W. W.; Colvin, V. L.; Monteiro-Riviere, N. A. *Toxicol. Appl. Pharmacol.* **2008**, *228*, 200.

(82)   Klimov, V. I. *Los Alamos Sci.* **2003**, *28*, 214.

(83)   Haugland, R. P. *Handbook of Fluorescent Probes and Research Products*; 9th ed.; Molecular Probes, Inc., 2002.

(84)   Murray, C. B.; Norris, D. J.; Bawendi, M. G. *Journal of the American Chemical Society* **1993**, *115*, 8706.

(85)   Peng, Z. A.; Peng, X. G. *Journal of the American Chemical Society* **2001**, *123*, 183.

(86)   Yu, W. W.; Qu, L. H.; Guo, W. Z.; Peng, X. G. *Chemistry of Materials* **2003**, *15*, 2854.

(87)   Hirai, T.; Watanabe, T.; Komasawa, I. *Journal of Physical Chemistry B* **1999**, *103*, 10120.

(88)   Kim, D.; Miyamoto, M.; Mishima, T.; Nakayama, M. *Journal of Applied Physics* **2005**, *98*, 4.

(89)   Farmer, S. C.; Patten, T. E. *Chemistry of Materials* **2001**, *13*, 3920.

(90)   Ponomareva, K. Y.; Kosobudsky, I. D.; Tret'yachenko, E. V.; Yurkov, G. Y. *Inorganic Materials* **2007**, *43*, 1160.

(91)   Wang, W. Y.; Liu, J.; Yu, X. B.; Yang, G. Q. *Journal of Nanoscience and Nanotechnology* **2010**, *10*, 5196.

(92)   Zelner, M.; Minti, H.; Reisfeld, R.; Cohen, H.; Feldman, Y.; Cohen, S. R.; Tenne, R. *Journal of Sol-Gel Science and Technology* **2001**, *20*, 153.

(93)   Julian, B.; Planelles, J.; Cordoncillo, E.; Escribano, P.; Aschehoug, P.; Sanchez, C.; Viana, B.; Pelle, F. *Journal of Materials Chemistry* **2006**, *16*, 4612.

(94)   Gaponik, N.; Talapin, D. V.; Rogach, A. L.; Eychmuller, A.; Weller, H. *Nano Letters* **2002**, *2*, 803.

(95)   Lesnyak, V.; Lutich, A.; Gaponik, N.; Grabolle, M.; Plotnikov, A.; Resch-Genger, U.; Eychmuller, A. *Journal of Materials Chemistry* **2009**, *19*, 9147.

(96)   Nirmal, M.; Dabbousi, B. O.; Bawendi, M. G.; Macklin, J. J.; Trautman, J. K.; Harris, T. D.; Brus, L. E. *Nature (London)* **1996**, *383*, 802.

(97)   Hines, M. A.; Guyot-Sionnest, P. *J. Phys. Chem.* **1996**, *100*, 468.

(98)   Dabbousi, B. O.; Rodriguez-Viejo, J.; Mikulec, F. V.; Heine, J. R.; Mattoussi, H.; Ober, R.; Jensen, K. F.; Bawendi, M. G. *J. Phys. Chem. B* **1997**, *101*, 9463.

(99)   Li, J. J.; Wang, Y. A.; Guo, W.; Keay, J. C.; Mishima, T. D.; Johnson, M. B.; Peng, X. *J. Am. Chem. Soc.* **2003**, *125*, 12567.

(100)   Mattoussi, H.; Mauro, J. M.; Goldman, E. R.; Anderson, G. P.; Sundar, V. C.; Mikulec, F. V.; Bawendi, M. G. *J. Am. Chem. Soc.* **2000**, *122*, 12142.

(101) Jaiswal, J. K.; Mattoussi, H.; Mauro, J. M.; Simon, S. M. *Nat. Biotechnol.* **2003**, *21*, 47.

(102) Zimmer, J. P.; Kim, S.-W.; Ohnishi, S.; Tanaka, E.; Frangioni, J. V.; Bawendi, M. G. *J. Am. Chem. Soc.* **2006**, *128*, 2526.

(103) Vannoy, C. H.; Xu, J.-M.; Leblanc, R. M. *J. Phys. Chem. C* **2010**, *114*, 766.

(104) Pathak, S.; Choi, S.-K.; Arnheim, N.; Thompson, M. E. *J. Am. Chem. Soc.* **2001**, *123*, 4103.

(105) Banerjee, S.; Kar, S.; Santra, S. *Chem. Commun. (Cambridge, U. K.)* **2008**, 3037.

(106) Duncan, T. V.; Mendez, P. M. A.; Kim, Y.; Park, S.-J. *J. Phys. Chem. C* **2009**, *113*, 7561.

(107) Derfus, A. M.; Chan, W. C. W.; Bhatia, S. N. *Nano Lett.* **2004**, *4*, 11.

(108) Jeong, S. Y.; Lim, S. C.; Bae, D. J.; Lee, Y. H.; Shin, H. J.; Yoon, S.-M.; Choi, J. Y.; Cha, O. H.; Jeong, M. S.; Perello, D.; Yun, M. *Appl. Phys. Lett.* **2008**, *92*, 243103/1.

(109) Noh, M.; Kim, T.; Lee, H.; Kim, C.-K.; Joo, S.-W.; Lee, K. *Colloids Surf., A* **2010**, *359*, 39.

(110) Mulvaney, P.; Liz-Marzan, L. M.; Giersig, M.; Ung, T. *J. Mater. Chem.* **2000**, *10*, 1259.

(111) Zhou, X.; Kobayashi, Y.; Romanyuk, V.; Ochuchi, N.; Takeda, M.; Tsunekawa, S.; Kasuya, A. *Appl. Surf. Sci.* **2005**, *242*, 281.

(112) Amato, G. *Nanoscale Res. Lett.* **2010**, *5*, 1156.

(113) Bentzen, E. L.; Tomlinson, I. D.; Mason, J.; Gresch, P.; Warnement, M. R.; Wright, D.; Sanders-Bush, E.; Blakely, R.; Rosenthal, S. J. *Bioconjugate Chem.* **2005**, *16*, 1488.

(114) Warnement, M. R.; Tomlinson, I. D.; Chang, J. C.; Schreuder, M. A.; Luckabaugh, C. M.; Rosenthal, S. J. *Bioconjugate Chem.* **2008**, *19*, 1404.

(115) Wang, Y. A.; Li, J. J.; Chen, H.; Peng, X. *J. Am. Chem. Soc.* **2002**, *124*, 2293.

(116) Liu, Y.; Brandon, R.; Cate, M.; Peng, X.; Stony, R.; Johnson, M. *Anal. Chem. (Washington, DC, U. S.)* **2007**, *79*, 8796.

(117) Goldman, E. R.; Anderson, G. P.; Tran, P. T.; Mattoussi, H.; Charles, P. T.; Mauro, J. M. *Anal. Chem.* **2002**, *74*, 841.

(118) Alivisatos, P. *Nat. Biotechnol.* **2004**, *22*, 47.

(119) Michalet, X.; Pinaud, F. F.; Bentolila, L. A.; Tsay, J. M.; Doose, S.; Li, J. J.; Sundaresan, G.; Wu, A. M.; Gambhir, S. S.; Weiss, S. *Science (Washington, DC, U. S.)* **2005**, *307*, 538.

(120) Chen, C.; Peng, J.; Xia, H.-S.; Yang, G.-F.; Wu, Q.-S.; Chen, L.-D.; Zeng, L.-B.; Zhang, Z.-L.; Pang, D.-W.; Li, Y. *Biomaterials* **2009**, *30*, 2912.

(121) Xiao, Y.; Barker, P. E. *Nucleic Acids Res.* **2004**, *32*, e28/1.

(122) Mueller, S.; Cremer, M.; Neusser, M.; Grasser, F.; Cremer, T. *Cytogenet. Genome Res.* **2009**, *124*, 351.

(123) Winter, J. O.; Liu, T. Y.; Korgel, B. A.; Schmidt, C. E. *Adv. Mater. (Weinheim, Ger.)* **2001**, *13*, 1673.

(124) Rosenthal, S. J.; Tomlinson, I.; Adkins, E. M.; Schroeter, S.; Adams, S.; Swafford, L.; McBride, J.; Wang, Y.; DeFelice, L. J.; Blakely, R. D. *J. Am. Chem. Soc.* **2002**, *124*, 4586.

(125) Gu, W.; Pellegrino, T.; Parak, W. J.; Boudreau, R.; Le, G. M. A.; Alivisatos, A. P.; Larabell, C. A. *Methods Mol Biol* **2007**, *374*, 125.

(126) Akerman, M. E.; Chan, W. C. W.; Laakkonen, P.; Bhatia, S. N.; Ruoslahti, E. *Proc. Natl. Acad. Sci. U. S. A.* **2002**, *99*, 12617.

(127) Kim, S.; Lim, Y. T.; Soltesz, E. G.; De, G. A. M.; Lee, J.; Nakayama, A.; Parker, J. A.; Mihaljevic, T.; Laurence, R. G.; Dor, D. M.; Cohn, L. H.; Bawendi, M. G.; Frangioni, J. V. *Nat. Biotechnol.* **2004**, *22*, 93.

(128) Lakowicz, J. R. *Principles of Fluorescence Spectroscopy*; 2nd ed.; Springer, 1999.

(129) Bruchez, M.; Moronne, M.; Gin, P.; Weiss, S.; Alivisatos, A. P. *Science* **1998**, *281*, 2013.

(130) Chan, W. C. W.; Nie, S. M. *Science* **1998**, *281*, 2016.

(131) Wang, H. Q.; Zhang, H. L.; Li, X. Q.; Wang, J. H.; Huang, Z. L.; Zhao, Y. D. *Journal of Biomedical Materials Research Part A* **2008**, *86A*, 833.

(132) Yordanov, G.; Simeonova, M.; Alexandrova, R.; Yoshimura, H.; Dushkin, C. *Colloids and Surfaces a-Physicochemical and Engineering Aspects* **2009**, *339*, 199.

(133) Wu, Y.; Weil, T. *Polym. Prepr. (Am. Chem. Soc., Div. Polym. Chem.)* **2010**, *51*, 786.

(134) Botsoa, J.; Lysenko, V.; Geloen, A.; Marty, O.; Bluet, J. M.; Guillot, G. *Appl. Phys. Lett.* **2008**, *92*, 173902/1.

(135) Jablonski, A. E.; Humphries, W. H. I. V.; Payne, C. K. *J. Phys. Chem. B* **2009**, *113*, 405.

(136) Lei, Y.; Tang, H. Y.; Feng, M. F.; Zou, B. S. *Journal of Nanoscience and Nanotechnology* **2009**, *9*, 5726.

(137) Jemal, A.; Murray, T.; Ward, E.; Samuels, A.; Tiwari, R. C.; Ghafoor, A.; Feuer, E. J.; Thun, M. J. *Ca-a Cancer Journal for Clinicians* **2005**, *55*, 10.

(138) Jemal, A.; Siegel, R.; Ward, E.; Hao, Y. P.; Xu, J. Q.; Thun, M. J. *Ca-a Cancer Journal for Clinicians* **2009**, *59*, 225.

(139) Chen, L. D.; Liu, J.; Yu, X. F.; He, M.; Pei, X. F.; Tang, Z. Y.; Wang, Q. Q.; Pang, D. W.; Li, Y. *Biomaterials* **2008**, *29*, 4170.

(140) Medintz, I. L.; Pons, T.; Trammell, S. A.; Grimes, A. F.; English, D. S.; Blanco-Canosa, J. B.; Dawson, P. E.; Mattoussi, H. *Journal of the American Chemical Society* **2008**, *130*, 16745.

(141) Lee, K. R.; Kang, I.-J. *Ultramicroscopy* **2009**, *109*, 894.

(142) Zhang, C. Y.; Hu, J. *Analytical Chemistry* **2010**, *82*, 1921.

(143) Zhang, L. W.; Yu, W. W.; Colvin, V. L.; Monteiro-Riviere, N. A. *Toxicology and Applied Pharmacology* **2008**, *228*, 200.

(144) Geys, J.; Nemmar, A.; Verbeken, E.; Smolders, E.; Ratoi, M.; Hoylaerts, M. F.; Nemery, B.; Hoet, P. H. M. *Environmental Health Perspectives* **2008**, *116*, 1607.

(145) Jiang, X.; Ahmed, M.; Deng, Z.; Narain, R. *Bioconjugate Chem.* **2009**, *20*, 994.

(146) Lin, C. H.; Chang, L. W.; Chang, H.; Yang, M. H.; Yang, C. S.; Lai, W. H.; Chang, W. H.; Lin, P. P. *Nanotechnology* **2009**, *20*.

(147) Fu, T.; Qin, H. Y.; Hu, H. J.; Hong, Z.; He, S. L. *Journal of Nanoscience and Nanotechnology* **2010**, *10*, 1741.

(148) Wu, C. H.; Shi, L. X.; Li, Q. N.; Jiang, H.; Selke, M.; Ba, L.; Wang, X. M. *Chemical Research in Toxicology* **2010**, *23*, 82.

(149) Hauck, T. S.; Anderson, R. E.; Fischer, H. C.; Newbigging, S.; Chan, W. C. W. *Small* **2010**, *6*, 138.

(150) Tan, S. J.; Jana, N. R.; Gao, S.; Patra, P. K.; Ying, J. Y. *Chem. Mater.* **2010**, *22*, 2239.

(151) Sperling, R. A.; Parak, W. J. *Philos. Trans. R. Soc., A* **2010**, *368*, 1333.

(152) Johnson, S. R.; Evans, S. D.; Brydson, R. *Langmuir* **1998**, *14*, 6639.

(153) Newman, J. D. S.; MacCrehan, W. A. *Langmuir* **2009**, *25*, 8993.

(154) Tan, J.; Liu, R.; Wang, W.; Liu, W.; Tian, Y.; Wu, M.; Huang, Y. *Langmuir* **2010**, *26*, 2093.

(155) Debnath, R. K.; Meijers, R.; Richter, T.; Stoica, T.; Calarco, R.; Luth, H. *Appl. Phys. Lett.* **2007**, *90*, 123117/1.

(156) Solov'yov, I. A.; Geng, J.; Solov'yov, A. V.; Johnson, B. F. G. *Chem. Phys. Lett.* **2009**, *472*, 166.

(157) Wang, J.; Zhang, L. Y.; Liu, P.; Lan, T. M.; Zhang, J.; Wei, L. M.; Zhang, Y. F.; Jiang, C. H. *Nano-Micro Lett.* **2010**, *2*, 134.

(158) Zhang, F.; Wong, S. S. *ACS Nano* **2010**, *4*, 99.

(159) Chen, J.; Wiley, B. J.; Xia, Y. *Langmuir* **2007**, *23*, 4120.

(160) Jiang, C.; Kiyofumi, K.; Wang, Y.; Koumoto, K. *Cryst. Growth Des.* **2007**, *7*, 2713.

(161) Kundu, P.; Halder, A.; Viswanath, B.; Kundu, D.; Ramanath, G.; Ravishankar, N. *J. Am. Chem. Soc.* **2010**, *132*, 20.

(162) Monson, C. F.; Woolley, A. T. *Nano Lett.* **2003**, *3*, 359.

(163) Ongaro, A.; Griffin, F.; Beecher, P.; Nagle, L.; Iacopino, D.; Quinn, A.; Redmond, G.; Fitzmaurice, D. *Chem. Mater.* **2005**, *17*, 1959.

(164) Kinsella, J. M.; Ivanisevic, A. *Langmuir* **2007**, *23*, 3886.

(165) Yu, R.; Chen, L.; Liu, Q.; Lin, J.; Tan, K.-L.; Ng, S. C.; Chan, H. S. O.; Xu, G.-Q.; Hor, T. S. A. *Chem. Mater.* **1998**, *10*, 718.

(166) Ye, X.-R.; Lin, Y.; Wang, C.; Wai, C. M. *Adv. Mater. (Weinheim, Ger.)* **2003**, *15*, 316.

(167) Cao, L.; Chen, H.-Z.; Zhou, H.-B.; Zhu, L.; Sun, J.-Z.; Zhang, X.-B.; Xu, J.-M.; Wang, M. *Adv. Mater. (Weinheim, Ger.)* **2003**, *15*, 909.

(168) Yang, B.; Kamiya, S.; Shimizu, Y.; Koshizaki, N.; Shimizu, T. *Chem. Mater.* **2004**, *16*, 2826.

(169) Schaper, A. K.; Hou, H.; Treutmann, W.; Phillipp, F. *J. Metastable Nanocryst. Mater.* **2005**, *23*, 301.

(170) Huh, Y.; Shao, L.; Tobias, G.; Green, M. L. H. *J. Nanosci. Nanotechnol.* **2006**, *6*, 3360.

(171) Yu, S.; Li, N.; Wharton, J.; Martin, C. R. *Nano Lett.* **2003**, *3*, 815.

(172) Bentley, A. K.; Farhoud, M.; Ellis, A. B.; Lisensky, G. C.; Nickel, A.-M. L.; Crone, W. C. *J. Chem. Educ.* **2005**, *82*, 765.

(173) Metwalli, E.; Moulin, J. F.; Perlich, J.; Wang, W.; Diethert, A.; Roth, S. V.; Mueller-Buschbaum, P. *Langmuir* **2009**, *25*, 11815.

(174) Brumlik, C. J.; Martin, C. R. *J. Am. Chem. Soc.* **1991**, *113*, 3174.

(175) Menon, V. P.; Martin, C. R. *Anal. Chem.* **1995**, *67*, 1920.

(176) Brumlik, C. J.; Martin, C. R.; Tokuda, K. *Anal. Chem.* **1992**, *64*, 1201.

(177) Brumlik, C. J.; Menon, V. P.; Martin, C. R. *J. Mater. Res.* **1994**, *9*, 1174.

(178) Nishizawa, M.; Menon, V. P.; Martin, C. R. *Science (Washington, D. C.)* **1995**, *268*, 700.

(179) Jirage, K. B.; Hulteen, J. C.; Martin, C. R. *Anal. Chem.* **1999**, *71*, 4913.

(180) Wirtz, M.; Martin, C. R. *Adv. Mater. (Weinheim, Ger.)* **2003**, *15*, 455.

(181) Martin, C. R.; Nishizawa, M.; Jirage, K.; Kang, M. *J. Phys. Chem. B* **2001**, *105*, 1925.

(182) Gasparac, R.; Taft, B. J.; Lapierre-Devlin, M. A.; Lazareck, A. D.; Xu, J. M.; Kelley, S. O. *J. Am. Chem. Soc.* **2004**, *126*, 12270.

(183) Lapierre-Devlin, M. A.; Asher, C. L.; Taft, B. J.; Gasparac, R.; Roberts, M. A.; Kelley, S. O. *Nano Lett.* **2005**, *5*, 1051.

(184) Roberts, M. A.; Kelley, S. O. *J. Am. Chem. Soc.* **2007**, *129*, 11356.

(185) Fang, Z.; Kelley, S. O. *Anal. Chem. (Washington, DC, U. S.)* **2009**, *81*, 612.

(186) Mbindyo, J. K. N.; Mallouk, T. E.; Mattzela, J. B.; Kratochvilova, I.; Razavi, B.; Jackson, T. N.; Mayer, T. S. *J. Am. Chem. Soc.* **2002**, *124*, 4020.

(187) Hernandez, R. M.; Richter, L.; Semancik, S.; Stranick, S.; Mallouk, T. E. *Chem. Mater.* **2004**, *16*, 3431.

(188) Kratochvilova, I.; Kocirik, M.; Zambova, A.; Mbindyo, J.; Mallouk, T. E.; Mayer, T. S. *J. Mater. Chem.* **2002**, *12*, 2927.

(189) Ugo, P.; Pepe, N.; Moretto, L. M.; Battagliarin, M. *J. Electroanal. Chem.* **2003**, *560*, 51.

(190) De, L. M.; Pereira, F. C.; Moretto, L. M.; Scopece, P.; Polizzi, S.; Ugo, P. *Chem. Mater.* **2007**, *19*, 5955.

(191) Mucelli, S. P.; Zamuner, M.; Tormen, M.; Stanta, G.; Ugo, P. *Biosens. Bioelectron.* **2008**, *23*, 1900.

(192) Wildt, B.; Mali, P.; Searson, P. C. *Langmuir* **2006**, *22*, 10528.

(193) Piraux, L.; Renard, K.; Guillemet, R.; Matefi-Tempfli, S.; Matefi-Tempfli, M.; Antohe, V. A.; Fusil, S.; Bouzehouane, K.; Cros, V. *Nano Lett.* **2007**, *7*, 2563.

(194) Garrett, R. H.; Grisham, C. M. *Biochemistry*; 2nd ed.; Brooks Cole, 1999.

(195) Garrett, R. H.; Grisham, C. M. *Principles of Biochemistry With a Human Focus*; 1st ed.; Brooks Cole, 2001.

(196) Mathews, C. K.; Van Holde, K. E.; Ahern, K. G. *Biochemistry*; 3rd ed.; Prentice Hall, 1999.

(197) Delehanty, J. B.; Medintz, I. L.; Pons, T.; Brunel, F. M.; Dawson, P. E.; Mattoussi, H. *Bioconjugate Chem.* **2006**, *17*, 920.

(198) Sapsford, K. E.; Pons, T.; Medintz, I. L.; Higashiya, S.; Brunel, F. M.; Dawson, P. E.; Mattoussi, H. *J. Phys. Chem. C* **2007**, *111*, 11528.

(199) Berti, L.; D'Agostino, P. S.; Boeneman, K.; Medintz, I. L. *Nano Res.* **2009**, *2*, 121.

(200) Hu, G.; Llinas, M.; Li, J.; Preiser, P. R.; Bozdech, Z. *BMC Bioinformatics* **2007**, *8*, 350.

(201) Kinoshita, K.; Fujimoto, K.; Yakabe, T.; Saito, S.; Hamaguchi, Y.; Kikuchi, T.; Nonaka, K.; Murata, S.; Masuda, D.; Takada, W.; Funaoka, S.; Arai, S.; Nakanishi, H.; Yokoyama, K.; Fujiwara, K.; Matsubara, K. *Nucleic Acids Res.* **2007**, *35*, e3/1.

(202) Abramov, M.; Schepers, G.; Van, A. A.; Van, H. P.; Herdewijn, P. *Biosens. Bioelectron.* **2008**, *23*, 1728.

(203) Val, G.; Marin, S.; Mellado, R. P. *Microb Ecol* **2009**, *58*, 108.

(204) Hai, T.; Hein, S.; Steinbuchel, A. *Microbiology (Reading, U. K.)* **2001**, *147*, 3047.

(205)   Cammarata, P. R.; Chu, S.; Moor, A.; Wang, Z.; Yang, S.-H.; Simpkins, J. W. *Exp. Eye Res.* **2004**, *78*, 861.

(206)   Zhang, W.-J.; Yang, J.; Yu, Y.-H.; Shen, Y.-F. *J. Eukaryotic Microbiol.* **2005**, *52*, 356.

(207)   Cuadrado, A.; Jouve, N. *Cytogenet Genome Res* **2007**, *119*, 91.

(208)   Ghanim, M.; Brumin, M.; Popovski, S. *J. Virol. Methods* **2009**, *159*, 311.

(209)   Stoecker, K.; Dorninger, C.; Daims, H.; Wagner, M. *Appl. Environ. Microbiol.* **2010**, *76*, 922.

(210)   Ulmer, K. M. *Science (Washington, D. C., 1883-)* **1983**, *219*, 666.

(211)   Tsuchiya, Y.; Morioka, K.; Shirai, J.; Yoshida, K.; Inumaru, S. *Nucleic Acids Symp. Ser.* **2006**, 275.

(212)   Burbelo, P. D.; Ching, K. H.; Han, B. L.; Klimavicz, C. M.; Iadarola, M. J. *Am. J. Transl. Res.* **2010**, *2*, 381.

(213)   Skoog, D. A.; Holler, F. J.; Nieman, T. A. *Principles of Instrumental Analysis*; 5th ed.; Brooks Cole, 1998.

(214)   Abramowitz, M.; Davidson, M. W. 2011.

(215)   Zhou, W.; Wang, Z. L. *Scanning Microscopy for Nanotechnology: Techniques and Applications*; Springer, 2007.

(216)   Williams, D. B.; Carter, C. B. *Transmission Electron Microscopy: Basics*; Springer, 1996.

(217)   Egerton, R. F. *Physical principles of Electrons Microscopy: An introduction to TEM, SEM, and AEM*; Springer, 2005.

(218)   Chang, E.; Miller, J. S.; Sun, J.; Yu, W. W.; Colvin, V. L.; Drezek, R.; West, J. L. *Biochem. Biophys. Res. Commun.* **2005**, *334*, 1317.

(219)   Medintz, I. L.; Uyeda, H. T.; Goldman, E. R.; Mattoussi, H. *Nat. Mater.* **2005**, *4*, 435.

(220)   Wirde, M.; Gelius, U.; Nyholm, L. *Langmuir* **1999**, *15*, 6370.

(221)   Yam, C.-M.; Pradier, C.-M.; Salmain, M.; Marcus, P.; Jaouen, G. *J. Colloid Interface Sci.* **2001**, *235*, 183.

(222)   Vance, A. L.; Willey, T. M.; Nelson, A. J.; van, B. T.; Bostedt, C.; Terminello, L. J.; Fox, G. A.; Engelhard, M.; Baer, D. *Langmuir* **2002**, *18*, 8123.

(223)   Peng, Z. A.; Peng, X. *J. Am. Chem. Soc.* **2001**, *123*, 183.

(224)   Peng, Z. A.; Peng, X. *J. Am. Chem. Soc.* **2001**, *123*, 1389.

(225)   Yu, W. W.; Qu, L.; Guo, W.; Peng, X. *Chem. Mater.* **2003**, *15*, 2854.

(226)   Hood, L.; Galas, D. *Nature (London, U. K.)* **2003**, *421*, 444.

(227)   Jiang, G.; Susha, A. S.; Lutich, A. A.; Stefani, F. D.; Feldmann, J.; Rogach, A. L. *ACS Nano* **2009**, *3*, 4127.

(228)   Whitesides, G. M.; Grzybowski, B. *Science (Washington, DC, U. S.)* **2002**, *295*, 2418.

(229)   Kamien, R. D. *Science (Washington, DC, U. S.)* **2003**, *299*, 1671.

(230)   Sapp, S. A.; Mitchell, D. T.; Martin, C. R. *Chem. Mater.* **1999**, *11*, 1183.

(231)   Mbindyo, J. K. N.; Reiss, B. D.; Martin, B. R.; Keating, C. D.; Natan, M. J.; Mallouk, T. E. *Adv. Mater. (Weinheim, Ger.)* **2001**, *13*, 249.

(232)   Reiss, B. D.; Mbindyo, J. N. K.; Martin, B. R.; Nicewarner, S. R.; Mallouk, T. E.; Natan, M. J.; Keating, C. D. *Mater. Res. Soc. Symp. Proc.* **2001**, *635*, C6.2/1.

(233)	Braun, E.; Eichen, Y.; Sivan, U.; Ben-Yoseph, G. *Nature (London)* **1998**, *391*, 775.

(234)	Martin, B. R.; Dermody, D. J.; Reiss, B. D.; Fang, M.; Lyon, L. A.; Natan, M. J.; Mallouk, T. E. *Adv. Mater. (Weinheim, Ger.)* **1999**, *11*, 1021.

(235)	Gu, Q.; Haynie, D. T. *Mater. Lett.* **2008**, *62*, 3047.

(236)	Ongaro, A.; Griffin, F.; Beecher, P.; Nagle, L.; Iacopino, D.; Quinn, A.; Redmond, G.; Fitzmaurice, D. *Chem. Mater.* **2005**, *17*, 1959.

(237)	Hostetler, M. J.; Stokes, J. J.; Murray, R. W. *Langmuir* **1996**, *12*, 3604.

(238)	Gooding, J. J.; American Scientific Publishers: 2004; Vol. 1, p 17.

(239)	Ang, T. P.; Wee, T. S. A.; Chin, W. S. *J. Phys. Chem. B* **2004**, *108*, 11001.

(240)	Belser, T.; Stoehr, M.; Pfaltz, A. *J. Am. Chem. Soc.* **2005**, *127*, 8720.

(241)	Laaksonen, T.; Pelliniemi, O.; Quinn, B. M. *J. Am. Chem. Soc.* **2006**, *128*, 14341.

(242)	Zhang, S.; Jamison, A. C.; Schwartz, D. K.; Lee, T. R. *Langmuir* **2008**, *24*, 10204.

(243)	Zhang, S.; Leem, G.; Lee, T. R. *Langmuir* **2009**, *25*, 13855.

(244)	Marshall, S. T.; O'Brien, M.; Oetter, B.; Corpuz, A.; Richards, R. M.; Schwartz, D. K.; Medlin, J. W. *Nat. Mater.* **2010**, *9*, 853.

(245)	Jana, N. R.; Gearheart, L.; Murphy, C. J. *The Journal of Physical Chemistry B* **2001**, *105*, 4065.

(246)	Jana, N. R.; Gearheart, L.; Murphy, C. J. *Chemistry of Materials* **2001**, *13*, 2313.

(247)	Gai, P. L.; Harmer, M. A. *Nano Letters* **2002**, *2*, 771.

(248)	Zhou, H.; Zhou, W.-p.; Adzic, R. R.; Wong, S. S. *The Journal of Physical Chemistry C* **2009**, *113*, 5460.

(249)	Hill, H. D.; Millstone, J. E.; Banholzer, M. J.; Mirkin, C. A. *ACS Nano* **2009**, *3*, 418.

(250)	Cao; Jin, R.; Mirkin, C. A. *Journal of the American Chemical Society* **2001**, *123*, 7961.

(251)	Tamerler, C.; Sarikaya, M. *ACS Nano* **2009**, *3*, 1606.

(252)	Lu, X.; Bai, H.; He, P.; Cha, Y.; Yang, G.; Tan, L.; Yang, Y. *Anal. Chim. Acta* **2008**, *615*, 158.

(253)	Willard, D. M.; Carillo, L. L.; Jung, J.; van, O. A. *Nano Lett.* **2001**, *1*, 469.

(254)	Tran, P. T.; Goldman, E. R.; Anderson, G. P.; Mauro, J. M.; Mattoussi, H. *Phys. Status Solidi B* **2002**, *229*, 427.

(255)	Patolsky, F.; Gill, R.; Weizmann, Y.; Mokari, T.; Banin, U.; Willner, I. *J. Am. Chem. Soc.* **2003**, *125*, 13918.

VITA

  The author was born in HoChiMinh City, Vietnam. She obtained her B.A. in Chemistry from the Department of Chemistry at University of New Orleans in May of 2004. She then continued her graduate education with the Department of Chemistry at the University of New Orleans and became a member of Professor Zeev Rosenzweig's research group. August of 2008, Professor Matthew A. Tarr became her second advisor.